University of Glasgow

Analysing and Controlling the Self-assembly of Gelation

Thesis submitted in fulfilment
of the requirements for the degree
of Doctor of Philosophy

Emily Ruth Cross
May 2020

To my parents, for raising me to believe that:

‘*Whatever the mind can conceive and believe, the mind can achieve regardless of how many times you may have failed in the past or how lofty your aims and hopes may be.*’

-Napoleon Hill

Abstract

We describe new methods to analyse and control the self-assembly of gelation leading to exciting new soft materials. These materials have been shown to be of use to a wide range of applications including antimicrobial coatings, OPV devices, thermochromic materials and biomedical materials. Many of the described methods are novel or go beyond the state of the art.

One of the analytical methods probes the surface chemistry of self-assembled hydrogel fibres to determine their pK_a. This method not only determines the gel's pK_a but whether indeed a gel would form from a small molecule and what its rheological stiffness would be. This is the first incident of electrochemistry being used to determine the rheology of gels. Furthermore, a method to probe in the real time the self-assembly kinetics of a gelator to form a gel using multiple pulse amperometry is described. This method is expanded to complex multicomponent systems.

Electrochemically fabricated hydrogels are developed and for the first time we show how the rheological properties can be controlled by controlling the electrochemical parameters. In addition to controlled rheological properties, the gels formed have unique mesh sizes and thermochromic properties.

We introduce a new gelation trigger method for low molecular weight hydrogels. Dopamine autoxidation can be used to control the self-assembly of small molecules to form gels and we go on to describe how these gels can be used for antimicrobial purposes.

To expand on the electrochemically fabricated hydrogels, we propose the oxidation of dopamine as a new electrochemical trigger. We describe how the rheological properties of the gels can be controlled and how they are potentially suitable for biomedical applications.

Finally, we describe a method to control the self-assembly of both single and multi-component gel networks by temperature and use an array of analytical

techniques to show this. We expand on this work to show how the temperature control can form gels with varying networks which lead directly to changes in the efficiency of electron transfer.

Acknowledgements

Most importantly I would like to say a massive thank you to my supervisor, Prof. Dave Adams. I am so thankful for all of the support and guidance that you have given me over the years, as well as inspiring me during my undergraduate years to pursue a PhD in Chemistry. It has been a fantastic honour and pleasure to have worked within your group.

Dr. Kate McAulay and Ana María Fuentes Caparrós you have both always been there for me when I've needed you to be. Thank you for all the moral support, laugher and memories I will never forget! To Bart Dietrich who has been the constant rock to which everything can depend upon, you were there from day one, thank you for all your wise words and friendship. To the current generation of Adams group, thank you for educating me in the interesting topics you are covering in your theses and for all the fun times we have had together. Thank you to all of the project students I had the honour to work with including Kevin Lamontagne, Jules Dutrieux and Euan Herdman.

Thank you to those in the department who assisted me during my PhD including Dr David Adam with NMR assistance and the members of the Symes group for helping with the electrochemistry.

A massive thank you goes to Dr Ben Alston who, in addition to Prof. Dave Adams, inspired me and gave me the confidence to pursue a PhD in the first place.

To Sam Donnelly, who has always supported me and made my final years during the PhD so wonderful.

To my family who have been there at both the highest highs and lowest lows of this journey, thank you. Olivia Davison and Simran Channa, you are basically family, so this includes you.

Finally, I need to thank Fiona Gray, as without her continued guidance this thesis would cease to exist.

List of publications arising from this thesis

E. R. Cross, S. Coulter, A. M. Fuentes-Caparros, K. McAulay, R. Schweins and D. J. Adams, 'Tuning the antimicrobial activity of low molecular weight hydrogels using dopamine' Chemical Communications, 2020, **56**, 8135-8138

S. Panja, A. M. Fuentes-Caparros, E. R. Cross, Cavalcanti, Leide and D. J. Adams 'Annealing supramolecular gels by a reaction relay' Chemistry of Materials, 2020, 32, **12**, 5264–5271

E. R. Cross, 'The electrochemical fabrication of hydrogels: a short review', Springer Nature Applied Sciences, 2020, **2**, 397.

E. R. Cross, K. McAulay and D. J. Adams, 'Forming low molecular weight hydrogels by electrochemical methods' in Methods in Molecular Biology: Peptide nanomaterials, Springer Nature, currently in publication.

E. R. Cross and D. J. Adams, 'Probing the self-assembled structures and pKa of hydrogels using electrochemical methods', Soft Matter, 2019, **15**, 1522-1528.

E. R. Cross, S. Sproules, R. Schweins, E. R. Draper and D. J. Adams, 'Optimising low molecular weight hydrogels for automated 3D printing' Journal of the American Chemical Society, 2018, **140**, 8667-8670.

M. C. Nolan, A. M. Fuentes Caparrós, B. Dietrich, M. Barrow, E. R. Cross, M. Bleuel, S. M. King and D. J. Adams, 'Optimising low molecular weight hydrogels for automated 3D printing', Soft Matter, 2017, **13**, 8426-8432.

List of abbreviations

Ag/AgCl	Silver/silver chloride
Cryo-TEM	Cryo-transmission electron microscopy
CV	Cyclic voltammetry
D_2O	Deuterium oxide
DCl	Deuterium chloride
DNA	Deoxyribonucleic acid
EPR	Electron paramagnetic resonance
FTO	Fluorine doped tin oxide
G'	Storage modulus
G"	Loss modulus
GdL	Glucono-δ-lactone
H_2O_2	Hydrogen peroxide
H_2O	Water
HCl	Hydrochloric acid
HOMO	Highest occupied molecular orbital
HPMC	(hydroxypropyl)methyl cellulose
HQ	Hydroquinone
ITO	Indium tin oxide
KCl	Potassium chloride
LED	Light emitting diode
LMWG	Low molecular weight gelator
LUMO	Lowest unoccupied molecular orbital
MPA	Multiple pulse amperometry
NaOD	Sodium deuteroxide
NaOH	Sodium hydroxide
NMR	Nuclear magnetic resonance
OPV	Organic photovoltaic
PBS	Phosphate buffered saline
Pt wire	Platinum wire reference electrode
Redox	Reduction and oxidation
Ref	Reference
RQC	Residual quadrupole coupling
SANS	Small angle neutron scattering
SEM	Scanning electron microscopy
SLD	Scattering length density
STD	Saturated transfer difference
TEM	Transmission electron microscopy
TM	$[Ru(NH_3)_6]Cl_3$
UV	Ultraviolet
UV/Vis	Ultraviolet/visible

Table of contents

List of tables

List of equations

List of figures

Declaration of authorship

I declare that, except where explicit reference is made to the contribution of others, that this thesis is the result of my own work and has not been submitted for any other degree at the University of Glasgow or any other institution.

Signed:

Date: 25th May 2020

CHAPTER 1

Introduction

Hydrogels are a class of soft material that consist of a solid entangled network which immobilises water.[1, 2] The solid network which encompasses the liquid gives the gels viscoelastic properties. Hydrogels have applications in many industries such as food,[3] electronics,[4] pharmaceutical,[5] and cosmetics.[6] Due to the increasing need to study cell and tissue physiology, hydrogels have become increasingly popular as they provide a three-dimensional matrix suitable to culture cells and engineer tissue.[5, 7] In addition, hydrogels can be used to encapsulate drugs for topical, parenteral and ocular administration.[5, 8] A hydrogel and drug combination provides controlled drug release which is advantageous compared to administration of the drug alone.[5]

Hydrogel networks can be formed from a variety of materials such as synthetic polymers,[9, 10] naturally occurring polymers,[11, 12] and low molecular weight gelators (LMWG).[13-15] Unlike polymer based hydrogels that are held together by covalent bonds, LMWG are held together only by intermolecular forces such as hydrogen bonding (H-bonding) and π-π stacking (Figure **1.1**).[14] This allows for reversibility and greater control over the assembly process which is advantageous for applications where the gels transition due to a triggered response from changes in the gels' environment is required. Due to the opportunity to create new methods to control gelation for exciting new LMWG, this thesis will focus on using gels formed from LMWG.

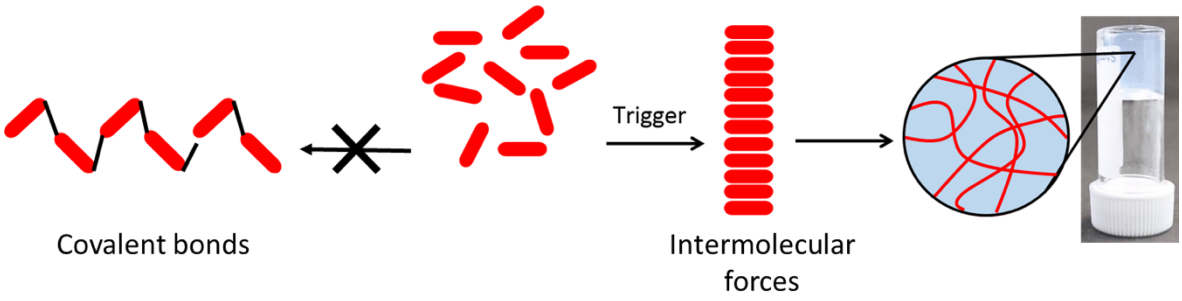

Figure 1.1 Schematic diagram showing how gels formed from LMWG (red) undergo self-assembly once a trigger is applied to form aggregated structures held together by intermolecular forces which entangle to immobilise water. This is a different method of gelation compared to polymer gels which are formed by the LMWG (red) covalently bonding together.

To form LMWG hydrogels, typically the gelator molecules are initially dissolved in water. When a trigger is applied which reduces the solubility of the gelator, self-assembly begins.[16] The self-assembly leads to larger structures, usually long fibres, which entangle and/or crosslink to immobilised water.

The self-assembly of gelation is still not fully understood. However, the use of ^{1}H NMR spectroscopy, small angle neutron scattering, small angle X-ray scattering and rheology can be used to gain more insight into the assembled networks as this introduction will explain.

1.1 Gelation triggers

The work within this thesis focuses on gelation of LMWG triggered by pH switch shown in Figure **1.2** a and b. However, pH triggered gelation is only one of many gelation triggers.[13] All of these triggers use the same principles as shown in Figure **1.2** b. First, a gelator which is soluble is dissolved in a solvent. Next, the solvent environment changes which reduces the solubility of the gelator. This change in solubility leads to an increase in strength of the intermolecular forces between the gelator molecules and the solvent, resulting in the rearrangement of the gelator molecules into a self-assembled aggregate. These self-assembled structures immobilise the solvent which results gel formation.

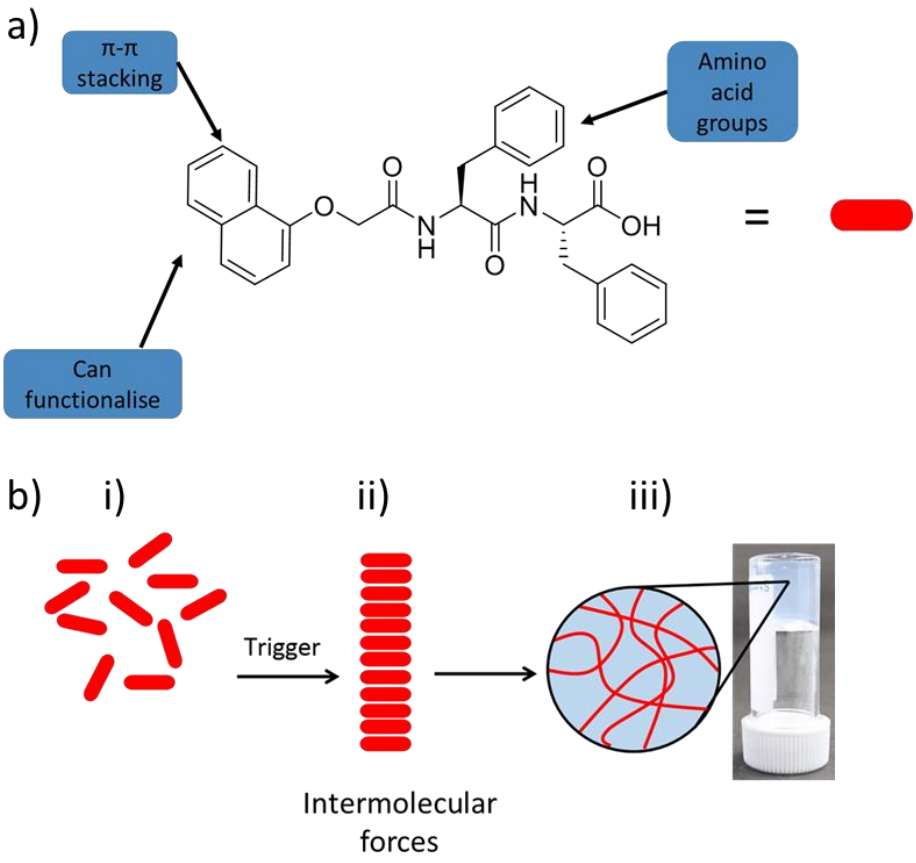

Figure 1.2 a) A typical LMWG consisting of a conjugated functional group which allows for π-π stacking and can be functionalised to increase or decrease solubility. This LMWG has a dipeptide chain consisting of two phenylalanine amine groups, other LMWG have short peptide chains consisting of mainly hydrophobic amino acids. The carboxylic acid functional group on the end of the peptide chain allows for pH triggered gelation. b) i) Schematic diagram showing the LMWG in i) dissolved at high pH. ii) A trigger is applied which reduces the solubility of the gelator, in this case a pH decrease where the carboxylate functional group is re-protonated. iii) The hydrophobic aggregated structures entangle which immobilises water and forms a gel.

1.1.1 Solvent switch

Solvent switch gelation involves dissolving gelator molecules in an organic solvent. A miscible solvent is then added which reduces the solubility of the gelator and triggers self-assembly. An example of this is water added to dimethyl sulfoxide. As the change in solubility is rapid, the rate of gelation is fast compared to other

gelation triggers. The final gel properties are determined by the ratio of the two solvents, the type of gelator used and the concentration of gelator.[17]

1.1.2 Temperature switch

Temperature change is a common gelation trigger. Gelators are usually soluble at high temperature but, at low temperatures insoluble (Figure **1.3**).[18] This change in solubility triggers self-assembly. The rate of gelation can be controlled by the temperature change gradient, which leads to a range in rheological properties.[18]

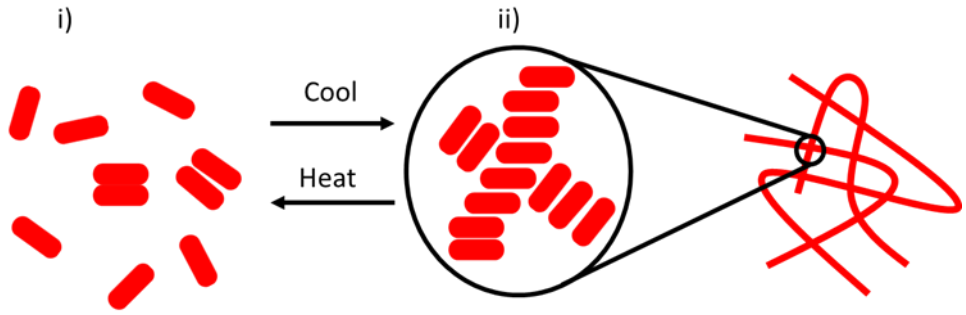

Figure 1.3 A heat cool gelation mechanism i) The gelators (red) are heated which increases solubility. ii) the solution is cooled, and a sol-gel transition is observed. This process can be reversed, and heat-cool cycles can be set up.

1.1.3 Enzyme

Enzymes are biological catalysts used throughout biology and chemistry by providing alternative reaction pathways. As they are naturally occurring, they are useful for preparing gels for physiological applications, but also require gelation conditions to be within specific temperature and pH ranges. As a trigger, enzymes can be used to either make or break bonds such as covalently bonding two gelator components which result in fibre formation or breaking covalent bonds from the solubilising group on a gelator molecule making the gelator insoluble.[19, 20]

1.1.4 Salt addition

The addition of a salt with metal ions such as Ca^{2+}, Mg^{2+} and Fe^{3+}, can be used to trigger gelation by screening charges (Figure **1.4**).[21] Aggregated structures such as micelles with exposed functional groups can bind to the metal ions to form a cross-linking network.[22, 23] This network can immobilise solvent and produce a gel. The

ion-fibre binding dynamics play an important role in determining the physical properties of the gels.[13]

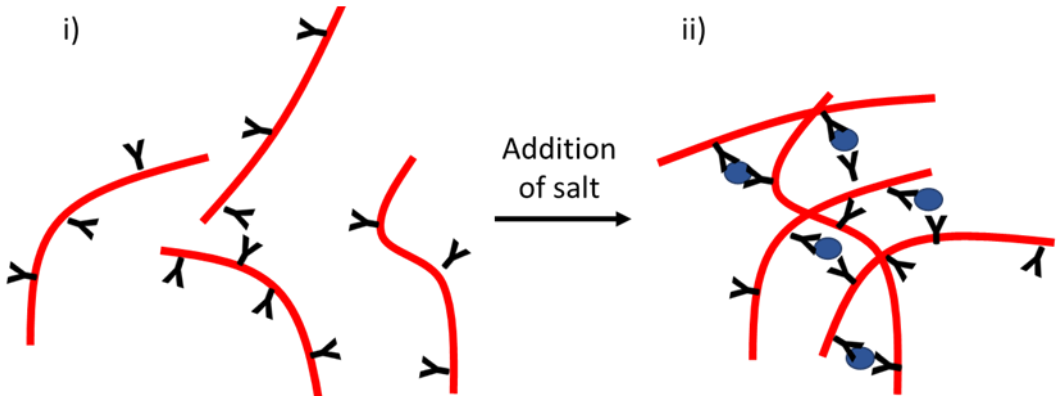

Figure 1.4 i) Worm-like micelles (red lines) with exposed charged functional groups (Y shape) in solution ii) Trigger of gelation by the addition of a salt (blue circles) which screens the charges of the worm-like micelles. The crosslinking of the worm-like micelles entraps water molecules resulting in a gel.

1.1.5 pH switch

pH triggers can be used when the gelator molecule has a functional group that be either be protonated or de-protonated, such as amines or carboxylic acids. In the case of gelators with a carboxylic acid, at high pH the carboxylic acid become de-protonated and the gelators are free in solution. A decrease in the pH of a gelator solution past its pK_a, causes the carboxylic acid group to become protonated,[24] and the stability from the electrostatic interactions between the acid and water is lost making the gelator hydrophobic.[24] To lower the energy of the system, the gelator then forms aggregates.

By choosing the method to lower pH, the gelation kinetics can be controlled. Using a mineral acid such as hydrochloric acid dropwise causes localised gelation which can result in non-homogeneous gels.[25] Forming non-homogeneous gels is impractical due to irreproducibility and the loss of advanced spatial control. Adams et al. developed a method to form homogenous gels *via* the addition of glucono-δ-lactone (GdL).[26] GdL hydrolyses in water lowering the pH gradually, these gels are more reproducible (Figure **1.5**).[25, 27]

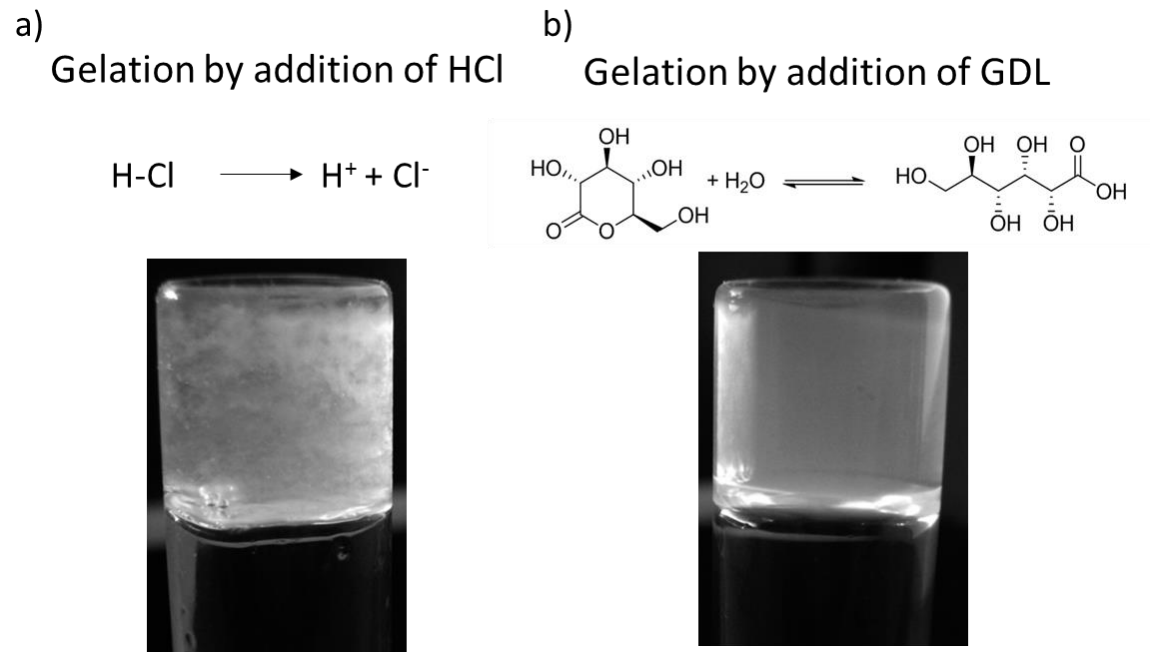

Figure 1.5 pH gelation triggers showing differences in homogeneity. a) addition of a mineral acid causes instant localised gelation resulting in a gel that is visibly inhomogeneous. b) addition of GdL slowly lowers the pH of the gelator solution as it hydrolyses, this results in a visibly homogeneous gel. Adapted from ref.[25] with permission from the Royal Society of Chemistry.

1.2 Electrochemical gelation

Electrochemical gelation is a common term used to describe the process of preparing hydrogels on an electrode surface. However, other phrases such as electrochemical fabrication, electrodeposition, bio-assembly, bio-printing, e-gels and electrogelation are also used to describe this process. Hydrogels can be prepared by changing the solubility of the gelating component on the electrode surface. [28-30] There are a variety of reduction and oxidation (redox) methods used to induce this change in solubility. Commonly, methods are chosen considering a combination of the gelator type, solution composition and the desired properties of the final product. These methods require either the reduction or oxidation of a species in the gelator solution (Table **1.1**).

Table 1.1 Methods for electrochemical hydrogel fabrication

Redox triggers	Gelator	References
Oxidation:		
Water oxidation	Silk Alginic acid Hyaluronic acid	31-35 36 37
Hydroquinone (forms benzoquinone and H^+)	Low molecular weight gelators (-COOH terminus)	29, 38, 39
Fe(II) (forms Fe^{3+})	Alginate Poly acrylic acid	40 41
Catechol (forms quinone)	Polyallylamine hydrochloride	42, 43
Cu(0) (forms Cu^{2+})	Chitosan Carboxymethylcellulose	44 45
Cl_2	Putative crosslinking of chitosan	46
Enzymes	Covalent crosslinking specific to enzyme type	47, 48
Reduction:		
Water reduction	Collagen Chitosan	11, 12 30, 49-53
Ruthenium complex $[Ru(bpy)_2]Cl_2$	Chitosan	54

Although the methods to fabricate hydrogels on an electrode surface may differ, the fundamental principles are similar. In general, these methods create a solubility gradient in which the gelator is soluble in the bulk solution but insoluble at the electrode surface. This change in solubility triggers the assembly of gelator components into hydrogels on the electrode surface, while in the bulk solution the gelator components remain soluble. Figure **1.6** shows how the redox trigger hydroquinone (HQ) can be oxidised on an electrode surface, producing benzoquinone and protons. The protons set up a pH gradient where the pH is low on the electrode surface and high in the bulk solution.[29, 38] The resulting low pH triggers gel formation which continues to grow as the HQ is continuously oxidised.

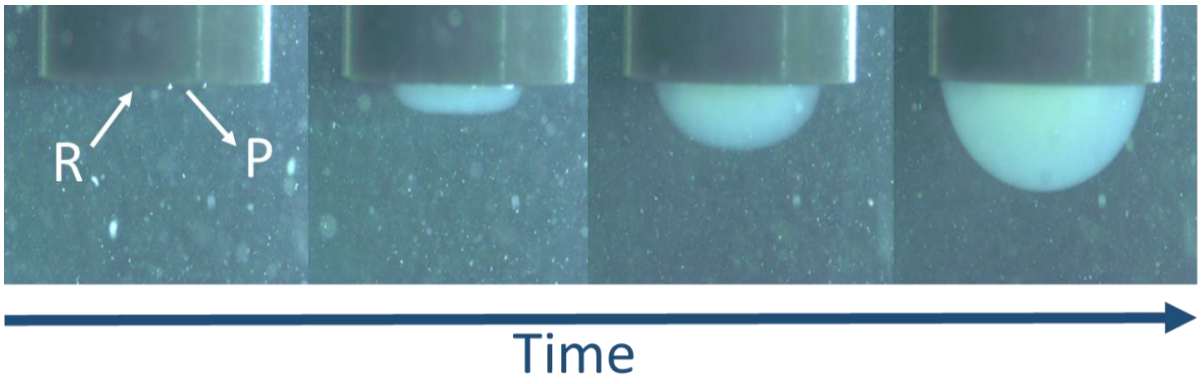

Figure 1.6 Image of a gel growing on a glassy carbon electrode as a fixed current is applied over time. **R** represents the redox trigger diffusing to the electrode surface, reacting to form a product, **P**, which triggers gelation. The volume of the gel on the surface increases with time. Figure from unpublished data

Common electrochemical set ups include a working electrode such as a glassy carbon, platinum, or FTO (fluorine doped tin oxide)/ITO (indium doped tin oxide) coated glass, within a three-electrode system. Electrode surfaces can be patterned in order for a hydrogel of a specific shape to be prepared (see Section 1.5). Electrode pens have the advantage of being mobile and can be used to sketch regions within a bulk gelator solution. The sketched regions are less soluble than the bulk which triggers the self-assembly of the gelator.[55] Gelation by an electrode pen allows for greater spatial control within a bulk solution than regular triggers. Affixing an electrode pen to a mechanical arm allows for programmed three-dimensional printing of hydrogels.[55] Figure **1.7** shows examples of both stationary and mobile electrochemical fabrication techniques.

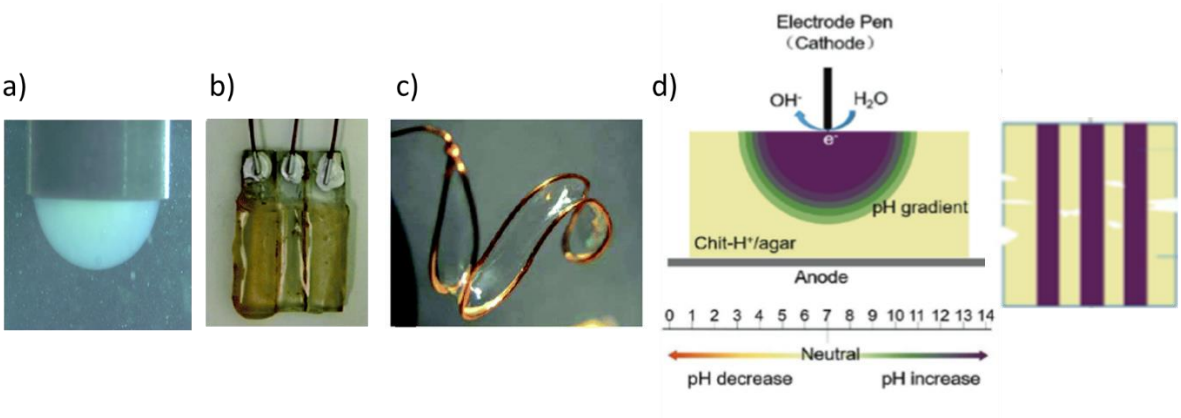

Figure 1.7 a) Low molecular weight hydrogel grown on a glassy carbon electrode. b) Low molecular weight hydrogel grown on a FTO glass electrode, reproduced from Ref. [38] with permission from The Royal Society of Chemistry. c) Three-dimensional silk gel grown on a copper wire electrode, reproduced from Ref. [34] with permission from The Royal Society of Chemistry. d) Schematic diagram of: left, an electrode pen dipping into the surface of a bulk solution containing protonated chitosan and agar causing electrolysis, an increase in pH and subsequently chitosan gel formation; right, the resulting sketched line regions of chitosan gel surrounded by the bulk solution. Reproduced from ref. [55] with permission from ©2018 WILEY-VCH Verlag GmbH & Co. KGaA, Weinheim.

Recent advances in potentiostat production have made potentiostats available which are small, do-it-yourself, portable and cheap allowing for greater access for fabrication techniques. [56-59] The rest of this introduction will discuss some of the challenges that are shared between electrochemical hydrogel fabrication methods and how these have been addressed. The methods used to analyse gels will also be highlighted.

1.3 Applications of electrochemically fabricated hydrogels

Electrochemical hydrogel fabrication provides new opportunities for construction on at the micro- and nanoscale.[60, 61] Unlike gels formed in bulk which take the shape of the container they are poured into when liquid, electrochemically fabricated hydrogels can be formed on any conductive surface which provides a high level of spatiotemporal control. Gels can then be used to encapsulate enzymes, nanomaterials, drugs or cells as shown in Figure **1.8**.[62] The potential for

new opportunities for fabricayion at the micro- and nano-scale is attracting increasing attention in a large range of potential applications, including synthesis of conducting polymers;[63] for use in regenerative medicine;[64, 65] and the rapidly growing field of biosensors and microfluidic devices.[66-70] Electrochemically fabricated hydrogels can also be used to create antibacterial surfaces,[71] and the coating of medical implants.[72, 73]

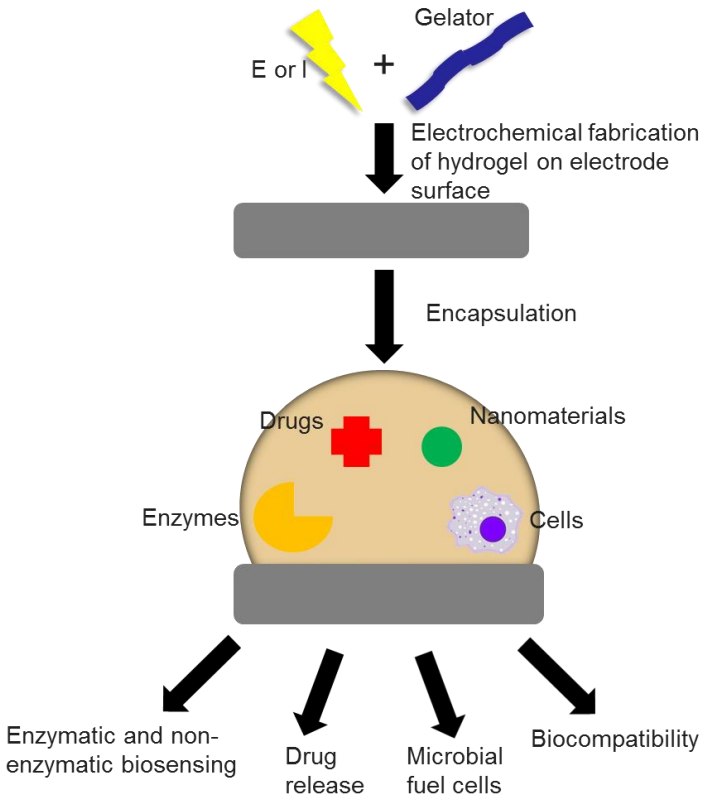

Figure 1.8 Schematic representation of the process for electrochemical fabrication of hydrogels, allowing the encapsulation of enzymes, drugs, nanomaterials, or cells, these processes are applied in several applications, such as biosensors,[66-69] corrosion prevention,[74] antimicrobial coatings, drug-release,[75] , barrier properties and cell encapsulation.[70]

1.4 Biological versus synthetic

There are a wide range of gelators that can be used to form hydrogels on an electrode surface. These include synthetic gelators and materials deriving from biological sources.[39] Chitosan was the first biopolymer gel to be formed on an electrode surface.[76] When using gelators originating from biological sources, there can be issues of batch-to-batch variation such as inconsistencies in molecular

weight, purity and possible contamination. All of these can mean that the final hydrogels have irreproducible properties. Other production-related issues with the use of chitosan produced from shellfish is the seasonality of the industrial harvest. When using naturally-occurring chitosan, there is also a significant risk of reticent anaphylaxis which limits clinical use.[10] Purified biologically-sourced gelators can of course be formed but this comes at an inflated cost.

Synthetic gelators can be used to mimic biological materials.[9, 77] These materials are usually based on covalently cross-linked polymer networks such as TrueGel3D™, Hystem® and HydroMAtrix™. As described earlier in Chapter 1 synthetic hydrogels are held together with only physical interactions without the need for covalent cross-linkers, such as low molecular weight gelators.[13-15] These gelators form reproducible gels in both the bulk,[25] and fabricated on an electrode.[38] Hydrogels formed using low molecular weight gelators can also be converted into polymers on an electrode.[63] The biocompatibility of hydrogels formed from synthetic gelators can be somewhat challenging. In order for the gels to be used in cell culture, they must be formed at a compatible pH (generally physiological pH) and cannot contain any materials that would induce cell death. Forming gels at physiological pH is difficult with certain pH triggered methods as they usually results in gels with high or too low a pH.[29]

For biological applications, both biologically derived and synthetic gels are often required to be placed in pH buffered cell media. The contents of cell media can include a mixture of glucose, antibiotics and buffered salt solutions. It is necessary therefore to test whether the effect of leaving the gels in a buffered solution affects the properties which are to be controlled electrochemically.

1.5 Spatiotemporal control

Spatiotemporal control is the term used to describe the fabrication of a gel by controlling the parameters of time and space, such as controlling the rate of growth and the resulting size and thickness of the gel.

Hydrogels can be prepared on a range of electrode surfaces with any geometry, within a stationary electrode system, they can also be sketched, or printed using a mobile electrode pen.[55, 78] Stationary electrodes can be any shape and size on

any length scale with the desired gel forming on the surface.[28, 79, 80] Conductive glass electrodes such as ITO and FTO can be etched to allow for regions of conductive/non-conductive areas,[38] which results in gels only forming on the conductive regions.[29, 38] As well as forming gels in a two-dimensional plane, three-dimensional gels can be formed by simply bending a two-dimensional electrode into an additional plane.[34] Bressner et al. showed a bent copper wire forming a closed loop electrode could be used to prepare the first electro fabrication of silk gels in three-dimensions.[34] Photocathodes can also be used to produce patterned gels. The photocathodes selectively produce electrode surface reactions. Jiang and co-workers controlled the illumination pattern on a digital micro-mirror device in order to produce chitosan gels with difference shaped and sizes and as well as multiplexed micro-patterning.[81]

Electrode pens can be formed from a variety of conductive materials and sizes. Su et al. formed a cathodic electrode pen from a stainless-steel acupuncture needle.[55] The pen once placed on the surface of a bulk gelator solution can create regions where gelation is triggered. The writing speed and holding time can determine the thickness of the gels formed.[55] Figure **1.9** shows examples of the spatial temporal control from both stationary and mobile electrodes.[45, 55]

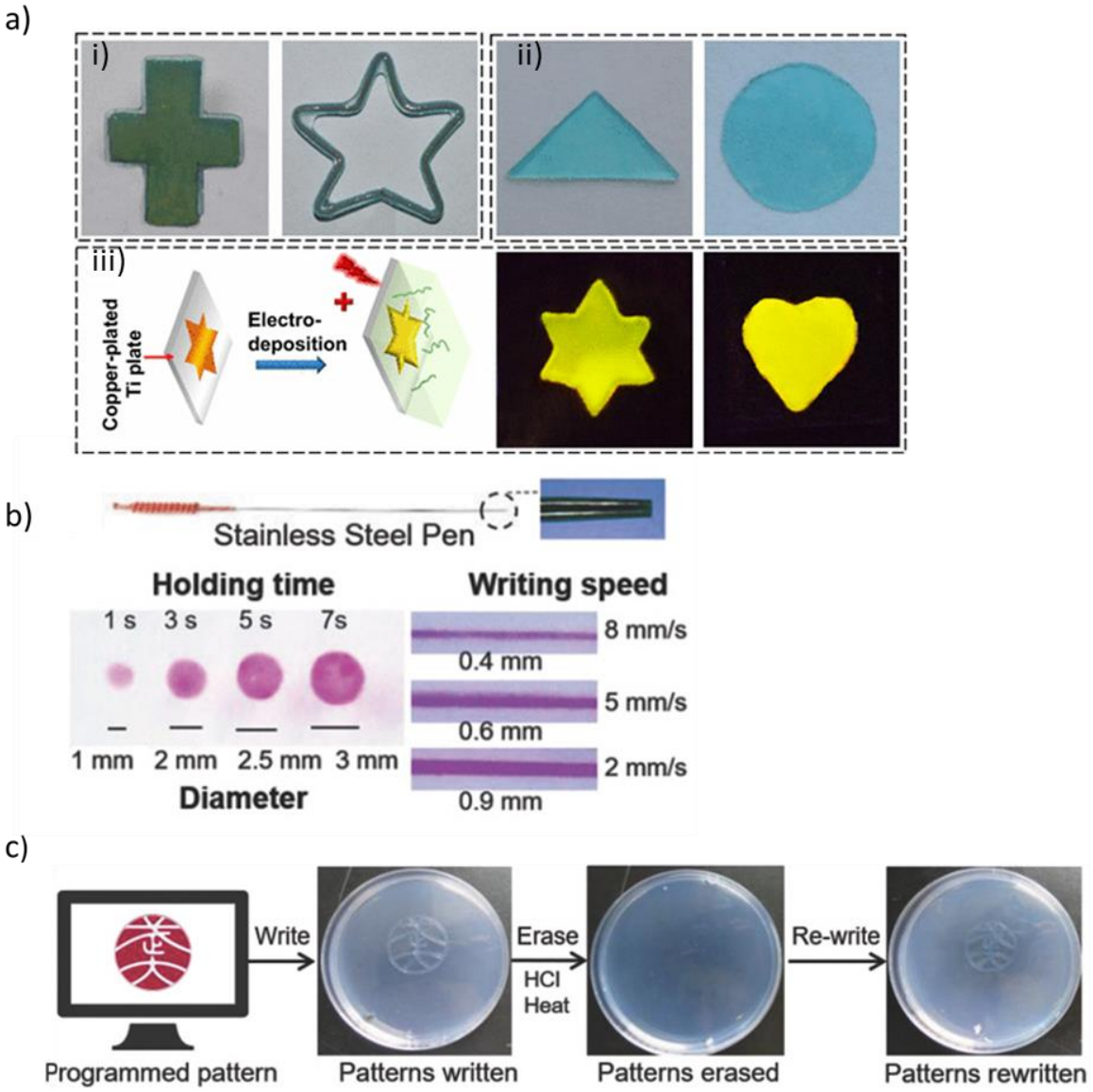

Figure 1.9 a) i) Images of deposited films on a copper plate and copper wire electrodes, ii) Images of deposited films with different shapes detached from copper plates. iii) Schematic illustration for fabricating fluorescence patters on the deposited film on a copper-plated titanium plate, and images of the fluorescence patterns under 254 nm UV light. All images for a) were reprinted by permission from Springer: Springer, Cellulose, [45] © 2018. b) cathodic writing on a chitosan/agarose hydrogel using a stainless-steel pen electrode. The longer holding times result with a gel of a larger area. The slower writing speed produces gels with greater thickness. c) A programmed pattern written onto the gel surface which can be erased and rewritten. Both b) and c) are reprinted by permission from ©2018 WILEY-VCH Verlag GmbH & Co. KGaA, Weinheim.

Further spatiotemporal control can be achieved by controlling the electrical input to the electrode. Yan et al. have shown the formation of chitosan hydrogels on a glassy carbon electrode can be controlled by oscillating electrical signals.[82] This oscillation in electrical signal enables segmented structures to be generated, which are consistent with the clock and wavefront framework.[82] Controlling the electrical signals also allows for the sequential assembly of gelators. This can be applied to multicomponent gelators systems on the same electrode. Controlling the applied current can selectively trigger individual gelators within multicomponent systems as Raeburn et al. have shown for pH triggered gelators of differing pK_a values.[38] Layered structures can also be prepared on separate electrodes within the same system as demonstrated by Wang et al.[83] Sequential assembly of gels is of particular interest for microfluidic channels for lab-on-a-chip applications,[83] and for use as conductive materials.

1.6 Homogeneity

In order to form reproducible gels, there needs to be homogeneity within gel phases.[25] This can be difficult to analyse. Fabrication methods which produce gas on the electrode surface may form bubbles within the gel or leave holes were the gas has diffused out. This can compromise mechanical stiffness, gel clarity and can act as an electrical insulator that slows down continued gel formation.[34, 84] A camera can be used to analyse the size and distribution of the bubbles within the gel which can keep track of bubbles forming and analyse the size of the gel.[29] Kaplan and Migliaresi have both shown how the rate of bubble formation can be minimised by regulating the current within solution.[32, 84]

1.7 Removing the gel from the electrode surface

In the cases where the gels do not form any chemical bonds to the electrode surface, they can be removed by gently tapping or scraping the gel from the surface.[34] In addition, there are methods which can remove gels from a surface remotely. These methods either reduce the solubility of the gelator at the electrode surface and gel interface,[85] or by producing a gas which pushes the gel off of the electrode.[80] This can be done by reversing the applied current.[84] Payne and co-workers have shown how pH switch gels formed by the reduction of water can be removed from the surface of the electrode by reversing the potential where

the oxidation of water occurs causing acidification. This induced acidification of chitosan gels can induce multilayer disassembly. [86] Potential reversal has also been used to remove gels from a patterned microelectrode surface as shown in Figure **1.10**.[80]

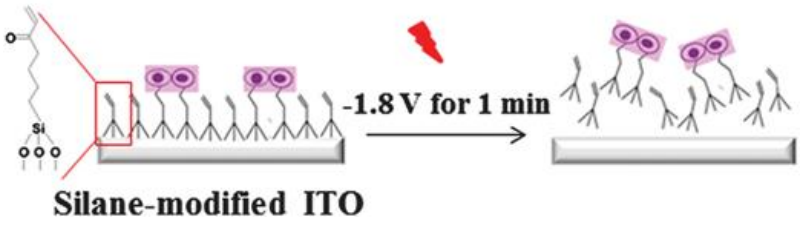

Figure 1.10 Electrochemical detachment of HepG2 cells inside herapin based hydrogels from a modified ITO electrode. Electrochemical detachment was triggered by a negative potential of -1.8 V being applied for 1 minute. Reproduced from Ref. [80] with permission from The Royal Society of Chemistry.

1.8 Self-assembly and gel property analysis

In order to analyse gels, the techniques must not distort the physical properties of the material.[87] An ideal method for gel analysis must have the following characteristics:

- Represent the three-dimensional hydrogel, not just the surface.
- Be a process that does not require environmental conditions that modify the materials morphology to an unknown degree e.g. cryogenically freezing, swelling, pressure changes or placing in a salt buffered solution.
- Have a sample preparation process that does not alter the matrix or self-assembly process e.g. avoid methods where samples are manually cut after freezing, coated in gold, or the addition of probe particles.

If these conditions are not met, analysis results can end up inaccurate. For example, Mears et al. showed how the drying of gels can affect the structural network.[88] Comparing the fibre width of a low molecular weight gel using scanning electron microscopy (SEM), cryo-transmission electron microscopy (cryo-TEM) and

small angle neutron scattering (SANS) measurements and revealed how the fibre widths differed between gels that were hydrated and dried.[88]

1.8.1 pH determination

Measuring the pH during gelation is important for pH triggered gels as the rate of pH change determines the rate of gelation.[55] As gelation occurs once the pH has passed the pK_a of a pH-triggered gelator,[89] the rate of pH change controls the rate of gelation which can yield gels of different physical properties.[90]

It is difficult to measure the pH of a gel or the bulk solution when a current is flowing, as the current interferes with the moving ions in the pH electrode tip. Although this can provide pH data with a range of error depending upon the concentration of ions in solution, the pH values are still usually reported. pH indicators such as universal indicator and methyl red can be added to the gelator solution which changes colour as the pH is changed.[34, 35] This can provide a simple approach to determine areas of different pH. Using an indicator is useful for measuring parts of the gel visible by the human eye or by spectrometry. However, to the best of our knowledge, a method to determine the exact pH at the electrode and gel interface during gelation has not been identified.

1.8.2 Optical Imaging of electrofabricated Hydrogels

In situ imaging is an essential tool to analyse gel growth. Images can be used to analyse the rate of gel growth and determine the shape and size of the gel.[28, 29, 38, 82] As the development of mobile phone camera resolution has progressed, in some cases a phone camera is all that is needed to record rate of gel growth, shape and area. Open source software such as ImageJ can be used to trace the outline of the gel on the electrode surface and calculates its area as well as analysing any bubble formation in the gel (Figure **1.11**).[91]

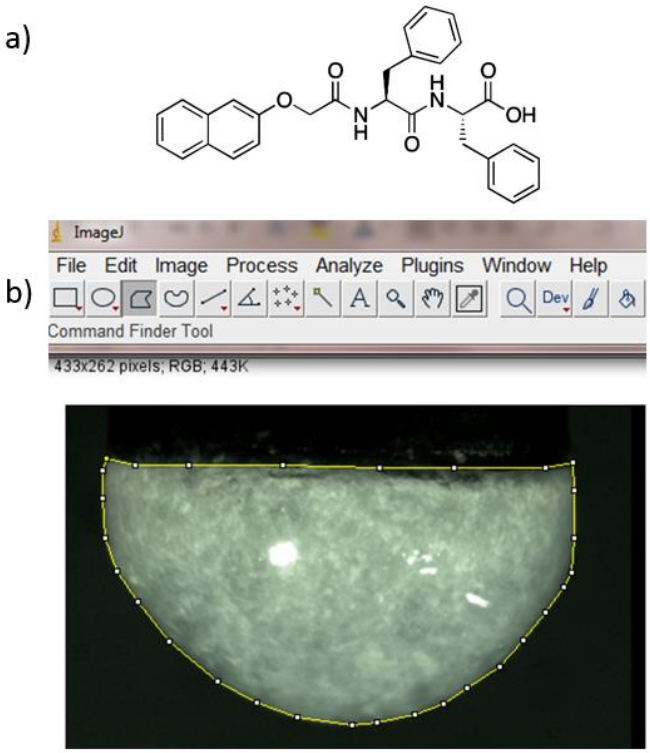

Figure 1.11 a) Low molecular weight gelator that is fabricated on a glassy carbon electrode. b) gel formed from gelator in a) on a glassy carbon electrode. ImageJ software is used to trace around the gel area to determine its volume.

1.8.3 Nuclear magnetic resonance (NMR)

Advances in in-situ analysis techniques for gelation such as NMR spectroscopy [92-94] have limited use in electrochemical gels due to the inability to physically apply the methods. Wallace et al. have shown how NMR spectroscopy can be used to determine the gelator pK_a and pore size in bulk gelation.[92-94] Development of these techniques for an electrochemical system would allow for greater analysis of gelation kinetics. For gels formed on an electrode, the self-assembly process can be followed by NMR detectable gelator molecules e.g. approximately smaller than 25 kDa.[95] Large gelators experience slow tumbling in solution which leads to faster relaxation of transverse magnetisation, this causes the gelator to appear invisible in the spectra.[95] NMR self-assembly analysis involves removing the gel from the electrode surface at different time points during gelation, freeze drying the gels then placing in a deuterated solvent and analysing using NMR spectroscopy. The NMR peaks are then integrated against a known standard to determine gelator concentration.[38, 96] Following the self-assembly during gelation allows for the

content of the gel to be identified, which is of particular use for multicomponent systems as shown in Figure **1.12**.

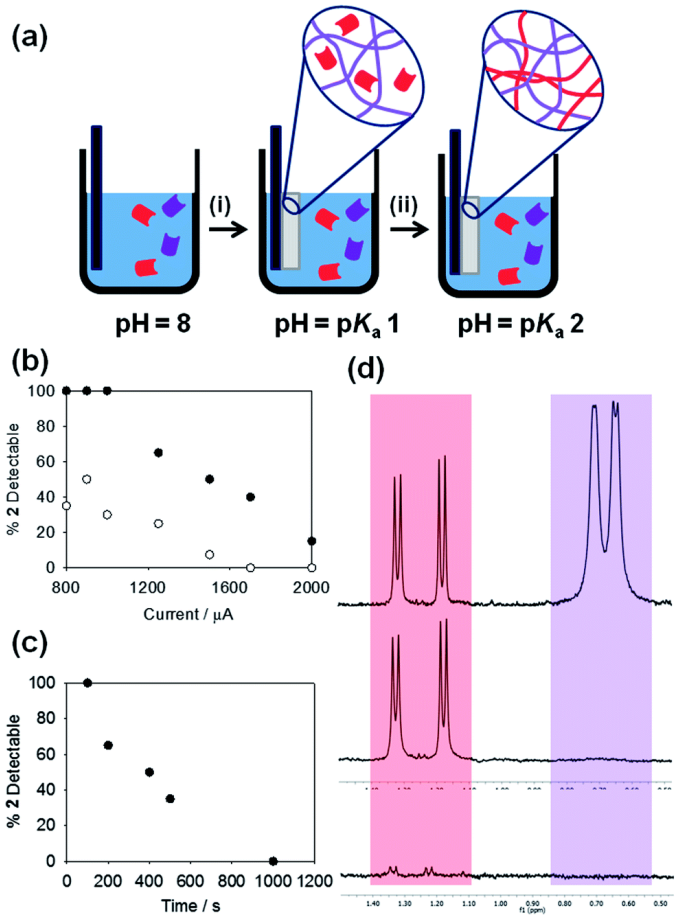

Figure 1.12 a) Schematic showing the sequential assembly of two gelators in a multi-component system. (i) The gelator with the highest pK_a will assemble first as the pH is decreased, whilst the second gelator will remain in solution until (ii) its pK_a is reached. (b) Percentage of the gelator with the highest pK_a (**1**) detectable in the NMR spectrum of a gelled 1:1 mixture the two gelators; gels formed at different currents for times of (black circles) 100 s and (White circles) 300 s. (c) Percentage of gelator with the lower pK_a (**2**) detectable in the NMR spectrum of a gelled 1:1 mixture of both gelators; gels formed at a current of 800 mA for different times. (d) Partial NMR spectra for (top) stock solution of both gelators, the purple peaks are from the gelator **1** and the red peaks are gelator **2**; (middle) application of a current of 1250 mA for 100 s results in loss of the peaks from **1** whilst **2** remains in solution; (bottom) application of a current of 2000 mA for 300 s results in the loss of peaks from both **1** and **2**, showing that both have gelled. Reproduced from Ref. [38] with permission from The Royal Society of Chemistry.

1.8.4 Characterisation of hydrogel nano/microstructures

Electron imaging techniques such as SEM or TEM can produce images of dried gel surfaces to reveal the morphologies of micelles, polymers and the overlapping of fibres.[97] From these images, the analysis of fibre width, length and pore size are often acquired. Three-dimensional images can be obtained by cryogenically freezing the gels then fracturing the matrix to reveal a cross section.[98] However, the disadvantages of using SEM, TEM and other in situ techniques include the vacuuming or cryogenically freezing of the gels. The collapsing of the matrix due to vacuum and the expansion of the matrix due to water freezing can dramatically modify the gels morphology making it difficult to accurately analyse the gels quantitatively without an unknown degree of error.[88] However, SEM imaging can be useful to qualitatively analyse different structural regions within a gel as shown in Figure **1.13**.[82]

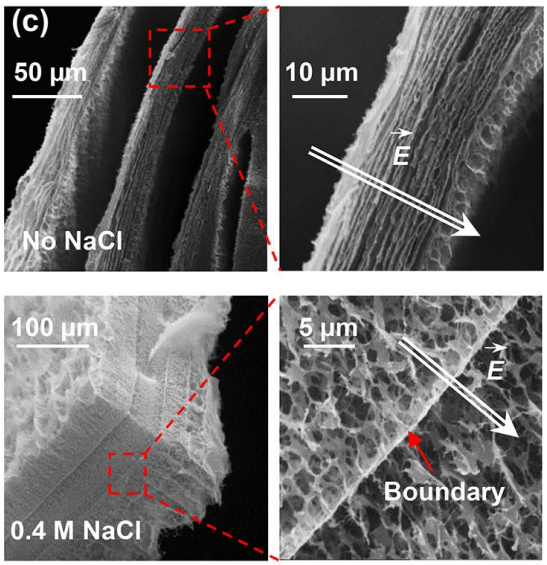

Figure 1.13 SEM images of segmented chitosan hydrogels show aligned segments for gels deposited in the absence of NaCl, while gels deposited in the presence of salt show porous random structures. Arrows indicate electric field. Adapted with permission from [82]. Copyright 2018 American Chemical Society.

Quantitative polarised light microscopy (qPLM) can be used to identify microstructural organisation within fabricated gels. Yan et al. used Brillouinn spectroscopy to show how gradients in mechanical properties and differences within internal patters can be identified during and after gelation. By combining

both qPLM and Brilloiun spectroscopy, they were able to clarify the mechanisms responsible for the emergence of segmented structure during chitosan's electrodeposition (Figure **1.14**).

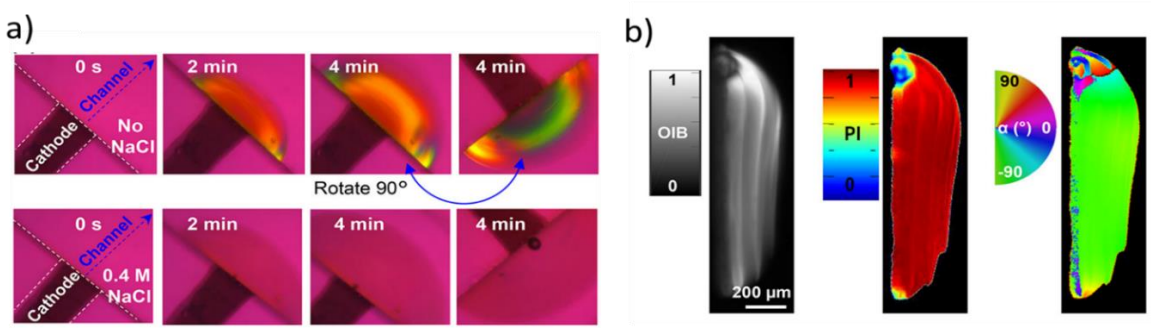

Figure 1.14 Electrical control of emerging nanostructures. a) Time lapse images that show gels deposited in the absence of NaCl are birefringent whereas gels deposited in the presence of NaCl show little birefringence. B) Quantitative polarised light microscopy metrics of orientation-independent birefringence, parallelism index, and local optical axis orientation of chitosan electrodeposited in the absence of salt. Adapted with permission from [82]. Copyright 2018 American Chemical Society.

1.8.5 Diffraction

Conventional X-ray diffraction generally gives broad, amorphous patterns for gels meaning that analysis is difficult. However, it can be a useful technique to identify fabricated crystalline structures within an amorphous gel such as chitosan's self-assembly into crystals.[55] Small angle scattering can be used to analyse gel properties such as fibre length, shape, fractional dimensions, alignment and size. [99, 100] Small angle scattering can be applied on many length scales ranging from 0.1 nm to 1000 nm which can be combined to observe a large range. In bulk gelation, contrast matching of gel fibres can be used to differentiate different components within a multicomponent system.[90] This can be used to determine if fibres are composed of self-sorted or co-sorted gelators.[90] Methods such as these would be useful to analyse electrochemical gelation.

1.8.6 Rheology

Oscillatory rheology can be used to determine homogeneity, stiffness and strength of a gel.[101] Rheology is carried out using a rheometer. Tests such as frequency and strain sweeps are used to measure the storage modulus, how solid like the material is (G') and the loss modulus, how liquid like the material is (G"). When G' is approximately an order of magnitude larger than G", and the G"/ G' value (tanδ) is less than 0.1 the material is considered a gel. Frequency tests can be used to determine how the gels react under increasing frequency which can be used to determine how stiff the gel is. The higher the G' and G" values, the stiffer the gel.

The strain tests then measure how much strain is needed to break the gel, and so can be used to determine the strength of the gel. The strain at which the gel begins to decrease its G' value is called the critical strain. Complete breakdown of the gel is where G" has become larger than G', and the sample is now more liquid-like than solid-like.

Variations in sample loading allow for both bulk and electrochemically formed gels to be measured however, it is important to note that rheological properties of gels can only be compared if they have been used on the same measuring system. Si et al. used a rheological approach, tensiometry, to show how the mechanical properties of a chitosan gel were enhanced by using a cathodic writing pen versus a chitosan gel that was unwritten.[55]

Rheology is an extremely useful tool for biofabricated gels. The stiffness of the gels amongst other factors controls the differentiation pathway of stem cells into tissue.[102] For those with a biology background, rheology data is usually provided giving the Young's modulus, whereas a chemical/engineering background usually provides the storage and loss moduli which can cause some confusion. However, the relationship between the two is relatively simple and shown in Equation 1.1

a) $E = G^*(2v + 1)$

b) $G^* = \mathrm{G}' + iG''$

Equation 1.1 Rheological equations to show the a) Young's modulus and b) the complex modulus where E represents Young's modulus, G* the complex modulus, v the Poisson ratio which is usually 0.5 for a hydrogel,[103] i the imaginary component, G' the storage modulus and G" the loss modulus.

1.9 Work in this thesis

The aim for this thesis was to discover new methods to understand and control the processes which lead to gelation. These newfound controls would be used to produce gels with specific properties in order to suit the application intended such as photoconductive and thermochromic devices; antimicrobial gels and cell models. The new controls developed in this thesis will include temperature controlled multicomponent gelation were one network can be formed in the absence of another or both at the same time. Another example of new controls includes the development of electrochemically fabricated hydrogels were the final gel properties can be tuned by the current input that is applied. Furthermore, a gelation method using dopamine oxidation both spontaneous in air and electrochemically driven will provide new materials with exciting application.

This thesis also aims to develop new analytical methods of gel characterisation such as the electrochemical determination of pK_a and rheology, ensuring that these improvements have the potential for wide accessibility and cheap usage.

1.10 References

1. M. D. Loos, B. L. Feringa and J. H. v. Esch, *J. Org. Chem*, 2005, **17**, 3615-3631.

2. P. Terech and R. G. Weiss, *Chem. Rev*, 1997, **97**, 3133-3160.

3. A. Ali and S. Ahmed, *J. Agri. Food Chem*, 2018, **66**, 6940-6967.

4. S. S. Panda, H. E. Katz and J. D. Tovar, *Chem. Soc. Rev*, 2018, **47**, 3640-3658.

5. E. Caló and V. V. Khutoryanskiy, *Euro. Polym. J,* 2015, **65**, 252-267.

6. M. E. Parente, A. Ochoa Andrade, G. Ares, F. Russo and Á. Jiménez-Kairuz, *Int. J. Cosmet. Sci*, 2015, **37**, 511-518.

7. M. W. Tibbitt and K. S. Anseth, J. Biotechnol, 2009, **103**, 655-663.

8. C. R. Lynch, P. P. D. Kondiah, Y. E. Choonara, L. C. du Toit, N. Ally and V. Pillay, Front Bioeng Biotech, 2020, **8**, 228.

9. D. A. Gyles, L. D. Castro, J. O. C. Silva and R. M. Ribeiro-Costa, *Euro. Polym. J* 2017, **88**, 373-392.

10. D. B. Brown, D. Rehmann, N, Sigma Aldrich Material Matters, 2016, **11**, 3.

11. J. Zhuang, S. Lin, L. Dong, K. Cheng and W. Weng, *ACS Biomater-sci. Eng*, 2018, **4**, 1528-1535.

12. T. Ling, J. Lin, J. Tu, S. Liu, W. Weng, K. Cheng, H. Wang, P. Du and G. Han, *J Mater. Sci-mater. M, 2013*, **24**, 2709-2718.

13. E. R. Draper and D. J. Adams, Chem, **3**, 390-410.

14. S. Ghosh, V. K. Praveen and A. Ajayaghosh, *Annu. Rev. Mater. Res*, 2016, **46**, 235-262.

15. L. E. Buerkle and S. J. Rowan, *Chem. Soc. Rev,* 2012, **41**, 6089-6102.

16. B. Ding, Y. Li, M. Qin, Y. Ding, Y. Cao and W. Wang, *Soft Matter,* 2013, **9**, 4672-4680.

17. L. Chen, J. Raeburn, S. Sutton, D. G. Spiller, J. Williams, J. S. Sharp, P. C. Griffiths, R. K. Heenan, S. M. King, A. Paul, S. Furzeland, D. Atkins and D. J. Adams, *Soft Matter*, 2011, **7**, 9721-9727.

18. E. R. Draper, H. Su, C. Brasnett, R. J. Poole, S. Rogers, H. Cui, A. Seddon and D. J. Adams, *Angew. Chem*, 2017, **129**, 10603-10606.

19. R. Huang, Y. Wang, W. Qi, R. Su and Z. He, *Mater. Lett*, 2014, **128**, 216-219.

20. F. Trausel, F. Versluis, C. Maity, J. M. Poolman, M. Lovrak, J. H. van Esch and R. Eelkema, *Acc. Chem. Res*, 2016, **49**, 1440-1447.

21. B. Ozbas, J. Kretsinger, K. Rajagopal, J. P. Schneider and D. J. Pochan, *Macromolecules*, 2004, **37**, 7331-7337.

22. H. McEwen, E. Y. Du, J. P. Mata, P. Thordarson and A. D. Martin, *J. Mater. Chem. B*, 2017, **5**, 9412-9417.

23. Lin Chen, Tom O. McDonald and D. J. Adams, *RSC Adv*, 2013, **3**, 8714-8720.

24. C. Colquhoun, E. R. Draper, E. G. B. Eden, B. N. Cattoz, K. L. Morris, L. Chen, T. O. McDonald, A. E. Terry, P. C. Griffiths, L. C. Serpell and D. J. Adams, *Nanoscale*, 2014, **6**, 13719-13725.

25. D. J. Adams, M. F. Butler, W. J. Frith, M. Kirkland, L. Mullen and P. Sanderson, *Soft Matter*, 2009, **5**, 1856-1862.

26. D. J. Adams, *Macromol. Biosci*, 2011, **11**, 160-173.

27. A. Z. Cardoso, A. E. Alvarez Alvarez, B. N. Cattoz, P. C. Griffiths, S. M. King, W. J. Frith and D. J. Adams, *Faraday Discuss*, 2013, **166**, 101-116.

28. R. Fernandes, L.-Q. Wu, T. Chen, H. Yi, G. W. Rubloff, R. Ghodssi, W. E. Bentley and G. F. Payne, *Langmuir*, 2003, **19**, 4058-4062.

29. E. K. Johnson, D. J. Adams and P. J. Cameron, *J. Am. Chem. Soc*, 2010, **132**, 5130-5136.

30. X. Pang and I. Zhitomirsky, *Mater. Chem. Phys,* 2005, **94**, 245-251.

31. Q. Lu, Y. Huang, M. Li, B. Zuo, S. Lu, J. Wang, H. Zhu and D. L. Kaplan, *Acta. Biomater*, 2011, **7**, 2394-2400.

32. D. Maniglio, W. Bonani, G. Bortoluzzi, E. Servoli, A. Motta and C. Migliaresi, *J. Bioact. Compat. Pol*, 2010, **25**, 441-454.

33. A. P. Tabatabai, D. L. Kaplan and D. L. Blair, *Soft Matter,* 2015, **11**, 756-761.

34. J. E. Bressner, B. Marelli, G. Qin, L. E. Klinker, Y. Zhang, D. L. Kaplan and F. G. Omenetto, *J. Mater. Chem. B*, 2014, **2**, 4983-4987.

35. N. Kojic, M. J. Panzer, G. G. Leisk, W. K. Raja, M. Kojic and D. L. Kaplan, *Soft matter*, 2012, **8**, 6897-6905.

36. M. Cheong and I. Zhitomirsky, *Colloids Surf. A Physicochem. Eng.* Asp, 2008, **328**, 73-78.

37. R. Ma, R. F. Epand and I. Zhitomirsky, *Colloid. Surface. B*, 2010, **77**, 279-285.

38. J. Raeburn, B. Alston, J. Kroeger, T. O. McDonald, J. R. Howse, P. J. Cameron and D. J. Adams, *Mater. Horiz*, 2014, **1**, 241-246.

39. E. K. Johnson, L. Chen, P. S. Kubiak, S. F. McDonald, D. J. Adams and P. J. Cameron, *Chem. Comm*, 2013, **49**, 8698-8700.

40. Z. Jin, G. Güven, V. Bocharova, J. Halámek, I. Tokarev, S. Minko, A. Melman, D. Mandler and E. Katz, *ACS Appl. Mater. Inter*, 2012, **4**, 466-475.

41. S. He, B. Ren, X. Liu and Z. Tong, *Macromol. Chem. Phys*, 2010, **211**, 2497-2502.

42. L.-Q. Wu, R. Ghodssi, Y. A. Elabd and G. F. Payne, *Adv. Funct. Mater*, 2005, **15**, 189-195.

43. C. Maerten, T. Garnier, P. Lupattelli, N. T. T. Chau, P. Schaaf, L. Jierry and F. Boulmedais, *Langmuir*, 2015, **31**, 13385-13393.

44. G. F. Payne and S. R. Raghavan, *Soft matter*, 2007, **3**, 521-527.

45. Y. Wang, Z. Zhang, M. Wang, C. Guo, H. Liu, H. Zeng, X. Duan, Y. Zhou and Z. Tang, *Cellulose*, 2018, **25**, 105-115.

46. K. M. Gray, B. D. Liba, Y. Wang, Y. Cheng, G. W. Rubloff, W. E. Bentley, A. Montembault, I. Royaud, L. David and G. F. Payne, *Biomacromolecules*, 2012, **13**, 1181-1189.

47. Y. Liu, J. L. Terrell, C.-Y. Tsao, H.-C. Wu, V. Javvaji, E. Kim, Y. Cheng, Y. Wang, R. V. Ulijn, S. R. Raghavan, G. W. Rubloff, W. E. Bentley and G. F. Payne, *Adv. Funct. Mater*, 2012, **22**, 3004-3012.

48. J. Wang, X. Miao, Q. Fengzhao, C. Ren, Z. Yang and L. Wang, *RSC Adv*, 2013, **3**, 16739-16746.

49. T. Jiang, Z. Zhang, Y. Zhou, Y. Liu, Z. Wang, H. Tong, X. Shen and Y. Wang, *Biomacromolecules*, 2010, **11**, 1254-1260.

50. H. He, X. Cao, H. Dong, T. Ma and G. F. Payne, *Adv. Funct. Mater*, 2017, **27**, 1605665.

51. F. Wang, P. Huang, D. Huang, Y. Hu, K. Ma, X. Cai and T. Jiang, *J. Mater. Chem. B*, 2018, **6**, 2304-2314.

52. Y. Li, Y. Liu, T. Gao, B. Zhang, Y. Song, J. L. Terrell, N. Barber, W. E. Bentley, I. Takeuchi, G. F. Payne and Q. Wang, *ACS Appl. Mater. Inter*, 2015, **7**, 10587-10598.

53. X. Pang and I. Zhitomirsky, *Surf. Coat. Technol*, 2008, **202**, 3815-3821.

54. Y. Zhang and C. Ji, *Anal. Chem*, 2010, **82**, 5275-5281.

55. S. Wu, K. Yan, Y. Zhao, C.-C. Tsai, J. Shen, W. E. Bentley, Y. Chen, H. Deng, Y. Du, G. F. Payne and X. Shi, *Adv. Funct. Mater*, 2018, **28**, 1803139.

56. A. A. Rowe, A. J. Bonham, R. J. White, M. P. Zimmer, R. J. Yadgar, T. M. Hobza, J. W. Honea, I. Ben-Yaacov and K. W. Plaxco, PLOS ONE, 2011, **6**, e23783.

57. M. D. M. Dryden and A. R. Wheeler, PLOS ONE, 2015, **10**, e0140349.

58. A. Butterworth, D. K. Corrigan and A. C. Ward, *Anal. Methods*, 2019, **11**, 1958-1965.

59. A. Ainla, M. P. S. Mousavi, M.-N. Tsaloglou, J. Redston, J. G. Bell, M. T. Fernández-Abedul and G. M. Whitesides, *Anal. Chem*, 2018, **90**, 6240-6246.

60. T. K. Merceron and S. V. Murphy, *Essentials of 3D Biofabrication and Translation*, 2015, 249-270.

61. H. Yi, L.-Q. Wu, W. E. Bentley, R. Ghodssi, G. W. Rubloff, J. N. Culver and G. F. Payne, *Biomacromolecules*, 2005, **6**, 2881-2894.

62. C. Maerten, L. Jierry, P. Schaaf and F. Boulmedais, *ACS Appl. Mater. Inter*, 2017, **9**, 28117-28138.

63. P. S. Kubiak, S. Awhida, C. Hotchen, W. Deng, B. Alston, T. O. McDonald, D. J. Adams and P. J. Cameron, *Chem. Comm*, 2015, **51**, 10427-10430.

64. J. Groll, T. Boland, T. Blunk, J. A. Burdick, D.-W. Cho, P. D. Dalton, B. Derby, G. Forgacs, Q. Li, V. A. Mironov, L. Moroni, M. Nakamura, W. Shu, S. Takeuchi, G. Vozzi, T. B. F. Woodfield, T. Xu, J. J. Yoo and J. Malda, *Biofabrication*, 2016, **8**, 013001.

65. M. Lei, X. Qu, H. Liu, Y. Liu, S. Wang, S. Wu, W. E. Bentley, G. F. Payne and C. Liu, *Adv. Funct. Mater*, 2019, **29**, 1900065.

66. J. Gong, T. Liu, D. Song, X. Zhang and L. Zhang, *Electrochem. Commun*, 2009, **11**, 1873-1876.

67. W. Suginta, P. Khunkaewla and A. Schulte, *Chem. Rev*, 2013, **113**, 5458-5479.

68. P. Qi, Y. Wan and D. Zhang, *Biosens. Bioelectron*, 2013, **39**, 282-288.

69. T. Ahuja, I. A. Mir, D. Kumar and Rajesh, *Biomaterials*, 2007, **28**, 791-805.

70. J. F. Betz, Y. Cheng, C.-Y. Tsao, A. Zargar, H.-C. Wu, X. Luo, G. F. Payne, W. E. Bentley and G. W. Rubloff, *Lab Chip*, 2013, **13**, 1854-1858.

71. C.-M. Xie, X. Lu, K.-F. Wang, F.-Z. Meng, O. Jiang, H.-P. Zhang, W. Zhi and L.-M. Fang, *ACS Appl. Mater. Inter*, 2014, **6**, 8580-8589.

72. M. B. Thomas, N. Metoki, D. Mandler and N. Eliaz, *Electrochim. Acta*, 2016, **222**, 355-360.

73. O. Geuli, N. Metoki, N. Eliaz and D. Mandler, *Adv. Funct. Mater*, 2016, **26**, 8003-8010.

74. Q. Chen, U. P. de Larraya, N. Garmendia, M. Lasheras-Zubiate, L. Cordero-Arias, S. Virtanen and A. R. Boccaccini, *Colloids Surface B*, 2014, **118**, 41-48.

75. K. D. Patel, R. K. Singh, E.-J. Lee, C.-M. Han, J.-E. Won, J. C. Knowles and H.-W. Kim, *Surf Coat. Tech*, 2014, **242**, 232-236.

76. L.-Q. Wu, A. P. Gadre, H. Yi, M. J. Kastantin, G. W. Rubloff, W. E. Bentley, G. F. Payne and R. Ghodssi, *Langmuir*, 2002, **18**, 8620-8625.

77. J. Thiele, Y. Ma, S. M. C. Bruekers, S. Ma and W. T. S. Huck, *Adv. Mater*, 2014, **26**, 125-148.

78. K. Yan, Y. Xiong, S. Wu, W. E. Bentley, H. Deng, Y. Du, G. F. Payne and X.-W. Shi, *ACS Appl. Mater. Inter*, 2016, **8**, 19780-19786.

79. V. Lakshminarayanan, L. Poltorak, D. Bosma, E. J. R. Sudhölter, J. H. van Esch and E. Mendes, *Chem. Comm*, 2019, **55**, 9092-9095.

80. K. Gwon, M. Kim and G. Tae, *Int. J. Inter. Biol*, 2014, **6**, 596-602.

81. S.-H. Huang, L.-S. Wei, H.-T. Chu and Y.-L. Jiang, *Sensors*, 2013, **13**, 10711-10724.

82. K. Yan, Y. Liu, J. Zhang, S. O. Correa, W. Shang, C.-C. Tsai, W. E. Bentley, J. Shen, G. Scarcelli, C. B. Raub, X.-W. Shi and G. F. Payne, *Biomacromolecules*, 2018, **19**, 364-373.

83. Y. Wang, Y. Liu, Y. Cheng, E. Kim, G. W. Rubloff, W. E. Bentley and G. F. Payne, *Adv. Mater*, 2011, **23**, 5817-5821.

84. G. G. Leisk, T. J. Lo, T. Yucel, Q. Lu and D. L. Kaplan, *Adv. Mater*, 2010, **22**, 711-715.

85. Y. Liu, E. Kim, R. V. Ulijn, W. E. Bentley and G. F. Payne, *Adv. Funct. Mater*, 2011, **21**, 1575-1580.

86. J. Li, D. Maniar, X. Qu, H. Liu, C.-Y. Tsao, E. Kim, W. E. Bentley, C. Liu and G. F. Payne, *Biomacromolecules*, 2019, **20**, 969-978.

87. G. R. Weiss, *Gels*, 2018, **4**, 1-27.

88. L. L. E. Mears, E. R. Draper, A. M. Castilla, H. Su, Zhuola, B. Dietrich, M. C. Nolan, G. N. Smith, J. Doutch, S. Rogers, R. Akhtar, H. Cui and D. J. Adams, *Biomacromolecules*, 2017, **18**, 3531-3540.

89. E. R. Cross and D. J. Adams, *Soft Matter*, 2019, **15**, 1522-1528.

90. E. R. Cross, S. Sproules, R. Schweins, E. R. Draper and D. J. Adams, *J. Am. Chem. Soc*, 2018, **140**, 8667-8670.

91. C. A. Schneider, W. S. Rasband, and K. W Eliceiri, *Nat. Methods*, 2012, **9**, 671-675

92. M. Wallace, J. A. Iggo and D. J. Adams, *Soft Matter*, 2015, **11**, 7739-7747.

93. M. Wallace, J. A. Iggo and D. J. Adams, *Soft Matter*, 2017, **13**, 1716-1727.

94. M. Wallace, D. J. Adams and J. A. Iggo, *Anal. Chem*, 2018, **6**, 4160–4166

95. M. P. Foster, C. A. McElroy and C. D. Amero, *Biochemistry*, 2007, **46**, 331-340.

96. E. R. Draper, J. R. Lee, M. Wallace, F. Jackel, A. J. Cowan and D. J. Adams, *Chem. Sci*, 2016, **7**, 6499-6505.

97. E. R. Draper, T. O. McDonald and D. J. Adams, *Chem. Comm*, 2015, **51**, 6595-6597.

98. A. Leal-Egaña, U.-D. Braumann, A. Díaz-Cuenca, M. Nowicki and A. Bader, *J. of Nanobiotechnology*, 2011, **9**, 24.

99. R. V. Rughani, D. A. Salick, M. S. Lamm, T. Yucel, D. J. Pochan and J. P. Schneider, *Biomacromolecules*, 2009, **10**, 1295-1304.

100. A. D. Martin, J. P. Wojciechowski, A. B. Robinson, C. Heu, C. J. Garvey, J. Ratcliffe, L. J. Waddington, J. Gardiner and P. Thordarson, *Sci. Rep*, 2017, **7**, 43947.

101. A. Dawn and H. Kumari, *Chem. Eur*, 2018, **24**, 762-776.

102. F. Han, C. Zhu, Q. Guo, H. Yang and B. Li, *J. Mater. Chem. B*, 2016, **4**, 9-26.

103. K. S. Anseth, C. N. Bowman and L. Brannon-Peppas, *Biomaterials*, 1996, **17**, 1647-1657.

CHAPTER 2

Electrochemical gel analysis

2.1 Introduction

The surface chemistry of self-assembled hydrogel fibres - their charge, hydrophobicity and ion-binding dynamics - is recognised to play an important role in determining how the gels develop as well as their suitability for different applications.[1, 2] However, to date, advances to establish methodologies for the study of this surface chemistry are limited.[1] Here, we demonstrate how electrochemical techniques can be used to measure these surface chemical properties of the fibres and also determine their pK_a. Furthermore, we provide a new method which predicts whether a gelator will form an aggregate of either gel or crystal form. In this chapter, we will describe in more detail the methods of pK_a determination and highlight the trends observed for single and multicomponent hydrogels, as well as distinguishing molecules that do not gel by pH method.

Development of hydrogel materials is slowed down by the inability to fully understand and control the self-assembly process.[1, 3] As the decrease in pH can be controlled, we can observe the system before and after reaching the pK_a. The pK_a of each gelator is independent,[4] so as a result of increasing complexity in our systems identifying the pK_a of each gelator accurately is crucial.[5] For instance, we have previously shown in addition to the formation of single component networks, methods where we can control the formation of one network over another by using gelators with different apparent pK_a values (Figure **2.1**).[6] The networks can be further affected by adjusting the concentration of glucono-δ-lactone (GdL) added to a multicomponent gelator solution. This is because as the pH lowers past the pK_a of the first gelator, its self-assembly is triggered. Only after the pK_a of the second gelator is reached, self-assembly of the second gelator can occur. For both single and multicomponent gelator systems, the apparent pK_a is therefore clearly important, with the pH at which the gels are formed being related to the apparent pK_a.[7-10] We then question whether there would be any differences in the final properties of the hydrogel if the gelator with the lower pK_a forms either after or during the other gelator forms a network? Would this differ if we altered the length of time spent between the two pK_a values? It is therefore imperative to identify the correct pK_a value in these systems, these hypothetical questions will hopefully be answered as the field progresses.

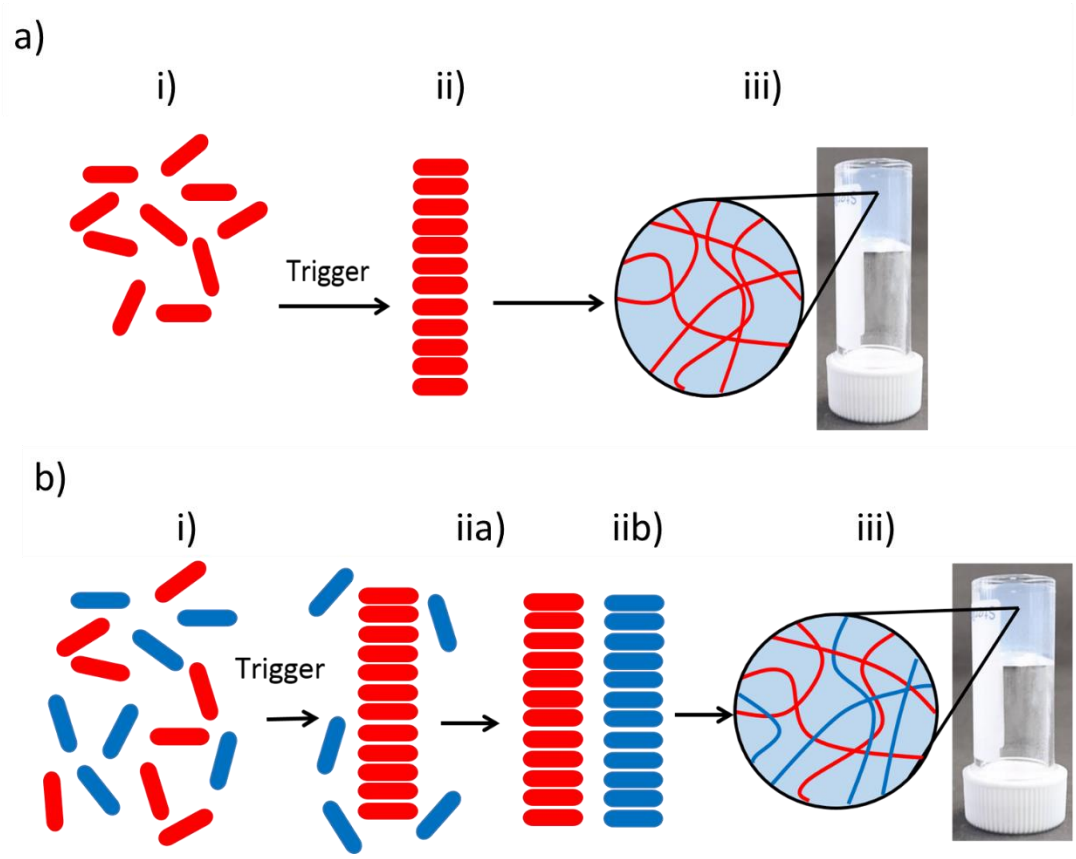

Figure 2.1 Schematic diagram showing the evolution of self-assembly as pH is lowered for a) single component system: i) gelators are free in solution, ii) a trigger is applied that causes the gelator molecules to self-assemble into one-dimensional fibres, iii) the fibres entangle and immobilise the solvent to give a gel. b) A multicomponent system: i) both gelators (blue and red) are initially free in solution, iia) a trigger is applied that causes one gelator to self-assemble into one-dimensional fibres, iib) the second gelator is triggered to self-assemble into one-dimensional fibres, iii) the fibres entangle and immobilise the solvent which results in a hydrogel.

Adding mineral acids can often result in systems that are strongly affected by kinetics, leading to issues with mixing.[11, 12] To get around this, Adams et al. developed methods to allow homogeneous gels to be formed. [21] One such method is to lower the pH by the addition of GdL (Figure **1.5**).[11, 12] GdL slowly hydrolyses to gluconic acid, which lowers the pH of the system without the need for stirring.[11] GdL produces gels which tend to have homogenous properties.[11]

2.1.1 Measuring pK_a

The gel properties are determined by the fibre network, and this is affected by the degree of charge on the fibres.[1, 2] However, there are limited methods available to readily determine the apparent pK_a and to probe the assembly process.[5] Methods to characterise the fibre interactions during self-assembly are also limited.[1] The charge, hydrophobicity and ion-binding dynamics of the gelators and fibres play an important role in self-assembly which ultimately determines the suitability of the gels for specific applications.[1]

For gelators with one pK_a value, the pK_a is defined as the pH value when 50% of the gelator molecules in aqueous solution exist in a protonated form and the other half are de-protonated. If there are gelators that form different aggregates, a multicomponent system or gelators with two pK_a values, then the explanation is not as simple. We are unable to accurately define whether 50 % of the gelator is protonated or not. Since Henderson, Hasselbalch and Sorenson's initial concept of a pK_a value at the turn of the 20th Century,[13, 14] many methods of pK_a determination have been developed (Figure **2.2**).[15] Some of these methods were of particular interest when the hydrogel field expanded at the turn of the 21st Century.[3]

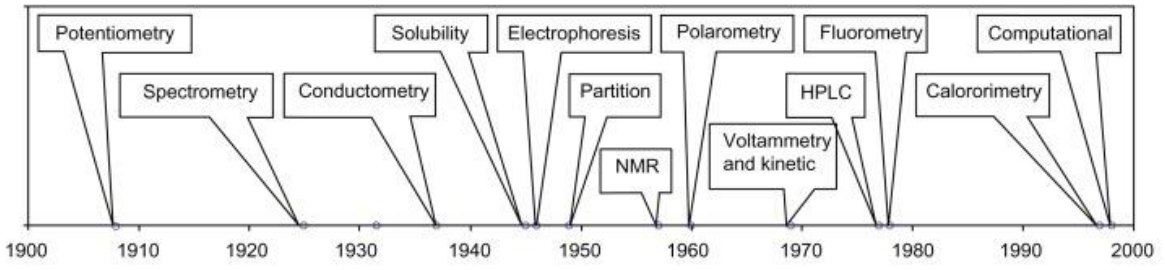

Figure 2.2 Timeline of the first notion of the various techniques to determine pK_a (dissociation constant, acid strength).[15]

2.1.1.1 Nuclear magnetic resonance (NMR)

In 1957, the use of NMR to determine pK_a was developed.[14] Grunwald et al. used ^{1}H NMR to determine the pK_a of mono-, di- and trimethyl-amine, hence determining the chemical shift of the triplet from the protons in the CH_3 groups as a function of pH.[16] A linear correlation was found between the chemical shift and the acid-base ratio, then a sigmoid curve was obtained from which the pK_a

was calculated.[17] Although solution state NMR spectroscopy is commonly used to measure the formation of a hydrogel, for this pK_a method to be useful the molecule must be detectable by NMR spectroscopy. This only occurs when the molecule has an atom with a $\frac{1}{2}$ spin ($\frac{1}{2}$, $\frac{3}{2}$ etc.), which can be excited and relaxed within the measurement time of the experiment. Larger molecules have longer relaxation times, so when gelator molecules aggregate and form a hydrogel network, the relaxation time is too long therefore not measurable by the spectrometer. Hence, we cannot measure the chemical shift between the acid-base ratio to calculate the pK_a value. In addition, most NMR experiments require deuterated liquid whereas most studies on gels are performed with their protonated analogues. Although the extent to which H-bonding, pH and even Van der Waals forces change in deuterated analogues is expected to be small, it should be kept in mind that protonated and deuterated gels may behave somewhat differently.[1]

Wallace et al. developed a new ^{1}H NMR method which allows the pH gradient in hydrogels to be established.[1, 5] They used $^{23}Na^{+}$, relaxation measurements to study the interaction between $^{23}Na^{+}$, probe molecules and the gelator gel fibre. The interaction of Na^{+} with the negatively charged gel fibres increases the relaxation time. Using a combination of residual quadrupole coupling (RQC) and saturated transfer difference (STD) the relative interaction between the probe and the fibre can be measured as a function of pH. As the pH is decreased, the affinity of the metal ion to the fibre decreases, resulting in less coupling between the fibre and metal ion. Therefore, if RQC is run at the frequency of the probe and then the STD is measured between the fibre before and after RQC, a lower coupling value would be obtained due to a higher relaxation time. At the same time, if RQC is measured between the metal ion and an oppositely charged probe then the resulting STD would show an increase in coupling due to a lower relaxation time. Finally, by plotting the changes in STD versus pH the pH where pK_a occurs can be determined. Wallace et al. further developed this method to determine pK_a, using ^{1}H NMR imaging techniques.[5] Although there is no volume addition, with both of these methods we may observe changes in the homogeneity as the pH change occurs from the top of the NMR tube to the bottom therefore non-uniform. These methods also require expert knowledge in programming the NMR spectrometer therefore cannot, at this moment in time, be universally optimised.

2.1.1.2 Spectrometry

Before the 19th Century, it was known that a change in acidity could change the colour of a substance. With visible light spectrometry it was possible to measure the pK_a of pH indicators.[18] Further developments showed that the presence of a chromophore near the ionisation site of a molecule could be used to observe differences between dissociated and non-dissociated forms of a molecule using UV/Vis spectrometry.[15, 16] By then selecting one of the wavelengths where this difference is observed, and one of the wavelengths where the difference cannot be observed and an absorption versus pH experiment can be conducted. From this a sigmoidal curve of absorption and pH can be calculated and the pK_a measured from the inflection point.[22] This method of pK_a determination is useful for those gelators that have a chromophore and are relatively translucent in solution. However, many gelators are opaque in solution and those that are clear may form turbid gels. Furthermore, some gelators do not have an absorption band in the UV/Vis region. This makes a large proportion of the gelator library unsuitable for spectral analysis techniques such as UV/Vis. Moreover, this also means that spectral analysis techniques can be used for the rest of the library of gelators with a chromophore that are relatively clear in both solution and gel form.

2.1.1.3 Electron-spin paramagnetic resonance (EPR) and fast field cycling relaxometry (FFCR)

Recently, pioneering experimental investigations into the mobility of gelators and solvent at the fibre-solution interface using electron-spin paramagnetic resonance[19, 20] or fast field cycling relaxometry[21] have been reported. However, these techniques require access to specialist equipment and labelling of the gelators, which hinder the uptake of these techniques by the broader research community.[1]

2.1.1.4 Conductometry and potentiometry

Acid dissociation constants can be determined by conductometry, assuming that strong electrolytes are completely dissociated at all concentrations and the weak electrolytes only attain complete dissociation at infinite dilution. The conductivity measured is a sum of all charged species in the system (Equation **2.1**). This makes

it difficult to identify a single molecule's pK_a in a solution where all molecules carry charge.

$$\Lambda = \Sigma \lambda_i$$

Equation 2.1 Conductance Λ, equals the sum of specific conductivity contributions λ, of species i.

Conventional pH probes use potentiometry to measure hydrogen ion activity in solution. To do this, potassium chloride (the solution contained in the pH probe tip) begins ion exchange with hydrogen ions in the sample solution. Charge builds up on the probe tip and the voltage difference between the inside solution and outside surface is measured. Interpolating the voltage difference with the voltages of calibration solutions of known pH, allows determination of the pH.

Previously, for use in gels, hydrochloric acid (HCl) titration methods have been used.[22] Here, volumes of HCl are added to the gelator solution and the pH is recorded simultaneously. Once the pK_a of the gelator is reached, buffering of the pH value is observed. This buffering corresponds to the pK_a. Although this method allows for the precise recording of results, the increase in volume alters the concentration of gelator in solution, to which the pK_a is dependent upon. Additionally, agitating the solution during the gelation process breaks any larger networks which have formed and alters the system to an unknown degree. The disadvantage of concentration increase and agitation can be overcome by measuring pH over time during gelation by GdL hydrolysis.[11] In this instance, the pH probe is placed in gelator solution at high pH, as the solubility decreases the change in pH is recorded. Again, once the pK_a is reached there is a buffering of the pH value. This method is a more accurate representation of the gelation system as it allows for the network to form. However, the slow hydrolysis of GdL buffers the gelator solution over a longer period of time and therefore the precision of pH value obtained decreases. Figure **2.3** show data from the pH probe measurements of pH change during gelation by GdL and acid titration.

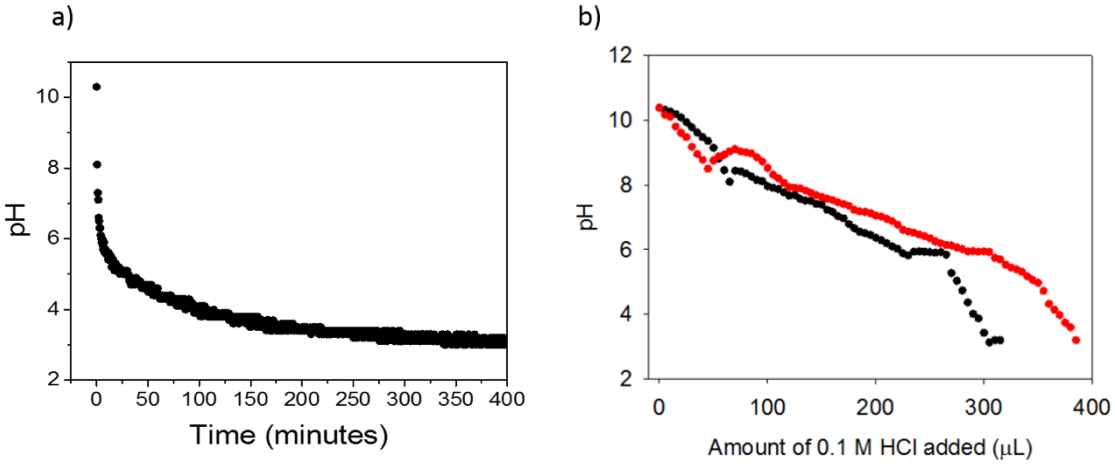

Figure 2.3 pH probe measurement for a gelator by method of a) pH evolution of GdL and b) HCl titration using addition of HCl. From these techniques alone, it is very difficult to determine the pK_a value. b) was taken from Draper et al.[23] open-access in Angewandte Chemie.

There are no methods to determine accurately whether 50% of the gelator is protonated or not without knowing the degree of aggregation. If aggregation occurs, this can result in stabilisation of charge and a pK_a that is higher than expected.[24, 25] Therefore, developing a method that can determine the pK_a of a gelator would significantly benefit the field.

If we want to gain greater control and expand our knowledge on the surface chemistry of our fibres, then we are required to propose a new method to study the surface chemistry that increases the accuracy, precision and efficiency of previous methods. This method would also need to be economically viable and accessible to the wider scientific community.

In this chapter, we show a new electrochemical method to analyse the surface chemistry of hydrogel fibres - their charge, hydrophobicities and ion-binding dynamics. From this, a pK_a determination method has been developed. This method provides improvements to previous methods that can be used in both simple and complex systems. We describe an electrochemical technique that can be used to analyse the interactions between the ions and the aggregated structure of the gelator (ion–fibre) during real-time gelation. The method allows us to determine the apparent pK_a values and follow the evolution of the ion-fibre

interactions as gelation occurs. This method can be applied to single as well as multicomponent systems.

The electrochemically reversible compound $[Ru(NH_3)_6]Cl_3$ (TM, Figure **2.4**) is introduced to the gelator solution at high pH. Based on previous work,[26-28] where the cross-linking or interactions of gelator fibres with cations produced hydrogels at high pH, we rationalised that cross-linking or interactions with the TM should also lead to a degree of immobilisation of the TM at high pH. As pH is decreased to below the pK_a of the gelator, the carboxylic acid will be protonated and the TM will then be free to diffuse through the solution. The electrochemical techniques rely upon this change in binding, shown schematically in Figure **2.5**.

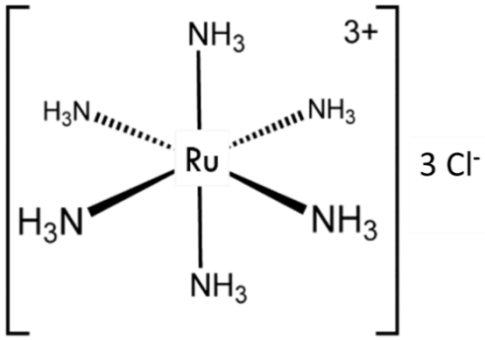

Figure 2.4 Lewis diagram of $[Ru(NH_3)_6]Cl_3$

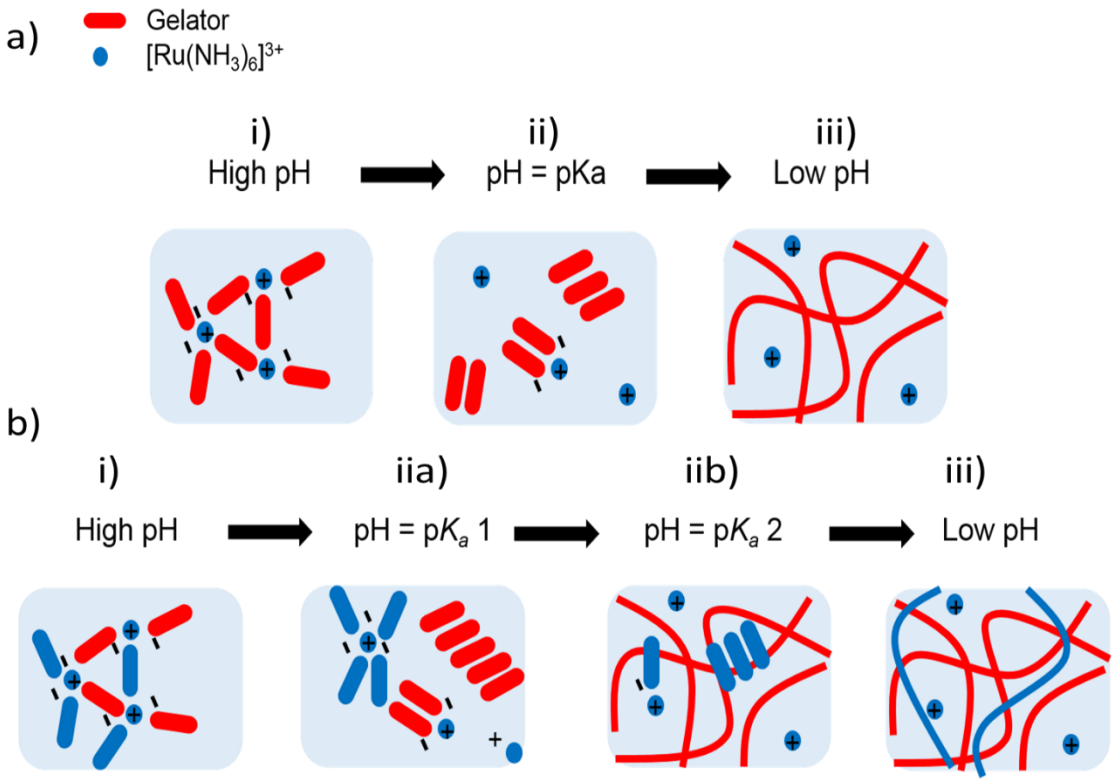

Figure 2.5 Schematic diagram showing the evolution of self-assembly as pH is lowered for: a) single component system i) At high pH, the TM (blue) is immobilised in solution by the crosslinking or interaction with the gelators (red). ii) When the pH equals the pK_a, the TM begins to dissociate from the gelators as they become protonated. iii) At low pH, the TM has fully dissociated from the fibres. The increase in the concentration of the dissociated TM results in an increase in current. b) Multicomponent system. i) At high pH, the TM (blue circles) is immobilised in solution by the crosslinking or interaction with the gelators (red and blue ovals). iia) When the pH equals the pK_a of the red gelator, the TM begins to dissociate from the red gelator as they become protonated. The increase in the concentration of dissociated TM results in a small increase in current. iib) When the pH equals the pK_a of the blue gelator, the TM begins to dissociate from the blue gelator as they become protonated. iii) At low pH the TM has fully dissociated from the fibres. The increase in the concentration of dissociated TM results in an increase in current.

Given the diffusion coefficient of the TM is dependent upon its radius of hydration and the viscosity it experiences through solution *via* the Stokes-Einstein equation Equation **2.2** we should observe an increase in diffusion coefficient when the transition metal becomes free in solution.

$$D = \frac{kT}{6\pi\eta R}$$

Equation 2.2 Stokes-Einstein equation where D is the diffusion coefficient, T is the temperature, ŋ is the viscosity, and R is the radius of hydration.

Using the Randles–Sevcik equation (Equation **2.3**), we can determine the change in diffusion coefficient by measuring the change in peak oxidation current of the TM as a function of pH or time.[29] When the TM is bound to the gelator at high pH, we expect the conductivity will be low due to the increase in the radius of diffusing species around the TM, whereas below the pKa we expect the conductivity of the TM to be higher due to the lower radius of hydration. We assume the free TM will be able to travel freely through the pores of the gel implying that the viscosity will be similar to water. A large increase in conductivity will therefore signify the pK_a value.

$$i_{\mathrm{p}} = 0.4463nFAC\left(\frac{nFvD}{RT}\right)^{\frac{1}{2}}$$

Equation 2.3 Randles-Sevcik equation where i_p is the peak oxidation or reduction current, n is the number of electrons transferred, F is Faraday's constant, A is the area of electrode, C is the concentration of TM, v is the scan rate, R is Rybergs constant, T is the temperature and finally D is the diffusion coefficient.

2.2 Experimental

2.2.1 Materials

All chemicals were purchased from Sigma-Aldrich. Milli-Q water was used throughout. The gelator molecules shown in Figure **2.6** were synthesised by Prof. Dave Adams and Dr. Bart Dietrich (University of Glasgow) depending on the batch, using previously established methods.[2, 25, 26, 30] All gelators contain an aromatic group, with either one or two amino acids on the periphery. These gelators were chosen based on their ability to either form gels or not.[4] A range of amino acid and aromatic groups were used to show the method could be applicable to a variety of hydrogels.

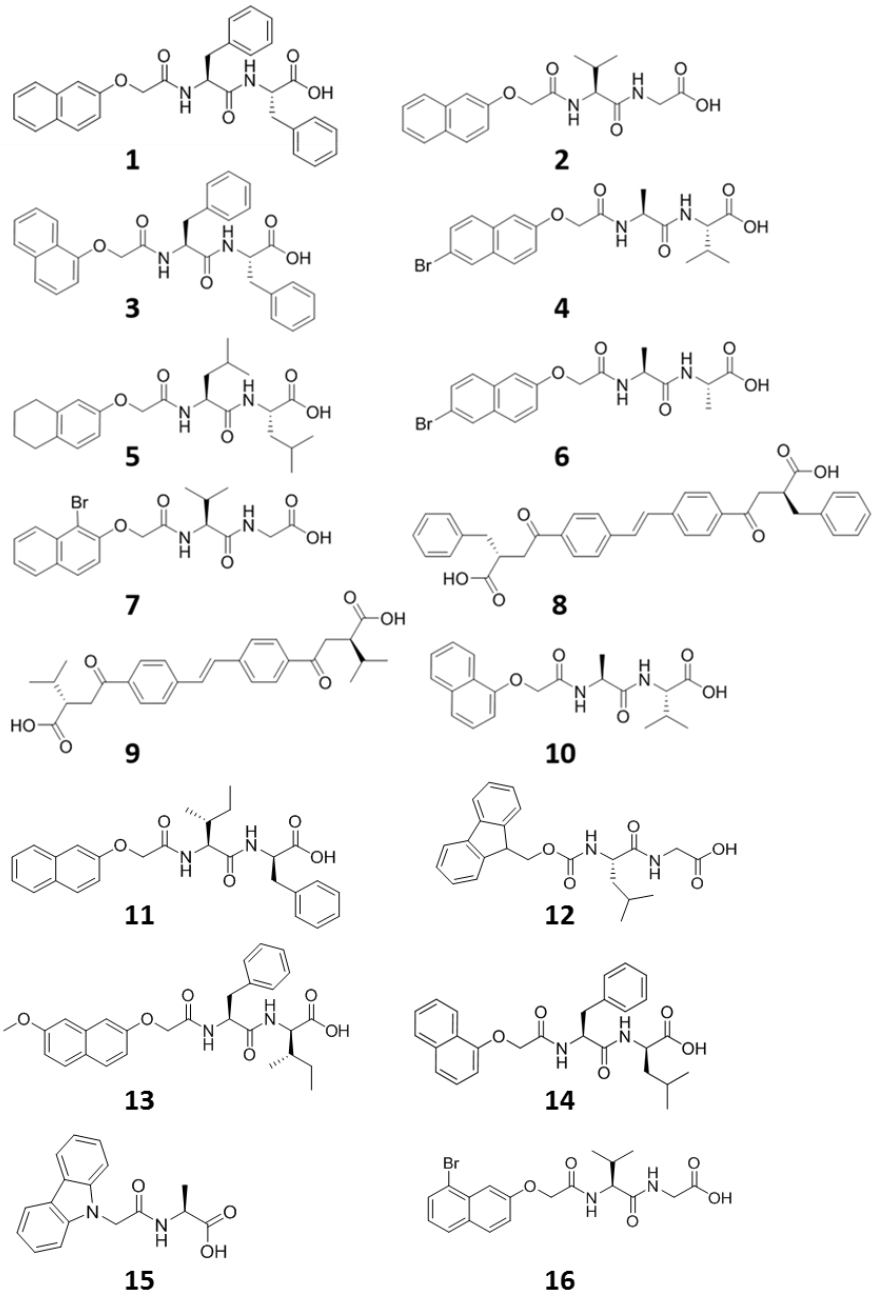

Figure 2.6 Chemical structures for gelators **1**-**16**.

HCl and GdL are used to lower the pH of the system. All gelator solutions are prepared using H_2O and NaOH (0.1 M aq). The redox-active transition metal complex used was TM. This TM was used due to it forming a cation that is electrochemically reversible in aqueous solution.[31] The metal complex is also widely used in electrochemistry and there are many publications citing the correct diffusion coefficient values.[32, 33]

2.2.2 Preparation of gelator solutions 1- 10

Each single component solution was prepared by weighing out 50 mg of gelator into 14 mL vials then adding deionised H_2O and NaOH (aq. 0.1 M, one molar equivalent for **1**-**6** and **8**-**10** and 2 molar equivalents for **7**) to a volume of 10 mL. The solution was stirred overnight to ensure all gelator had dissolved to provide solutions at a final concentration of each gelator of 5 mg/mL. For the multicomponent solution, single component solutions were prepared as above at a concentration of 10 mg/mL. The two single component solutions were then mixed in a ratio of 1:1 to provide a solution in which the concentration of each component were 5 mg/mL (so total gelator concentration of 10 mg/mL). All solutions were stored at room temperature.

2.2.3 Preparation of gelator solutions for electrochemical analysis

For each single component systems, 2 mL of the gelator solution were transferred using a pipette to a Sterilin vial containing 3.1 mg of TM (5 mM). The gelator solution was then transferred, by pouring, into a Sterilin vial containing 10 mg of GdL (5 mg/mL). Immediately after, a modified Sterilin vial lid containing three electrodes (glassy carbon working electrode, Ag/AgCl (3 M) reference, Pt wire counter) were added as shown in Figure **2.7**. Then, the electrochemical experiment was run as described in Sections 2.2.5 - 2.2.8. For the multicomponent systems, 1 mL of each gelator solution at a concentration of 10 mg/mL were mixed together (so the total gelator concentration of each component were 5 mg/mL). 2 mL of this gelator solution were transferred to a Sterilin vial containing 6.2 mg of TM (10 mM). The solution was poured into 20 mg of GdL (10 mg/mL) and the electrochemical experiments carried out.

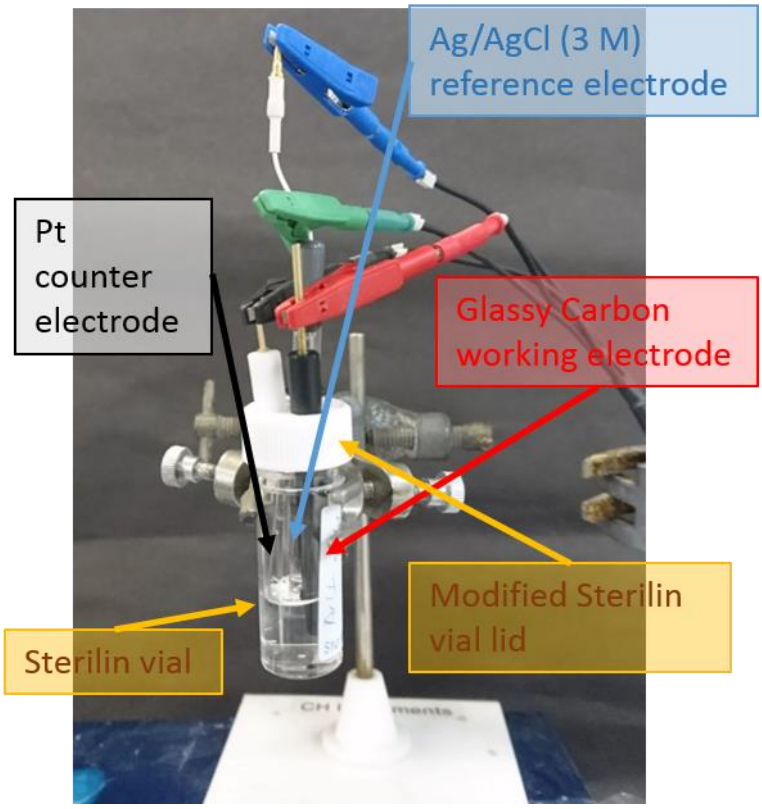

Figure 2.7 Image showing the electrochemical set up used here.

2.2.4 pH measurements

pH measurements were recorded using a Hannah PC turtle FC500 pH probe with a given error of ±0.1. For measuring the pH of gelation over time, 2 mL of gelator solution at pH 10 was added to GdL (5 mg/mL for single component and 10 mg/mL for multicomponent) in a 7 mL Sterilin vial. The pH measurements were recorded with an interval of 0.5 minutes over a period of 16 hours.

2.2.5 Cyclic voltammetry

The electrochemical set up as described in Section 2.2.3 was used to carry out cyclic voltammetry. Cyclic voltammetry measurements were carried out within a potential range of -0.5 to 0.2 V vs. an Ag/AgCl (3 M) ref. at a scan rate of 20, 40, 60, 80, 100, 200, 400, 600, 800, 1000 mV/s. Each CV measurement consisted of one scan. The diffusion coefficient was determined using the reduction current peak and the Randles-Sevcik equation (Equation **2.3**).

2.2.6 Cyclic voltammetry over time

Cyclic voltammograms were measured as described in Section 2.2.5 consecutively for 16 hours (Figure **2.8**). The peak reduction current was then converted to diffusion coefficient using the Randles-Sevcik equation (Equation **2.3**).

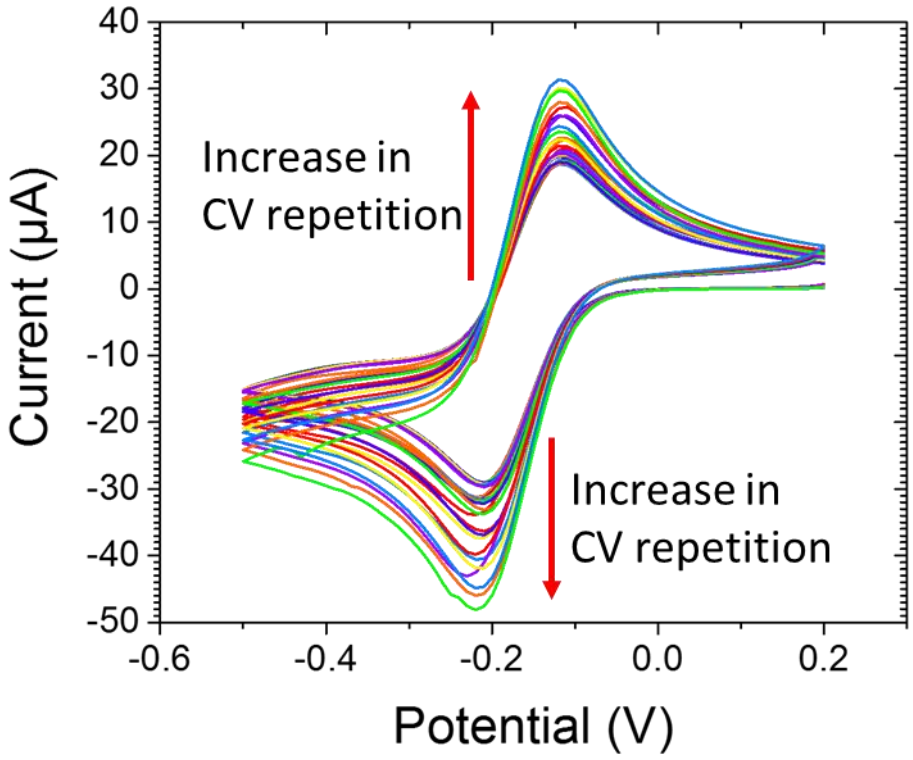

Figure 2.8 Example data for TM in the presence of **1** and GDL during gelation showing 20 continuous CVs at 0.2 V/s The increase in CV repetition number is shown by the red arrows. From these graphs the peak reduction current is measured as a function of time.

2.2.7 Gel or crystal determination

Cyclic voltammetry as described in Section 2.2.5 was used to measure the peak current of the TM at pH 9.5 and pH 4.5 (Figure **2.9**). The difference between the reduction current peak of 9.5 and 4.5 was calculated. This value indicated whether a crystal or gel formed as discussed in Section 2.3.2.

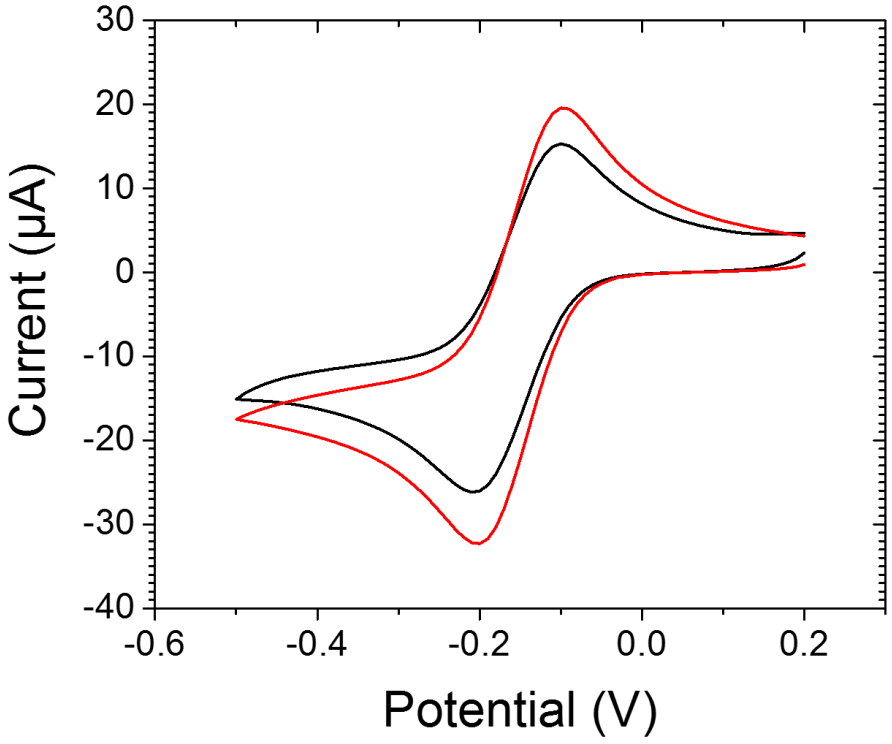

Figure 2.9 CVs of **1** at pH 9.5 (black) and at pH 4.5 (red).

2.2.8 Multiple pulse amperometry (MPA)

The same electrochemical set up was used for MPA as described in Section 2.2.3. MPA measurement were carried out at potentials of -0.12 and -0.20 V for 1 s each. This was continuously repeated for 16 hours.

2.2.9 Rheological measurements

Rheological measurements were carried out using an Anton Paar Physical MCR301 rheometer. Time sweeps were performed using 50 mm diameter parallel plates with an angular frequency of 10 rad/s with a strain of 0.5 %. For measuring the time sweep 2 mL of gelator and TM solution as described in Section 2.2.2 was poured onto the bottom parallel plate. Mineral oil was added to the edges of the parallel plate to prevent drying of the sample. A time delay of 15 seconds was maintained from addition of GdL to sample acquisition. The time sweeps were recorded over 16 hours.

For correlating electrochemistry and rheology in Section 2.3.3, gels were prepared by adding 8 mg/mL of GdL to a 2 mL gelator sample in a Sterilin vial. The gels were left for 16 hours before measuring. Frequency scans were performed from 1 rad/s to 100 rad/s under a constant strain of 0.5 %.

2.3 Results and discussion

2.3.1 Electrochemical reversibility of $[Ru(NH_3)_6]Cl_3$ (TM)

In order for the TM to be used in the pK_a studies, it is essential that the TM is electrochemically reversible in solution regardless of pH. These control studies would ensure that when determining the pK_a of a gelator any deviation from the control peak currents would be due to the presence of gelator and not the pH of the solution. Cyclic voltammetry was used to determine the electrochemical reversibility of the TM in control solutions with varying pH. Using scan rates between 0.02 and 1 V/s against an Ag/AgCl (3 M) reference electrode (see Section 2.2.5 for full experimental), the oxidation and reduction peak currents were obtained (Figure **2.10**). To determine electrochemical reversibility the peak currents were plotted against the square root of scan rate which revealed a linear regression R^2 value of 1.000 for all data. In addition, the potential at which the peak current occurred was independent of scan rate, we could therefore conclude that the TM was electrochemically reversible and pH independent.

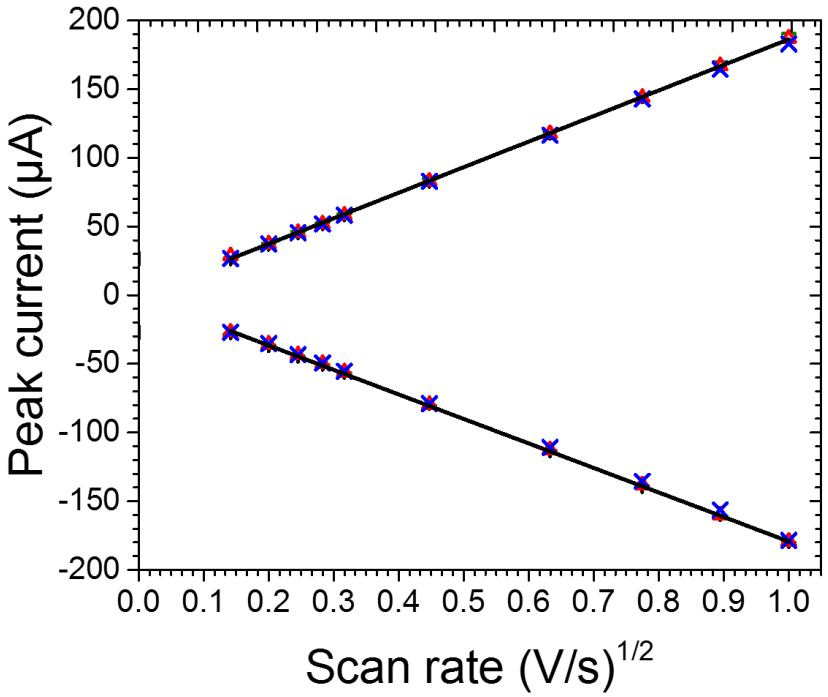

Figure 2.10 Randles-Sevcik analysis of the peak current vs scan rate$^{0.5}$ of TM in KCl (1 M) at pH: 3.0 (blue), 4.0 (red), 6.0 (black), 8.0 (green).

Next, the electrochemical reversibility of the TM in a viscous gelator solution was measured as the pH was lowered. We observed at scan rates below 0.08 V/s the peak current versus the square root of scan rate was linear (dashed line in Figure **2.11**). After this value, the peak current versus the square root of the scan rate was non-linear therefore the TM was not electrochemically reversible. This implies that at higher scan rates the concentration of TM diffusing to the electrode surface was limited and did not maintain the concentration required by the Nernst equation, due to the increase in radius of hydration and viscosity of the solution. For solutions at pH 7 and 9, which were above the pK_a value of the gelator we observed the same peak oxidation and reduction current values at each scan rate. Whereas, for solutions at pH 3 and 5, the peak oxidation and reduction values were not similar. This was the first indication that we could observe changes in ion-fibre surface chemistry above and below the pK_a of the gelator. Furthermore, these data suggest that the scan rate needs to be below 0.08 V/s for an electrochemically reversible system when running for cyclic voltammetry and MPA.

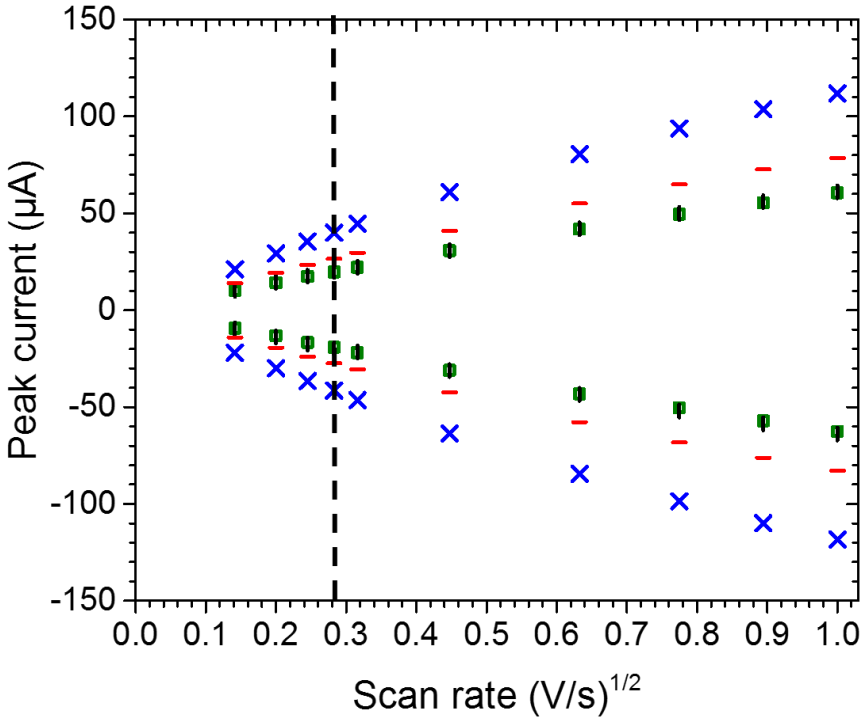

Figure 2.11 A Randles-Sevcik plot of the peak current vs scan rate$^{0.5}$ of TM in **1** at pH: 3.0 (blue), 5.0 (red), 7.0 (black), 9.0 (green).

During the electrochemical reversibility tests, it was observed that the oxidised TM turns deep purple over time. In water alone, the TM stains the inside of the vial and remains in solution whereas, when there is gelator present the TM separates from the water and does not stain the inside of the vial (Figure **2.12**). This alone suggests a useful application for this gelator, as a method to water purification or pollutant removal. Hydrogels are being developed by Smith et al. for removal of unwanted pollutants including: dyes, toxic anions, chemical weapons and the immobilisation of oil spills.[34] A similar phenomenon using gold nanoparticles was observed by Smith et al.[35]

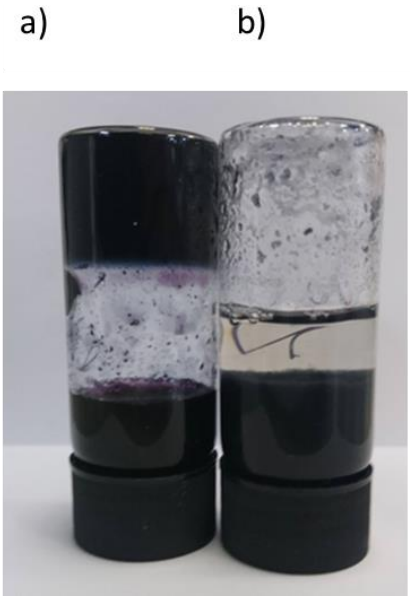

Figure 2.12 An image to show the effect the gelator has in separating the TM from solution b) and the same solution with no gelator a). We can see how the glass in a) is stained with TM whereas in b) the TM is confined in the gelator.

2.3.2 Acid titration

A common method of triggering gelation for dipeptide gelators with a carboxyl group is to use pH.[11, 36] Initially, a solution at high pH is prepared, and then gels are formed by lowering the pH using HCl.[37-39] When adding aliquots of HCl and measuring pH, a plateau around the pK_a value is observed.[25, 40] This conductivity method is commonly used to determine the apparent pK_a of such gelators.[24, 25] However, with this method the volume of gelator solution increases with the addition of acid which can be problematic if the pK_a is dependent upon concentration.[25]

Lowering the pH by additions of HCl aliquots, the TM-gelator interactions were recorded using cyclic voltammetry. The TM was added to the gelator solution at pH 10. After each addition of HCl (0.1 M), the pH was measured and a CV was recorded to observe the peak currents for the TM. When the peak currents are low, this suggests that the TM is bound to the gelators, due to the increase in apparent radius of the TM. For this family of gelator, typically worm-like micelles or diffuse aggregates are formed at high pH, which are stabilised by the de-protonated carboxylic acid.[26] Either kind of structure should be able to bind to the positively-charged TM. When the current peaks are high, we suggest the concentration of free TM in solution is high due to the apparent decrease in radius of the TM, resulting in a high diffusion coefficient. This implies that more gelator molecules are protonated and not binding to the TM.

The diffusion coefficient was calculated at different pH values exemplified for molecules **1**-**4** (Figure **2.13** a-d). For the molecules that form gels by this method, after initial additions of HCl, we observe small changes in the diffusion coefficient, as would be expected with a system above the pK_a. For **1** and **4**, there is a slight initial increase in diffusion coefficient as pH decreases, whereas for **2** and **3** there is a slight decrease in diffusion coefficient. This suggests differences in the self-assembly regime but could also be due to subtle changes in the viscosity as the pH is lowered. With subsequent additions of HCl, we observed a rapid linear increase in the diffusion coefficient. This is where we identify the pK_a to be. A similar trend was observed in all gelators measured where the change in gradient of diffusion coefficient and pH was used to determine the pK_a value. We note that the values determined agree well with the values previously measured by a pH titration.[25, 41] A summary of the pK_a values are shown in Table **2.1**.

Not all molecules in this family form gels.[4] When aliquots of HCl were added to a solution of a molecule that does not form a gel (e.g. **5** and **10**), there was again an initial small change in the diffusion coefficient (Figure **2.13** e and f). However, at a critical pH, there was a sharp decrease in diffusion coefficient. This sharp decrease in diffusion coefficient was a result of the gelator molecules forming a visible precipitate which sedimented to the bottom of the vial stopping the TM from diffusing to the electrode surface. We again associate this with the apparent pK_a.

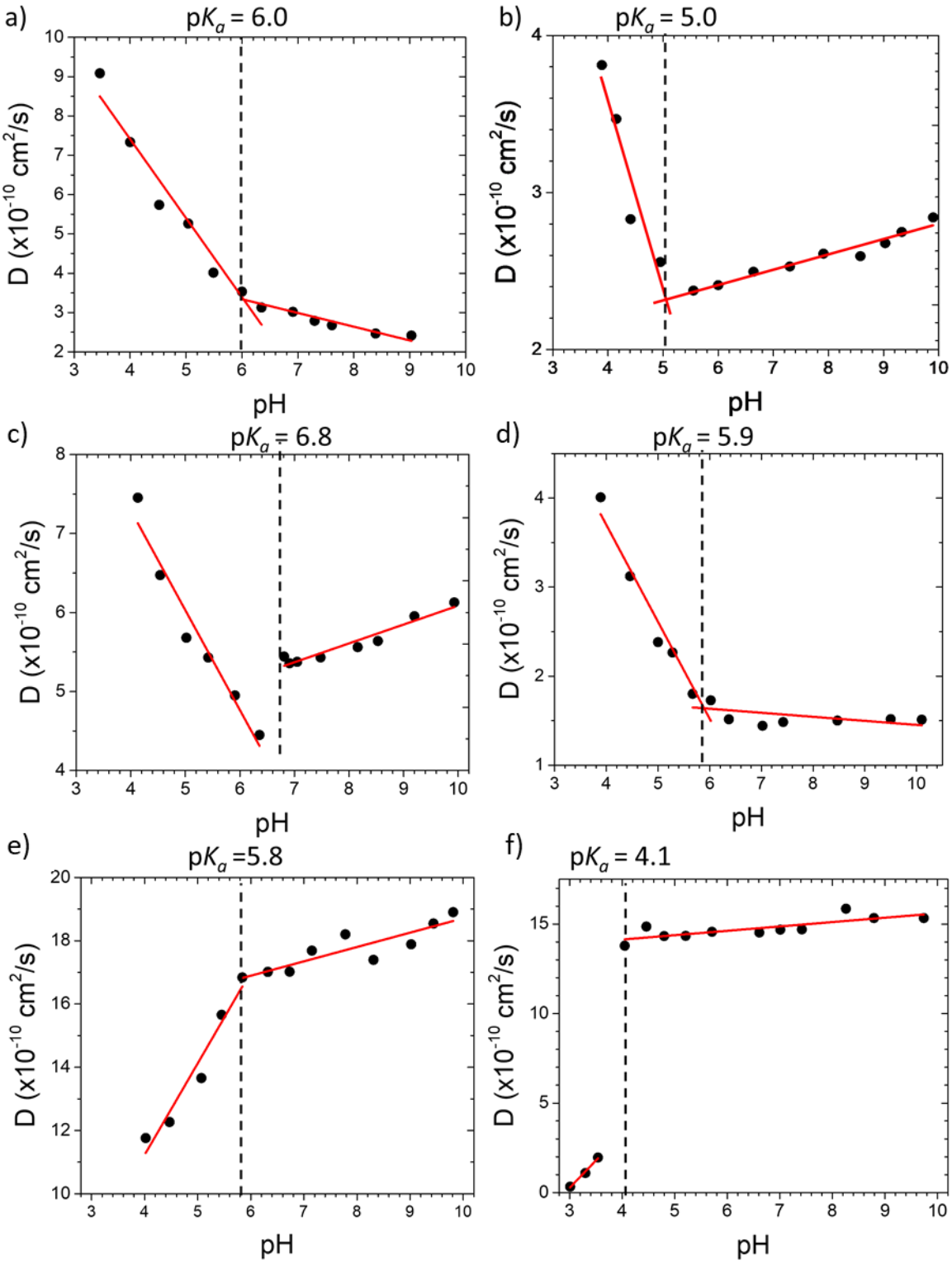

Figure 2.13 Change in the diffusion coefficient of the TM as pH is lowered by the addition of HCl (0.1 M) in a solution (5 mg/mL) of a) **1**, b) **2**, c) **3**, d) **4**. The dashed line represents the apparent pK_a values for these gelators. e) and f) show analogous data for e) **5** and f) **10**, where no gel is formed when the pH is decreased.

Table 2.1 Summary of p*Ka* values for gelator molecules.

Gelator	Literature pK_a value	pH titration pK_a value	Cyclic voltammetry method pK_a value	Multiple pulse amperometry method pK_a value	Gel or no gel
1	6.0[25]	6.0	~6.0	6.0	Gel
2	5.0[25]	5.0	-	5.0	Gel
3	-	6.8	-	-	Gel
4	5.8[25]	5.9	~5.8	-	Gel
5	-	5.8	-	5.7	No gel
6	4.9[25]	-	-	6.0	Gel
10	-	4.1	-	-	No gel
2 + **8** (in a multicomponent system)	5.8*[8] (**8**) & 5.0[25] (**2**)	-	-	6.6 (**8**) & 5.0 (**2**)	Gel

*Literature value states the gelator solution at 10 mg/mL.

By measuring the difference between the peak current at pH 9.5 and at pH 4.5, we can therefore use this method to screen whether a molecule has the potential to be an effective pH-triggered gelator or not (Figure **2.14**). A positive delta current value represents a molecule capable of forming a gel whereas, a negative value suggests precipitation. Whilst for some systems, this is no more effective than simply testing gelation by adding acid and inverting the vial, we highlight that pH-triggered gelation is highly dependent on the method of acid addition.[11, 42] Hence, this method can be used to show whether a gel *could* form or not, whilst a simple addition of acid to quickly lower the pH can sometimes result in samples where it is difficult to unambiguously demonstrate that a gel has formed.[4] Our method also has the potential to be used on small volumes, where again unambiguously assigning gelation is difficult. We envisage that this method could be installed as part of a high throughput screen.

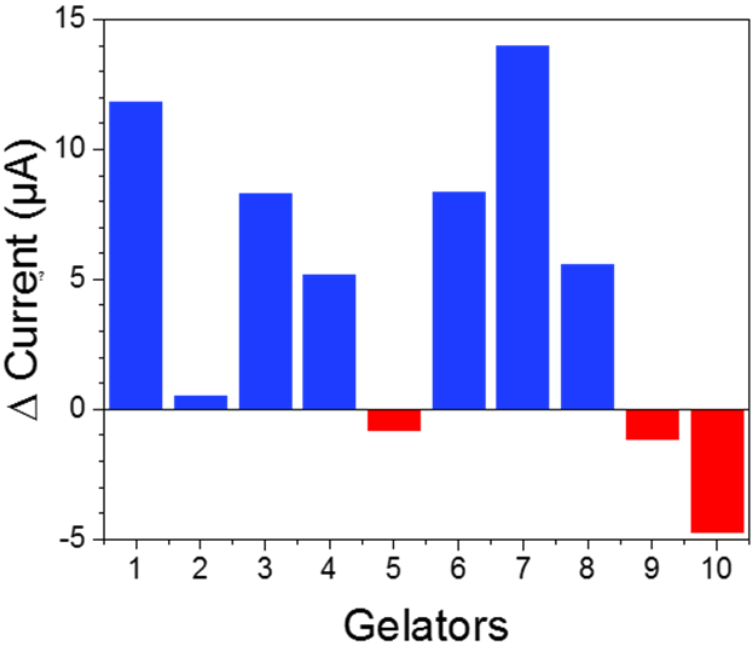

Figure 2.14 The change in current between pH 9.5 and 4.5 for the TM in solutions of gelators **1**-**10**. Gelators that form a gel are shown in blue and those that form precipitates are shown in red. The gelation ability was checked independently of the ΔCurrent measurements.

2.3.3 Correlating electrochemistry and rheology

The HCl titration and rheology methods described in Section 2.3.2 were used to determine whether there were any trends between the ability of a gelator to bind to a transition metal complex during self-assembly and its gel stiffness. Previous work has shown that the ion-binding dynamics and charge on the fibres that form gels play an important role in determining the gel properties.[1,2] Being able to predict the relative stiffness of gelator molecules using an electrochemical method on the starting gelator solution would be advantageous economically and environmentally as well as time saving.

Gelator solutions of **2**-**4**, **7**, and **11**-**16** were prepared as previously described,[1] at 8 mg/mL. For rheological measurements, 8 mg/mL of GdL was added to a 2 mL gelator sample and were left for gel for 16 hours before measuring. For electrochemical measurements, TM (3.1 mg/mL) was added to the gelator solution. This solution was placed into a three-electrode electrochemical cell with a glassy carbon working electrode, platinum counter electrode and an Ag/AgCl (3 M) reference electrode. A cyclic voltammogram was measured at pH 9.5 and at

pH 4, HCl ((0.1 M) was added to lower the pH). The difference between the peak oxidation currents of TM at pH 9.5 and 4 were calculated. A strong linear regression of 0.96139 was observed between gel stiffness and change in current. This data strongly implies that the electrostatic properties of the gelator and the ion-binding dynamics of self-assembly determine gel stiffness. The greater change in ion-binding dynamics the stiffer the gel. This method could be used to predict the stiffness of a gel by measuring the difference in current without having to measure the stiffness by conventional rheology methods.

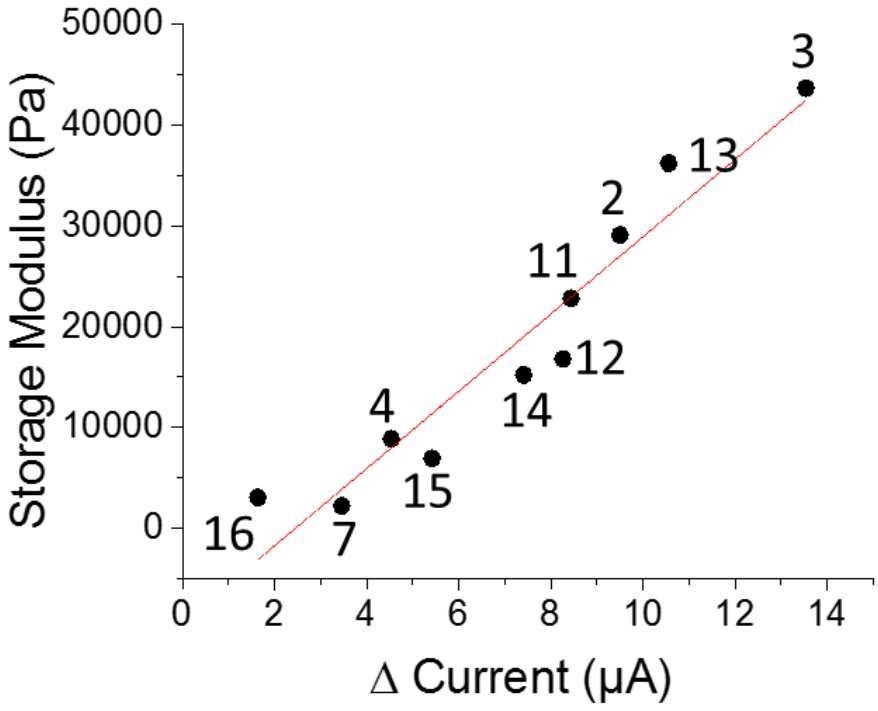

Figure 2.15 Storage modulus at 10 rad/s taken from frequency sweeps of gelators **2**-**4**, **7**, and **11**-**16** versus the difference in current at pH 9.5-4.

2.3.4 GdL hydrolysis cyclic voltammetry

GdL slowly hydrolyses to gluconic acid, which lowers the pH of the system without the need for stirring.[11] Due to this slow hydrolysis, and so the slow self-assembly process, to determine the pK_a we need a method that records data over the period of time and that does not distort the network. After adding GdL to a solution of a gelator, CVs were run over 16 hours with a scan rate of 0.04 V/s vs. an Ag/AgCl (3 M) reference electrode allowing the diffusion coefficient as a function of time to be determined. By measuring the evolution of pH at the same time as the CVs, we

expected to determine the pH when the increase in diffusion coefficient was observed. The results for gelator **1** and **4** are shown in Figure **2.16**. A very slight increase of diffusion coefficient was observed around pH 6.0 for **1** and pH 5.8 for **4**. Although these values correspond to the pK_a values obtained in the pH titration data above, the method itself did not provide data that was easy to interpret. The change in linearity of the diffusion coefficient is more gradual over a larger pH range compared to the sharp change with HCl titration. Therefore, this makes it more difficult to determine the pK_a value and the method not optimal.

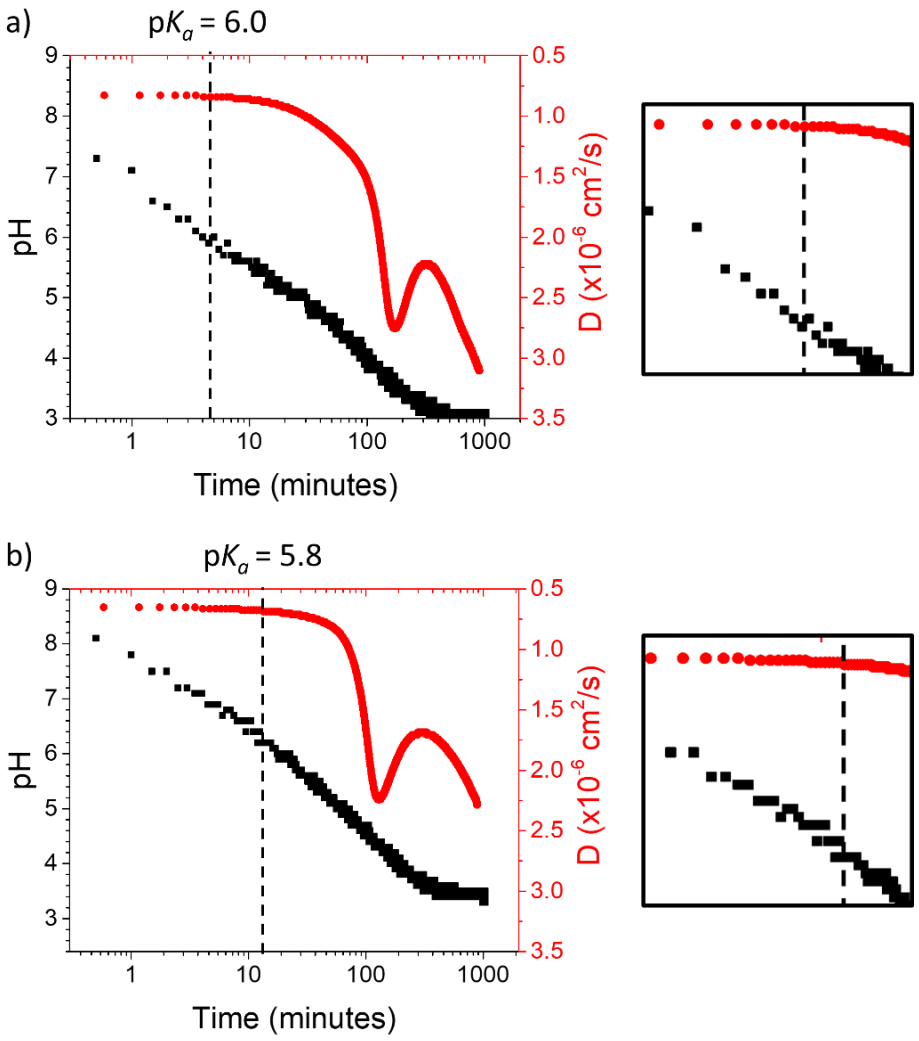

Figure 2.16 Evolution of pH (black squares) and diffusion coefficient from continuous CV (red circles) for a) **1** and b) **4** with time after addition of GdL to a solution at high pH. The dashed line represents the literature pK_a values for these gelators. The enlarged graph regions to the right of the original graph show a zoomed in version of the data around the pK_a value.

2.3.5 Multiple pulse amperometry (MPA)

Due to the difficultly in determining the pK_a from the data using continuous CVs, we moved to using MPA. In MPA, the potential is switched between the reduction and oxidation potential in a binary fashion. The method differs from cyclic voltammetry where the potential is instead swept linearly between two potentials (Figure **2.17**). MPA increased the number of data points that could be collected in unit time twenty-fold. MPA is also easy to set up experimentally and is more time and labour efficient compared to titration methods.

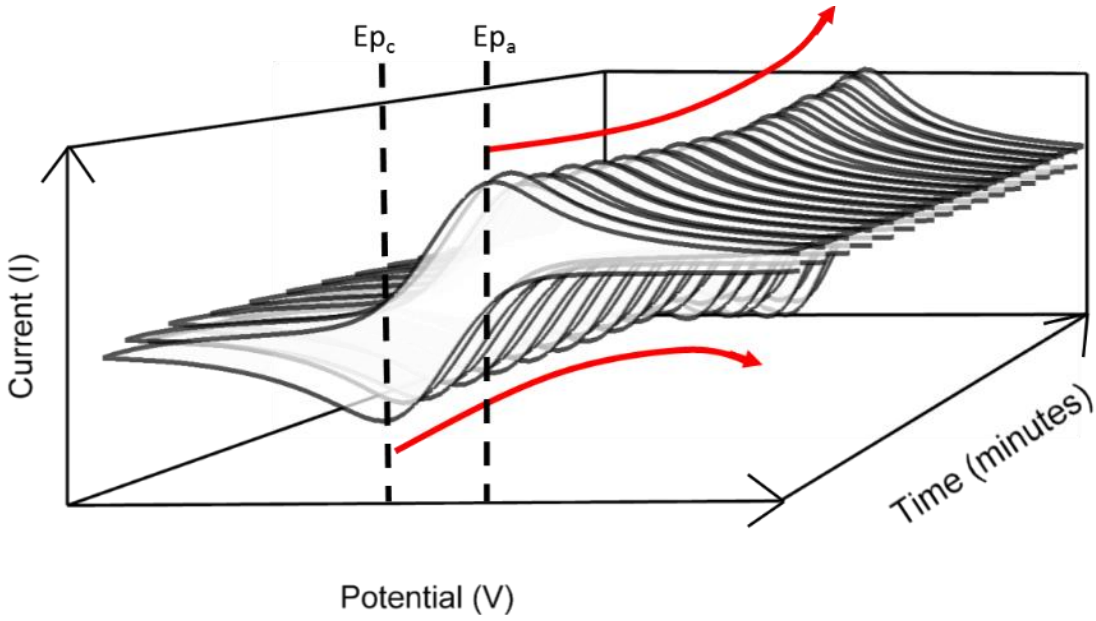

Figure 2.17 Example data to show how the methods of CV and MPA differ. For MPA the current is switched between the two values (Ep_c and Ep_a) in a binary fashion whereas, in CV the current is swept between and past the two values.

MPA was applied to a gelation system with GdL and the pH was measured over time. Figure **2.18** show the MPA and pH evolution for gelators **1** and **2** respectively. The maximum current 'peak' (least negative value) occurs at the pH where we expect pK_a to occur from data in Figure **2.18**. Measuring the rheology concurrently with the pH and current during gelation allows us to correlate between when the pK_a is observed and the onset of gelation. The onset of gelation can be identified as the large increase storage modulus (G′), this increase in G′ can be observed for **1** and **2** in Figure **2.18** a) and b), at the same time point as the current 'peak' (least negative value). We would expect this from our previous work.[25]

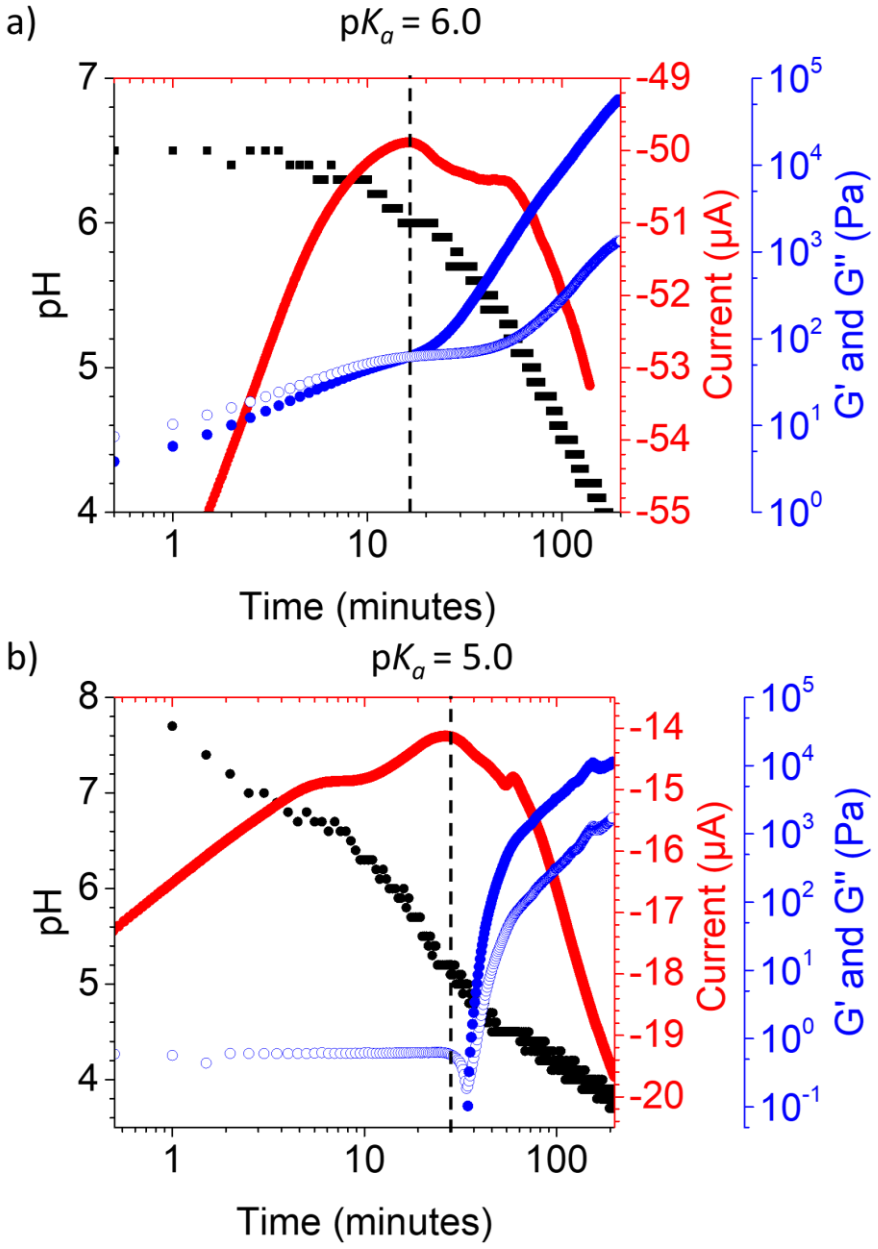

Figure 2.18 Evolution of pH (black squares), current (red circles) and storage (blue full circles) and loss (blue hollow circles) moduli with time on a log scale for a) **1**, b) **2** after addition of GdL. The dashed line represents the pK_a values for these gelators.

The situation for **1** and **2** is straightforward. The MPA method can however be used to understand less straightforward cases. For example, for **6** (Figure **2.19** a), we observe the maximum current 'peak' (least negative value) shown with the dashed line labelled i) at pH 6.0. As the pH buffers around this value there is an increase in G′ at the same pH shortly afterwards, shown with the dashed line labelled ii). This suggests that once the pK_a is reached at i), there is a time delay in the

formation of a network that immobilises water being formed. However, it is important to point out that both the current peak and G′ onset i) and ii), occur at the same pH value. When using this method for a system that does not form a gel, **5**, two peaks in the current were found (Figure **2.19** b, labelled i) and ii)). At points i) (pH 5.7) and ii) (pH 5.0), there appears to be a shift in charge. After peak at point i), the current value becomes more negative suggesting more TM is free in solution. After point (ii), the current value becomes less negative suggesting there is less TM free in solution. Coupling the MPA data with rheological time sweeps, there is an increase in G′ at point i). This suggests the formation of a network that immobilises water. Next, we can see the G′ peaks at point ii), it is at this point the gel is most stiff. Then after point ii), as the current tends to zero, the G′ value decreases. Finally, after second peak the current becomes more negative again, the change in G′ continues to decrease which corresponds to the formation of the precipitate.

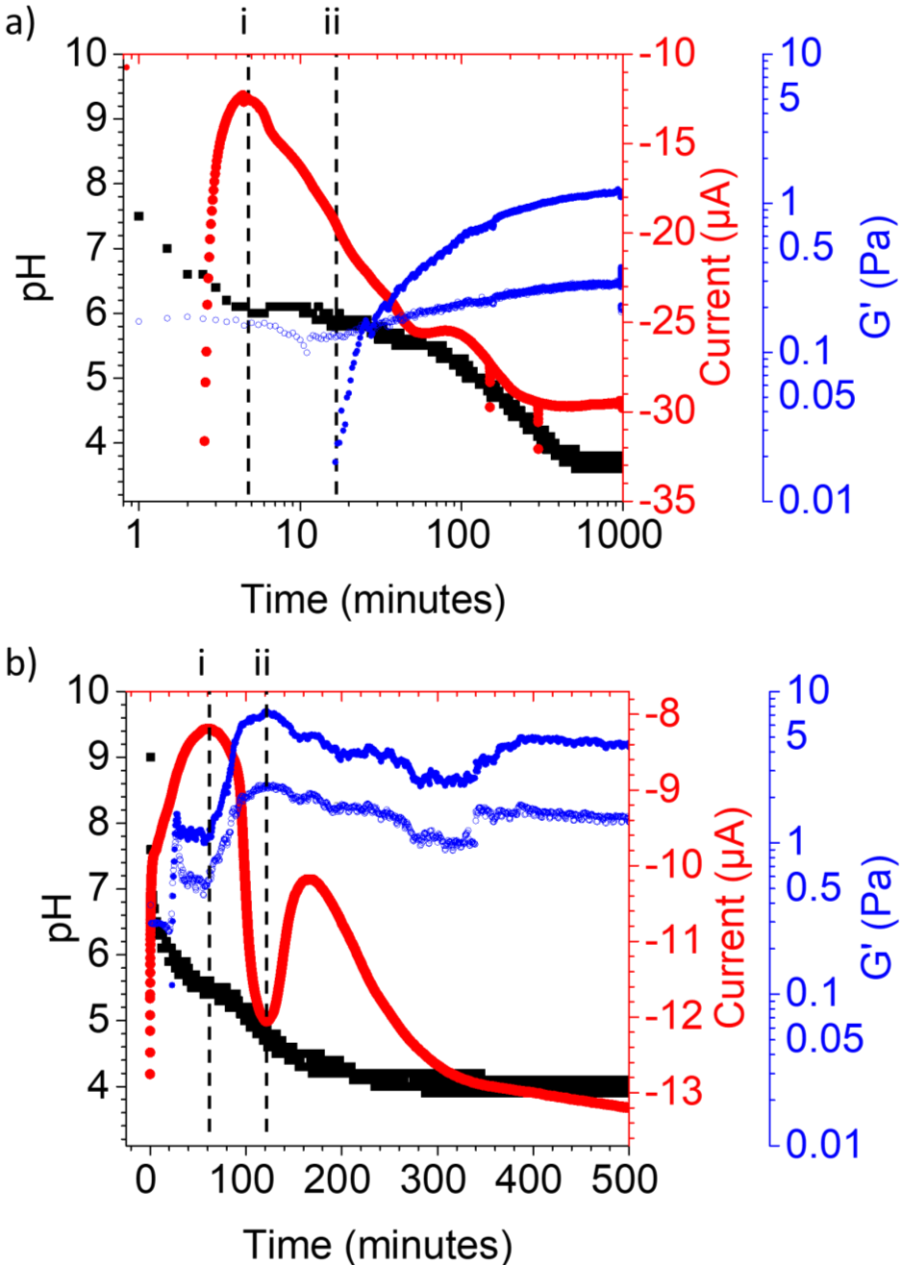

Figure 2.19 a) Shows the evolution of storage (blue full circles) and loss (blue hollow circles) moduli in addition to pH (black squares) and current (red circles) on a log scale for **6**. The dashed lines labelled i) and ii) represent when the pH equals the pK_a value b) Shows the pH (black squares), current (red circles) and storage (blue full circles) and loss (blue hollow circles) moduli for **5**. The dashed line labelled i) represents the pK_a value and the dashed line labelled ii) represents when the self-assembly process deviated from forming a gel.

2.3.6 Multicomponent systems

In multicomponent systems composed of two gelators, we would expect the TM to bind to both gelators at high pH. From our previous work, addition of GdL leads

to sequential assembly as long as the pK_a of each gelator is different (Figure **2.1**b).[6] As pH is lowered below the pK_a of the first gelator, we would expect displacement of the TM from this gelator by protons. This would increase the concentration of free TM in solution resulting in an increase in current. Then, as the pH reaches the pK_a of the second gelator, further displacement of TM and a final increase in current would be expected (shown schematically in Figure **2.5**b). We applied the MPA method to a multicomponent system consisting of gelators **2** and **8**. These dipeptides were chosen on the basis of the large difference in single component pK_a values.[8, 25] However, any combination could be used. The evolution of current, pH, storage and loss moduli are shown (highlighted are the two pKa values for **2** and **8**). Within two minutes after the addition of GdL, the pH decreased to the pK_a of gelator **8**. At this point, an increase in G′ is observed and we also just pass the first peak in current. This suggests **8** is forming a network in the absence of **2**. Once the pK_a of **2** has been reached, we observe a second increase in G′ and the beginning of a second current peak. This would suggest **8** is beginning to assemble.[6] Finally, at pH 3.8 the pK_a of GdL is observed, shown by another current peak.

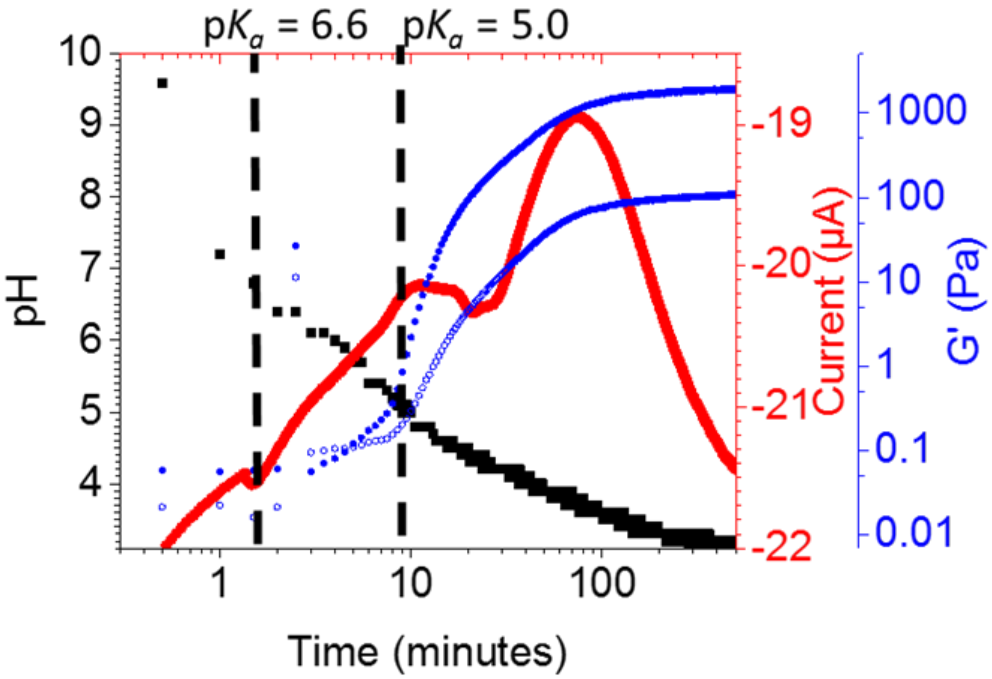

Figure 2.20 Evolution of pH (black squares), current (red circles) and storage (blue full circles) and loss (blue hollow circles) moduli for a multicomponent system of **2** and **8.** The dashed lines represents the pK_a values for these two gelators.

2.4 Conclusions

We have demonstrated how electrochemical techniques can be used to probe the surface chemistry of self-assembled hydrogel fibres including their charge and ion-binding dynamics. This included developing a new pK_a determination method for this class of amino acids or dipeptides. Not only were we able to determine whether a functionalised-dipeptide would self-assemble to form a hydrogel or precipitate, and at what pH this occurs, we determined its stiffness. This is the first time that gel rheology has been determined electrochemically. Furthermore, we developed a method to probe the real-time self-assembly kinetics of a functionalised-dipeptide using multiple pulse amperometry, rheology and pH evolution. Finally, we expanded this method to complex multicomponent systems and were able to observe the surface chemistry of the individual fibres forming as pH was lowered. The future scope of this work includes use in high-throughput screening for pH-triggered systems and further complex gelation systems.

2.5 References

1. M. Wallace, J. A. Iggo and D. J. Adams, *Soft Matter*, 2017, **13**, 1716-1727.

2. D. J. Adams, L. M. Mullen, M. Berta, L. Chen and W. J. Frith, *Soft Matter*, 2010, **6**, 1971-1980.

3. G. R. Weiss, *Gels*, 2018, **4**, 1-27.

4. J. K. Gupta, D. J. Adams and N. G. Berry, *Chem. Sci*, 2016, **7**, 4713-4719.

5. M. Wallace, D. J. Adams and J. A. Iggo, *Anal. Chem*, 2018, **6**, 4160–4166

6. K. L. Morris, L. Chen, J. Raeburn, O. R. Sellick, P. Cotanda, A. Paul, P. C. Griffiths, S. M. King, R. K. O'Reilly, L. C. Serpell and D. J. Adams, *Nat. Comm*, 2013, **4**, 1480.

7. E. R. Draper, M. Wallace, R. Schweins, R. J. Poole and D. J. Adams, *Langmuir*, 2017, **33**, 2387-2395.

8. E. R. Draper, E. G. B. Eden, T. O. McDonald and D. J. Adams, *Nat. Chem*, 2015, **7**, 848.

9. E. R. Cross, S. Sproules, R. Schweins, E. R. Draper and D. J. Adams, *J. Am. Chem. Soc*, 2018, **140**, 8667-8670.

10. D. J. Cornwell, O. J. Daubney and D. K. Smith, *J. Am. Chem. Soc*, 2015, **137**, 15486-15492.

11. S. Sörenson, *Biochem Z*, 1909, **21**, 131-200.

12. K. Hasselbalch, *Biochem Z*, 1916, **78**, 112-144.

13. J. Reijenga, A. van Hoof, A. van Loon and B. Teunissen, Anal. Chem Ins, 2013, **8**, 53-71.

14. S. G. Tajc, B. S. Tolbert, R. Basavappa and B. L. Miller, *J. Am. Chem. Soc*, 2004, **126**, 10508-10509.

15. M. Wallace, J. A. Iggo and D. J. Adams, *Soft Matter*, 2015, **11**, 7739-7747.

16. E. S. WC Holmes, *J. Am. Chem. Soc*, 1925, **47**. 2232-2236

17. A. Caragheorgheopol, W. Edwards, J. G. Hardy, D. K. Smith and V. Chechik, *Langmuir*, 2014, **30**, 9210-9218.

18. J. H. Ortony, C. J. Newcomb, J. B. Matson, L. C. Palmer, P. E. Doan, B. M. Hoffman and S. I. Stupp, *Nat. Mater*, 2014, **13**, 812-816.

19. J. Tritt-Goc, A. Rachocki and M. Bielejewski, *Soft Matter*, 2014, **10**, 7810-7818.

20. A. M. Castilla, E. R. Draper, M. C. Nolan, C. Brasnett, A. Seddon, L. L. E. Mears, N. Cowieson and D. J. Adams, *Sci. Rep*, 2017, **7**, 8380.

21. D. J. Adams, M. F. Butler, W. J. Frith, M. Kirkland, L. Mullen and P. Sanderson, *Soft Matter*, 2009, **5**, 1856-1862.

22. E. R. Draper, H. Su, C. Brasnett, R. J. Poole, S. Rogers, H. Cui, A. Seddon and D. J. Adams, *Angew. Chem*, 2017, **129**, 10603-10606.

23. C. Tang, A. M. Smith, R. F. Collins, R. V. Ulijn and A. Saiani, *Langmuir*, 2009, **25**, 9447-9453.

24. L. Chen, S. Revel, K. Morris, L. C. Serpell and D. J. Adams, *Langmuir*, 2010, **26**, 13466-13471.

25. Lin Chen, Tom O. McDonald and D. J. Adams, *RSC Adv*, 2013, **3**, 8714-8720.

26. H. McEwen, E. Y. Du, J. P. Mata, P. Thordarson and A. D. Martin, *J. Mater. Chem. B*, 2017, **5**, 9412-9417.

27. S. Roy, N. Javid, P. W. J. M. Frederix, D. A. Lamprou, A. J. Urquhart, N. T. Hunt, P. J. Halling and R. V. Ulijn, *Chem. Eur*, 2012, **18**, 11723-11731.

28. Y. Wang, J. Limon-Petersen and R. Compton, *J. Electroanal. chem* 2011, **652**, 13-17.

29. S. Awhida, E. R. Draper, T. O. McDonald and D. J. Adams, J. Colloid Interf. Sci, 2015, **455**, 24-31

30. N. A. Morris, M. F. Cardosi, B. J. Birch and A. P. F. Turner, *Electroanalysis*, 1992, **4**, 1-9.

31. T. Okajima, T. Ohsaka and N. Oyama, *J. Electroanal. Chem. Interf. Electrochem*, 1991, **315**, 175-189.

32. Y. Wang, J. G. Limon-Petersen and R. G. Compton, *J. Electroanal. Chem*, 2011, **652**, 13-17.

33. B. O. Okesola and D. K. Smith, *Chem. Soc. Rev*, 2016, 45, 4226-4251.

34. B. O. Okesola, S. K. Suravaram, A. Parkin and D. K. Smith, *Angew. Chem Int. Edit*, 2016, **55**, 183-187.

35. R. G. Weiss, Journal of the American Chemical Society, 2014, **136**, 7519-7530.

36. V. Jayawarna, M. Ali, T. A. Jowitt, A. F. Miller, A. Saiani, J. E. Gough and R. V. Ulijn, Advanced Materials, 2006, **18**, 611-614.

37. Y. Zhang, H. Gu, Z. Yang and B. Xu, *J. Am. Chem. Soc*, 2003, **125**, 13680-13681.

38. Z. Yang, G. Liang, M. Ma, Y. Gao and B. Xu, *J. Mater. Chem*, 2007, **17**, 850-854.

39. C. Tang, R. V. Ulijn and A. Saiani, *Eur. Phys. J. E*, 2013, **36**, 111.

40. K. A. Houton, K. L. Morris, L. Chen, M. Schmidtmann, J. T. A. Jones, L. C. Serpell, G. O. Lloyd and D. J. Adams, *Langmuir*, 2012, **28**, 9797-9806.

41. W. Helen, P. de Leonardis, R. V. Ulijn, J. Gough and N. Tirelli, *Soft Matter*, 2011, **7**, 1732-1740.

42. Y. Pocker and E. Green, *J. Am. Chem. Soc*, 1973, **95**, 113-119.

43. A. D. Martin, J. P. Wojciechowski, H. Warren, M. in het Panhuis and P. Thordarson, *Soft Matter*, 2016, **12**, 2700-2707.

CHAPTER 3

Tuning electrochemical hydrogels using hydroquinone

3.1 Introduction

To form gels using LMWG, a trigger needs to be applied to change the gelator molecules such that they become less soluble in the solvent or such that the solvent environment changes to decrease the solubility of the gelators.[1, 2] This change in solubility triggers self-assembly of the gelator molecules into aggregated structures such as one-dimensional fibres, which develop into a gel. In this chapter, we form gels using an electrochemical trigger.

Unlike gels formed in bulk, which take the shape of the container they are poured into when liquid, electrochemically fabricated hydrogels can be formed on any conductive surface which provides a potentially high level of spatiotemporal control.[3-9] This localised gelation method is ideal for producing thin film gels which are suitable for a variety of applications such as synthesis of conducting polymers;[10] for use in regenerative medicine;[11, 12] creating antibacterial surfaces,[13, 14] and the rapidly growing field of biosensors and microfluidic devices.[15-19]

Electrochemical hydrogel fabrication provides new opportunities for constructing at the micro- and nanoscale.[20, 21] These films can be prepared within seconds while thicker films can be prepared within minutes. Recently, there have been developments in using electrochemical techniques to form gels as discussed in Chapter 1. In this chapter, we use an electrochemically induced pH trigger with LMWG to form gels. The trigger occurs when hydroquinone (HQ), which is added to the gelator solution, is electrochemically oxidised at ~0.45 V producing benzoquinone and protons.[5, 6] The production of protons lowers the pH environment around the electrode surface which triggers self-assembly of the LMWG gelators which forms a gel film on the electrode. [5, 6]

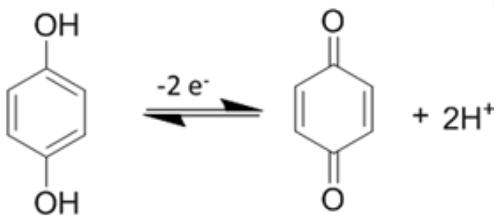

Figure 3.1 Oxidation of HQ

To grow gels of different thicknesses, fast potentiomentry can be used.[4, 5] In this method, an applied current oxidises the HQ over a fixed period of time (Figure **3.2**). The longer the HQ is oxidised the thicker the gel.

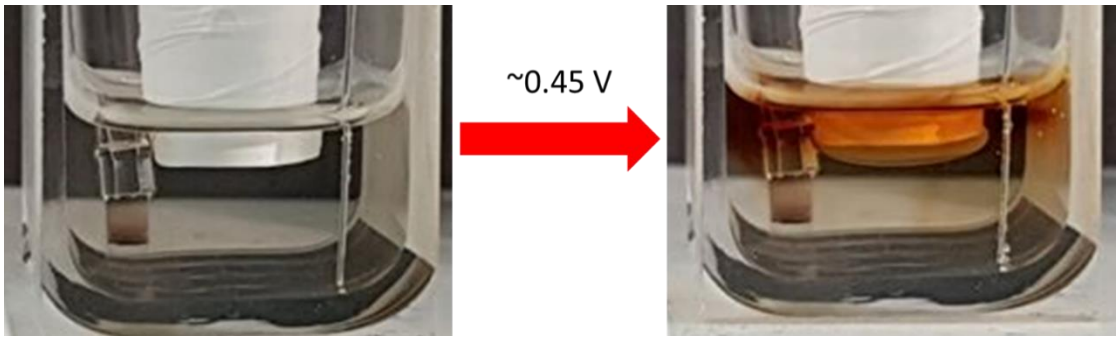

Figure 3.2 Image showing electrochemical gelation on a large glassy carbon electrode. The aqueous solution contains HQ and gelator. Once a potential of ~0.45 V is applied, self-assembly is triggered. The potential can be added over various length of time to achieve gels of different thicknesses.

Previous work has shown great spatiotemporal control in electrochemically fabrication of polymer gels.[5-7, 9, 22] However, there is little understanding of how electrochemical parameters affect the other physical properties of electrochemically fabricated gels such as stiffness and pore size. To the best of our knowledge, there are currently no data that show how the rheological properties of such gels can be controlled electrochemically. Growing gels with controlled rheological properties is a desirable prospect especially for potential use in cell culture, film coatings and regenerative medicine. In this chapter, for the first time, we show kinetic control over the rheological properties in electrochemical LMWG.

3.2 Experimental

3.2.1 Materials

Gelators **1** and **2** (Figure **3.5**) were prepared as previously reported.[23] [24] Gelator **1** was prepared by Prof. Dave Adams and Dr. Bart Dietrich (University of Glasgow) depending on the batch. All other chemicals were purchased from Sigma Aldrich.

3.2.2 Hydroquinone solution

A fresh 0.1 M solution of HQ in aqueous KCl (1 M) was prepared for use in electrochemical studies. The pH was adjusted to pH 8 using NaOH (0.01 M).

3.2.3 LMWG solution

LMWG solutions were prepared by weighing out 80 mg of **1** (Figure **3.5** a) into 14 mL vials then adding deionised H_2O (7.39 mL) and NaOH (aq. 0.1 M, one molar equivalent, 1.61 mL) to a volume of 9 mL. The solution was stirred overnight to ensure all gelator had dissolved. The gelator solutions were then pH adjusted to 8 with HCl (0.5 M) and de-ionised water, ensuring that the final volume was 10 mL which provides solutions at a final concentration of gelator of 8 mg/mL. Solutions were stored at room temperature.

Just before growing gels electrochemically, 50 mg of HQ was added to 10 mL of gelator solution followed by 100 µL of 0.1 M NaCl. The solution was gently swirled to ensure the HQ was dissolved then placed into the electrochemical cell for gel growth. It is essential that the gelator solution is not left to oxidise over a long period of time, should the solution turn orange a fresh solution should be prepared.

3.2.4 Electrochemistry set up

An electrochemical cell with dimensions 2.5 cm 2 cm x 7 cm (HxWxL) containing three electrodes (glassy carbon working electrode, Ag/AgCl (3 M) reference and platinum wire counter electrodes) was set up as shown in Figure **3.3**. The prepared LMWG solution was poured into the electrochemical cell for cell growth.

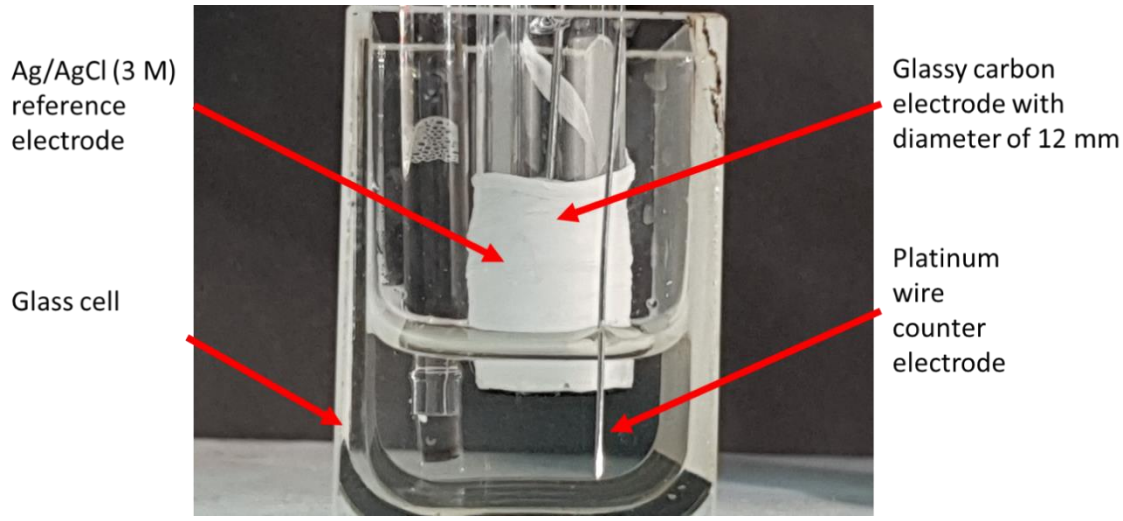

Figure 3.3 Image of electrochemical cell set up. Inside the cubic cell, the working electrode is the glassy carbon electrode, the counter electrode is connected to the platinum wire and the reference electrode is the Ag/AgCl (3 M) reference electrode.

Before using the glassy carbon electrode, it is polished using diamond polish with decreasing particle size (10, 3 then 1 μm). Polishing is continued with a fine alumina slurry polish. Polishing was carried out in a figure of 8 motion to ensure a flat electrode surface. The electrode was then placed in distilled water and sonicated for 1 minute to remove and alumina debris.

3.2.5 Cyclic voltammetry

All experiments were run using a Dropsens Potentiostat and a three-electrode system. The working electrode was a glassy carbon electrode, a platinum wire counter was used with an Ag/AgCl (3 M) reference electrode as described in Section 3.2.4. Cyclic voltammetry (CV) measurements were carried out within a potential range of -0.5 to 0.2 V vs. an Ag/AgCl (3 M) reference electrode at a scan rate of 20, 40, 60, 80, 100, 200, 400, 600, 800, 1000 mV/s. Each CV measurement consisted of one scan.

3.2.6 Fast potentiometry

Fast potentiometry was used to grow gels on the working electrode. Gelator solution as describe in Section 3.2.3 was placed into the electrochemical set up (see Section 3.2.4). A current between the range of 1000 and 2000 μA was applied

for between 270 to 810 seconds. During this time, the potential passed the oxidation potential of HQ at ~0.45 V which results in a gel being formed on the electrode surface. Once the applied current has stopped, the gel was carefully removed from the electrode surface using a scalpel.

3.2.7 Image analysis

Images of gelation were taken every 30 seconds using a mobile phone camera. These images were uploaded to the open source image analysis software 'ImageJ'. The outline of the gel can be traced, and the area of gel calculated.

3.2.8 Rheology

Rheological measurements were carried out using an Anton Paar Physica MCR301 rheometer. Parallel plates (12.5 mm diameter, smooth) were used to measure frequency and strain sweeps. For measuring the frequency and strain sweeps, the gels were removed from the electrode surface using a scalpel and placed onto the rheometer. Rheological measurements were recorded at 25 °C. Figure **3.4** a shows the gel carefully placed onto the bottom parallel plate while Figure **3.4** b shows the top plate once it has been lowered to a gap of 2 mm.

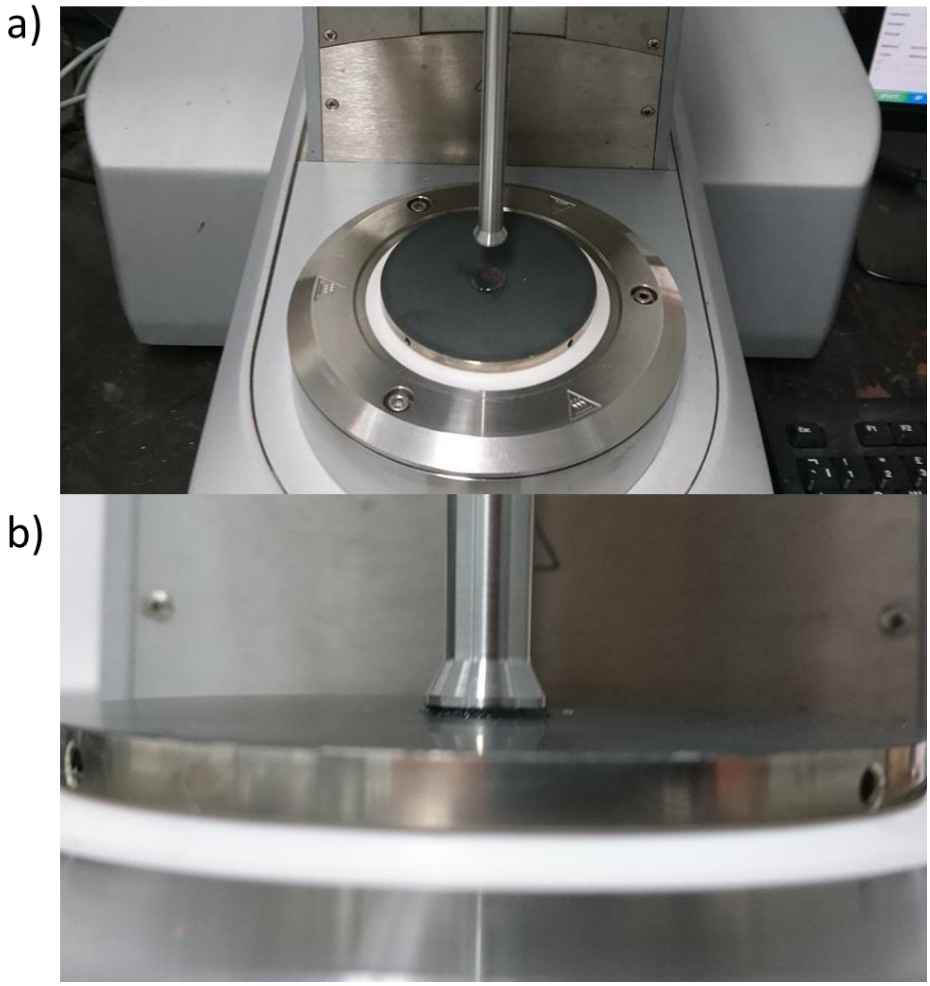

Figure 3.4 a) Image of an electrochemically grown gel carefully placed on the bottom parallel plate. b) The top parallel plate is lowered and sandwiches the gel between the bottom and top plate.

Strain sweep: Strain sweeps were measured from 0.01 % to 100 % with a constant frequency of 10 rad/s. Measurements were performed in duplicate and errors were calculated from the standard deviation.

Frequency sweep: Frequency scans were performed from 1 rad/s to 100 rad/s under a constant strain of 0.5 %. Measurements were performed in duplicate and errors were calculated from the standard deviation.

3.2.9 Nuclear magnetic resonance (NMR)

Gels were grown on the electrode as described in Section 3.2.6 and freeze dried overnight. The freeze-dried gels were then dissolved in 1 mL of dimethyl sulfoxide and 2 µL of ethanol was added as an internal standard. ^{1}H NMR spectra were

recorded using a Bruker Avance III 500 MHz spectrometer with the temperature internally controlled at 25 °C. The concentration of gelator present was calculated by comparing the proton environment peaks of the known concentration of ethanol internal standard against the proton environment peaks of the gelator.

3.2.10 Uptake and release kinetics

Gels were grown in triplicate as described in Section 3.2.6. Gels were rinsed with deionised water and placed into a 6 well plate. 5 mL of Direct Red 90 at pH 3 (0.090 M) was added on top of the gel and the gels were left covered for 16 hours. Next, all of the Direct Red 90 was removed and a 100 µL aliquot was used to measure the absorption to determine M_∞. 7 mL of deionised water at pH 3 was then added on top of the gel. After timed intervals, generally 30 minutes, 1.5 mL of water was aspirated slowly to ensure homogeneity of the aqueous phase and to ensure the gel was not damaged. 100 µL of the solution on top of the gel was removed and added to a 96 well plate and the absorption was recorded.

3.2.11 pH measurements

pH measurements were recorded using a Hannah PC turtle FC500 pH probe with a given error of ± 0.1.

3.2.12 UV/vis spectroscopy

Measurements were carried out using an Agilent Cary 60 UV−Vis spectrophotometer. Gel samples for UV-vis absorptions were placed into a 2 mm quartz cuvette. Kinetic measurements were collected for 6 minutes after freezing of sample.

3.3 Results and discussion

3.3.1 Oxidation of hydroquinone

To determine whether the oxidation of HQ in air can trigger bulk gelation over a 16 hour time period, HQ (16 mg) was added to a Sterilin vial containing 2 mL of gelator **1** (Figure **3.5** a) solution (8 mg/mL). After 16 hours, as a crude measure of rheology, inversion of the Sterilin vial showed no gel had formed (Figure **3.5** b, c). This suggests the oxidation of HQ in air does not trigger gelation and forms a control for the work in this chapter.

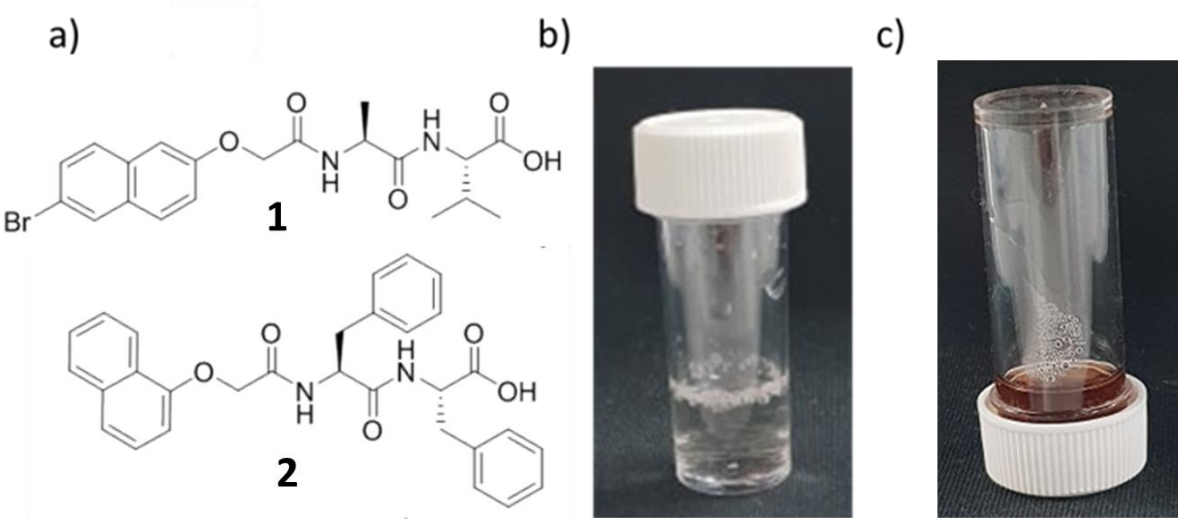

Figure 3.5 a) Chemical structures for gelators **1** and **2** which are used throughout this chapter. b) Shows a solution of **1** with the addition of HQ in a Sterilin vial. c) Shows the inverted Sterilin vial containing solution of **1** and HQ after 16 hours. This image shows that no gel has formed and the oxidation product benzoquinone which is orange in colour is present.

Localised oxidation of HQ can be controlled using electrochemistry. To investigate the electrochemical reversibility properties of HQ, 100 mg of HQ was added to 10 mL of KCl (1 M) and CVs were run with scan rates between 0.02 V/s and 1.00 V/s vs. Ag/AgCl (3 M) reference electrode. The resulting CVs in Figure **3.6** show an electrochemical quasi-reversible system. This implies that HQ has an intermediate rate of electron transfer on the electrode surface.

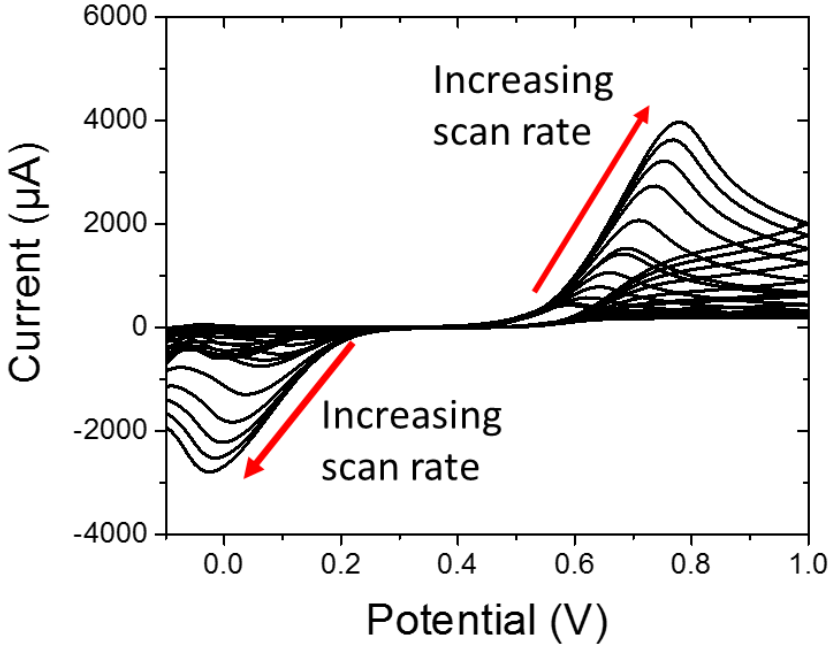

Figure 3.6 Overlapping CVs of HQ (10 mg/mL) in KCl (1 M) using scan rates between 0.02 and 1.00 V/s. Red arrows show how with increasing scan rate the peak oxidation and reduction current increases. The red arrows also show the peak oxidation and reduction current occurs at different potentials, which is typical of a quasi-reversible system.

3.3.2 Electrochemical fabrication parameters

3.3.2.1 Hydroquinone electrochemical reversibility parameters

Using the electrochemical oxidation of HQ on a glassy carbon electrode, a pH gradient is set up from low at the electrode surface to high in the bulk solution. This area of low pH triggers the self-assembly of LMWG at the electrode surface.[5, 6] The potential range at which HQ oxidises has a corresponding current range which is highlighted in the CV in Figure **3.7**. At low current values within this range, the concentration of HQ that oxidises is low whereas, at high current the concentration is higher. This implies the pH gradient is greatest when a higher current is applied.

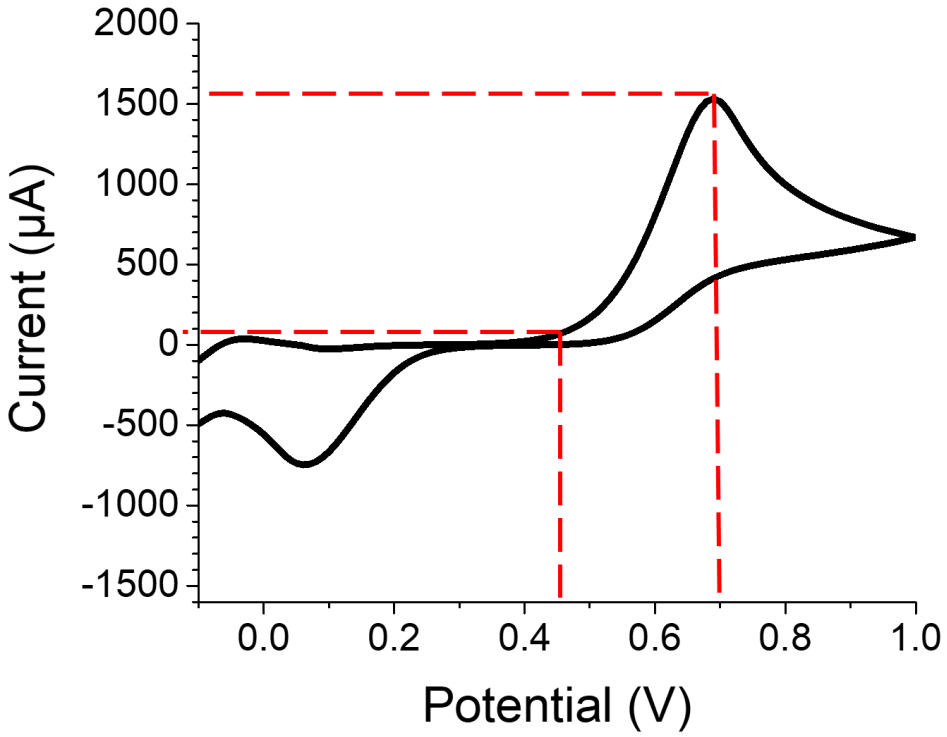

Figure 3.7 CV of HQ (5 mg/mL) in KCl (1 M) at a scan rate of 0.2 V/s. The oxidation potential range is highlighted by the vertical red dashed lines. The corresponding HQ oxidation current range is shown by the horizontal red dashed lines.

In order to investigate whether gels formed at different currents will have different physical properties, a CV was run for a 10 mL gelator **1** solution (8 mg/mL) containing HQ (50 mg) at 0.2 V/s versus an Ag/AgCl (3 M) reference electrode. Both the onset and peak oxidation potentials of HQ are highlighted in blue in Figure **3.8** the corresponding current ranges are highlighted in red. From these data, the current values of 1500 μA and 2000 μA were chosen for fast potentiometry to fabricate gels.

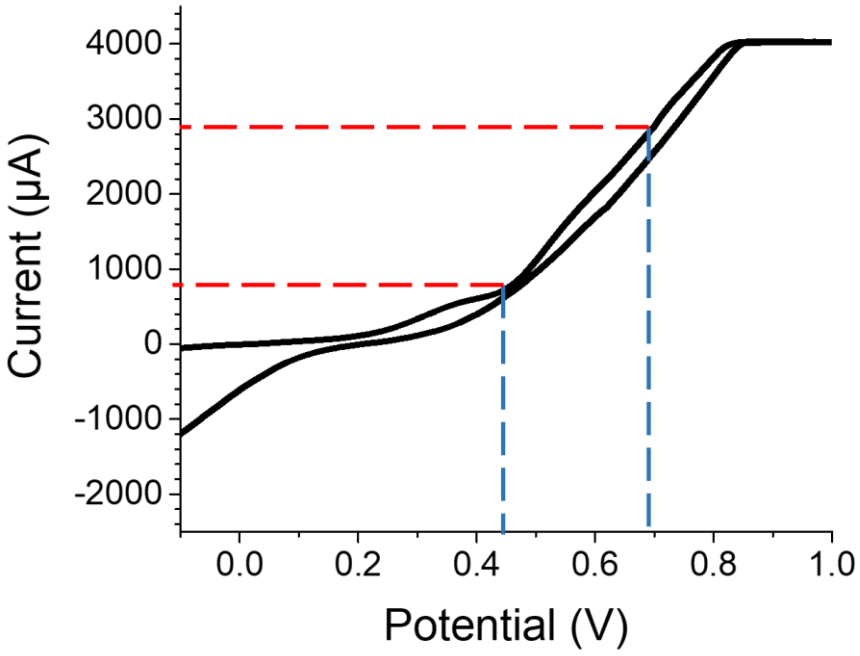

Figure 3.8 Cyclic voltammogram of **1** with HQ at a scan rate of 0.2 V/s. The blue dashed lines show the HQ oxidation potential range, the red dashed lines show the corresponding HQ oxidation current range.

3.3.2.2 Gel size parameters

It is important that the fabricated hydrogel has an even surface for reproducibility and for rheological analysis. For rheological analysis when the surface is flat, there is an equal force (stress) pushing the parallel plates apart whereas, with an uneven gel the force distributed is uneven. This uneven distribution of stress will distort the storage and loss moduli values when performing rheological measurements such as strain or frequency sweeps.

To investigate the best method to prepare an even surface, three electrode positioning scenarios were prepared as shown in Figure **3.9**. With the first scenario a) the working electrode is further away from the counter and reference electrode which are relatively closer together; this resulted in a gel growing on the working electrode that was uneven. Uneven gel growth was also the outcome when the electrode was moved into a larger vessel and the distance between the electrodes were increased as shown in b). Finally, the reference and counter electrode were

placed in opposite corners of the larger vessel with the working electrode in the middle. This ensured an even gel surface growth.

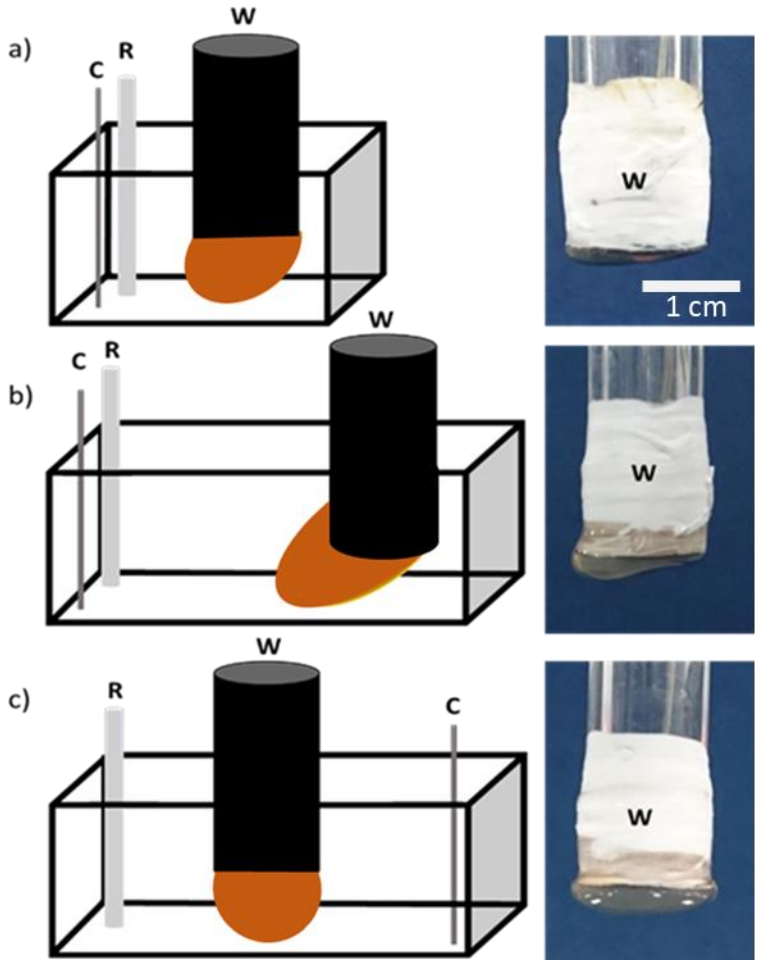

Figure 3.9 Electrochemical set up for gel growth including counter C, reference R, and working W electrodes with images of gels grown on the working electrode. a) Uneven gel growth with C and R together in a small cell. b) Uneven gel growth with C and R together in a large cell. c) Even gel growth with C and R equidistant apart in opposite corners.

Gels were grown on the electrode surface by fast potentiometry at either 1000 µA, 1500 µA and 2000 µA as described in Section 3.2.6. Figure **3.10** shows both gels of **1** and **2** grown at the corresponding applied current. As predicted the higher applied currents produced a higher potential which result in a greater concentration of HQ oxidation.

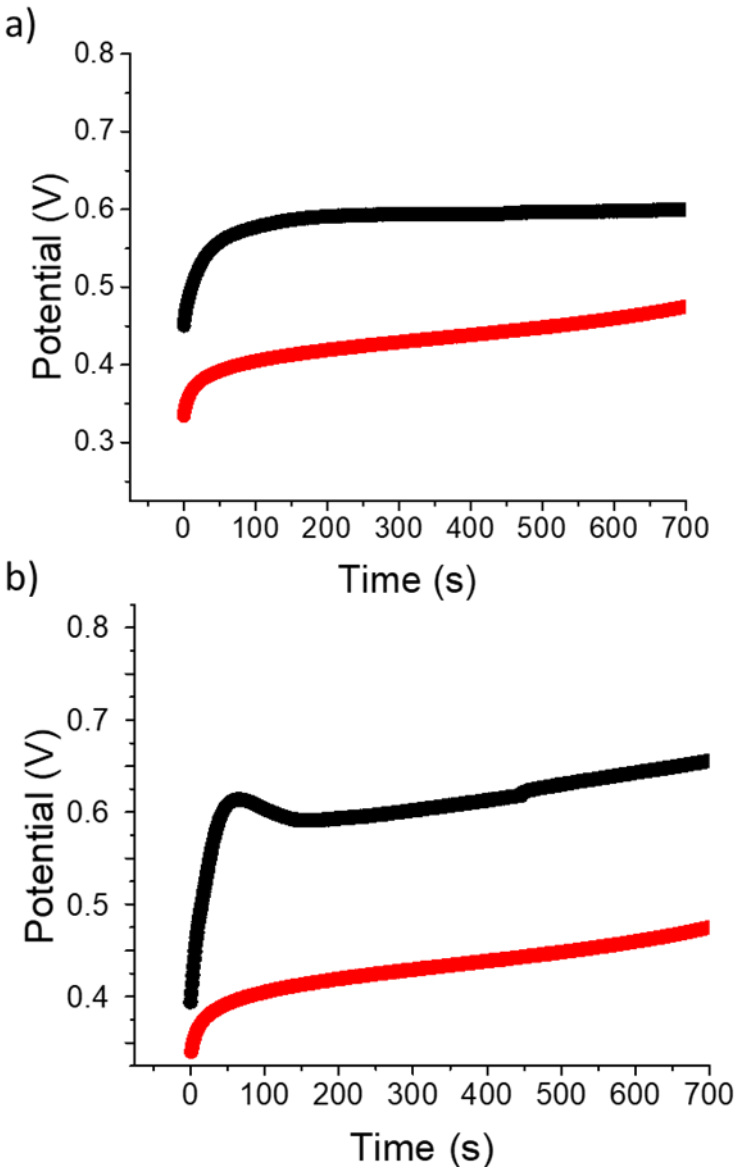

Figure 3.10 Fast potentiometry of a) 1 with the applied current of 1500 μA (red) and 2000 μA (black) as well as b) 2 with the applied current of 1000 μA (red) and 1500 μA (black). All potentials were recorded against an Ag/AgCl (3 M) reference electrode.

To ensure the volume of gel formed from both applied currents were identical for analysis, images were captured during gelation and the area of gel was measured using ImageJ software.[25] Figure **3.11** a) shows the measured gel areas of **1** grown at 1500 μA and 2000 μA . A gel area of 0.2 cm was chosen which corresponds to forming a gel at 2000 μA for 540 s and at 1500 μA for 810 s. We will call gels formed at 2000 μA for 540 s gel **1a**, and gels formed at 1500 μA for 810 s gel **1b** throughout. This gel area was chosen as these gels have an ideal thickness for rheological and small angle neutron scattering analysis. However, we do not expect that choosing

a different area would result in a different experimental outcome. Figure **3.11** b) shows the measured gel areas of **2** grown at 1500 μA and 1000 μA. A gel area was chosen which corresponds to forming a gel at 1500 μA for 270 s and at 1000 μA for 540 s. We will call gels formed at 1500 μA for 270 s gel **2a**, and gels formed at 1000 μA for 540 s gel **1b** throughout. A summary of gel parameters is shown in Table **3.1**.

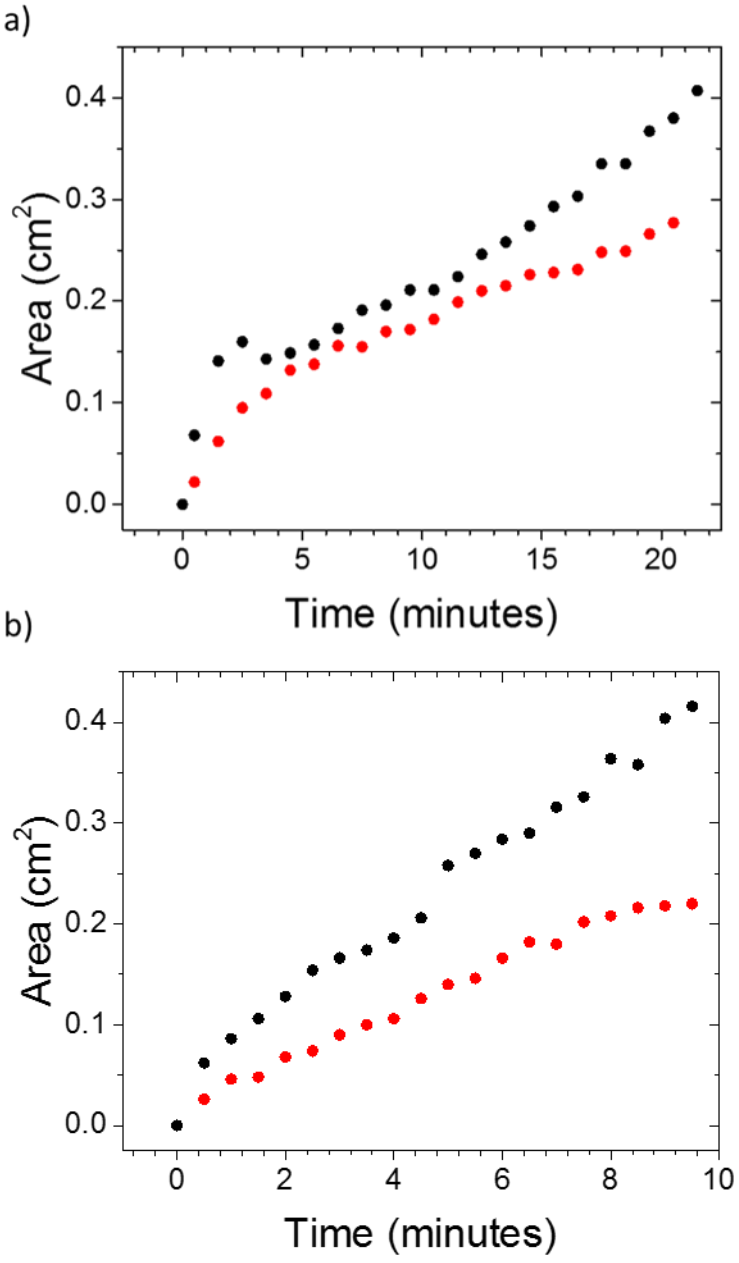

Figure 3.11 Area of gel forming on the electrode surface during potentiometry of a) **1** with applied current of 1500 μA (red) and 2000 μA (black). b) **2** with applied current of 1000 μA (red) and 1500 μA (black).

Table 3.1 Summary of electrochemical gelation parameters where the current applied and the length of time the current is applied for is shown for each gel.

Gel	Current applied (μA)	Time (s)
1a	2000	540
1b	1500	810
2a	1500	270
2b	1000	540

3.3.3 Characterisation of hydrogel properties

To identify whether controlling the rate of gelation results in gels with different physical properties, a range of analytical methods were used to characterise gel stiffness, control release kinetics, gel density and thermochromic properties.

3.3.3.1 Rheological analysis

Rheological frequency and strain sweeps were used to analyse the viscoelastic properties of the gels. Gels were prepared and removed from the electrode surface with a scalpel. The gels were then transferred onto the rheometer plate and both frequency and strain sweeps were carried out. All gels measured showed a linear viscoelastic property in the measured frequency range of 1-100 rad/s with reproducible data shown in Figure **3.12**.

A higher gel stiffness was observed for **1b** (326 ± 9.19 KPa at 10 rad/s) than **1a** (114 ± 0.707 KPa at 10 rad/s). **1b** also broke under a higher strain (10.00 % for **1b** versus 3.98 % for **1a**). In contrast, **2a** (stiffness of 9.03 ± 0.056 KPa at 10 rad/s and broke under 12.60 % strain) was stiffer and stronger than **2b** (stiffness of 3.81 ± 0.145 at 10 rad/s and broke under 7.90 % strain). The rheology data were collected from fresh samples in duplicate therefore, the differences in stiffness are statistically significant, and are not due to sample-to-sample variation. These differences in gel stiffness and strength suggest different network properties between gels formed from the same gelator but at different applied currents. The trends between the gel stiffness and strength are also dependent upon the gelator molecules.

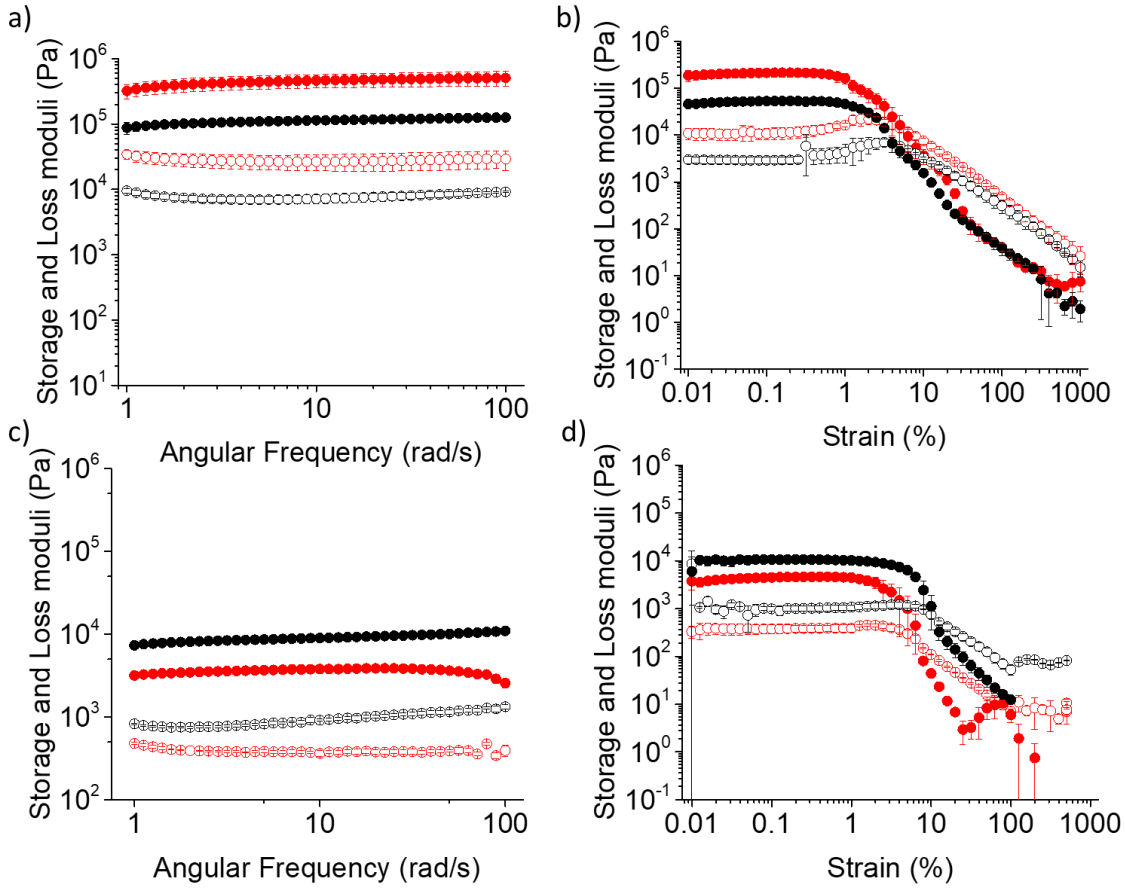

Figure 3.12 a) Frequency sweep of **1a** (black) and **1b** (red). b) Strain sweep of **1a** (black) and **1b** (red). c) Frequency sweep of **2a** (black) and **2b** (red). d) Strain sweep of **2a** (black) and **2b** (red). In all cases, the closed symbols represent G' and the open symbols represent G" and error bars were calculated from duplicated samples. Frequency sweeps were measured under a constant strain of 0.5 % and strain sweeps were measured under a constant frequency of 10 rad/s.

From the rheological data alone, we can hypothesise that gels formed from gelators that do not form large aggregated structures at high pH such as **1a** and **1b**, form layers on the electrode surface that depend upon the applied current. Higher currents induce faster gelation which may produce areas of gel that are inhomogeneous. In contrast, lower currents induce slower gelation that may produce longer fibres which during gelator self-assembly entangle forming a homogeneous network that is both stiffer and stronger. In comparison, gels formed from gelators that form worm-like micelles at high pH such as **2a** and **2b**, may entangle greater at higher current and gelation rates, producing stiffer and stronger gels.

Ideally, SANS data would be collected to determine the length and radius of the gel fibres within the network. This analysis, in addition to the work carried out in this chapter, would be able to conclude whether the differences in network properties between the gels of different applied currents are due to differences in the fibre length and radius or due to the entanglement of the fibres. SANS was attempted but due to issues with sample preparation the data could not be fitted.

3.3.3.2 Nuclear magnetic resonance (NMR)

^{1}H NMR spectroscopy was used to determine the concentration and density of gelator in gels **1a**,**1b, 2a** and **2b**. The proton environments for each gelator were integrated against an ethanol internal standard (2 µL per 1 mL of sample). A higher concentration of gelator was found for gels grown at the higher current (**1a** and **2a**) than at the lower current (**1b** and **2b,** Figure **3.13**). The higher concentration of gelator within the same gel volume implies that the networks of **1a** and **2a** are denser than the corresponding gels grown at lower current (**1b** and **2b**)**.**

As there is no common trend between the density of the gels and their rheology, it is more than likely that the gel networks that are forming are unique to each gelator. This would correspond to the hypothesis described in Section 3.3.3.1 where gels formed from a gelator with worm-like micelles or smaller aggregates at high pH do not follow the same rheological trends.

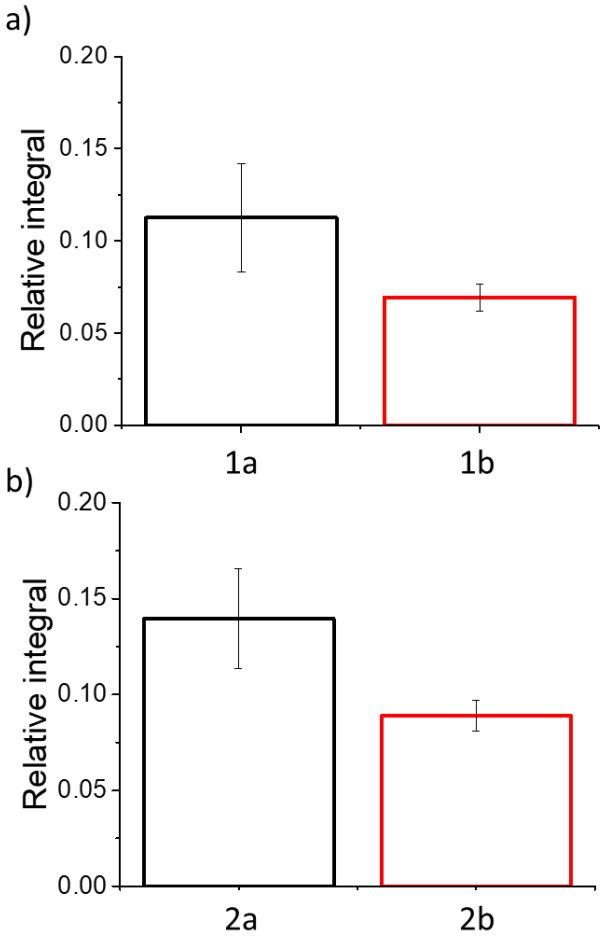

Figure 3.13 Relative integrals measured by ^{1}H NMR spectroscopy for a) **1a** and **1b** and b) **2a** and **2b**, against an ethanol internal standard.

3.3.3.3 Uptake and release

To investigate whether the differences in gel network result in differences in the gel mesh size, uptake and release studies were carried out. Gels of **1a**,**1b**,**2a** and **2b** were prepared and the maximum concentration uptake of Direct red 90 was measured. The release kinetics of Direct Red 90 were measured over a period of 6 hours. Figure **3.14** show the uptake and release data.

Gels of **1a** and **1b** showed an average maximum uptake over 16 hours of 34.0 % and 27.2 % respectively. This difference in uptake of 6.8 % between gels **1a** and **1b** coincide with the differences in the gel network. It is possible there is greater entanglement between the fibres in **1a** which may reduce network pore size and reduce the rate of uptake. This can be further explained by the release kinetics of Direct Red 90 being slower in **1a** than **1b**.

Gels of **2a** and **2b** showed an average maximum uptake over 16 hours of 44.6 % and 46.5 %. Although **2b** shows a higher average uptake of Direct Red 90, the data of **2a** falls within the error bars of **2b**. Furthermore, the release kinetics of **2a** and **2b** are more similar than **1a** and **1b**. This may suggest only a small difference in the mesh size of gels **2a** and **2b**.

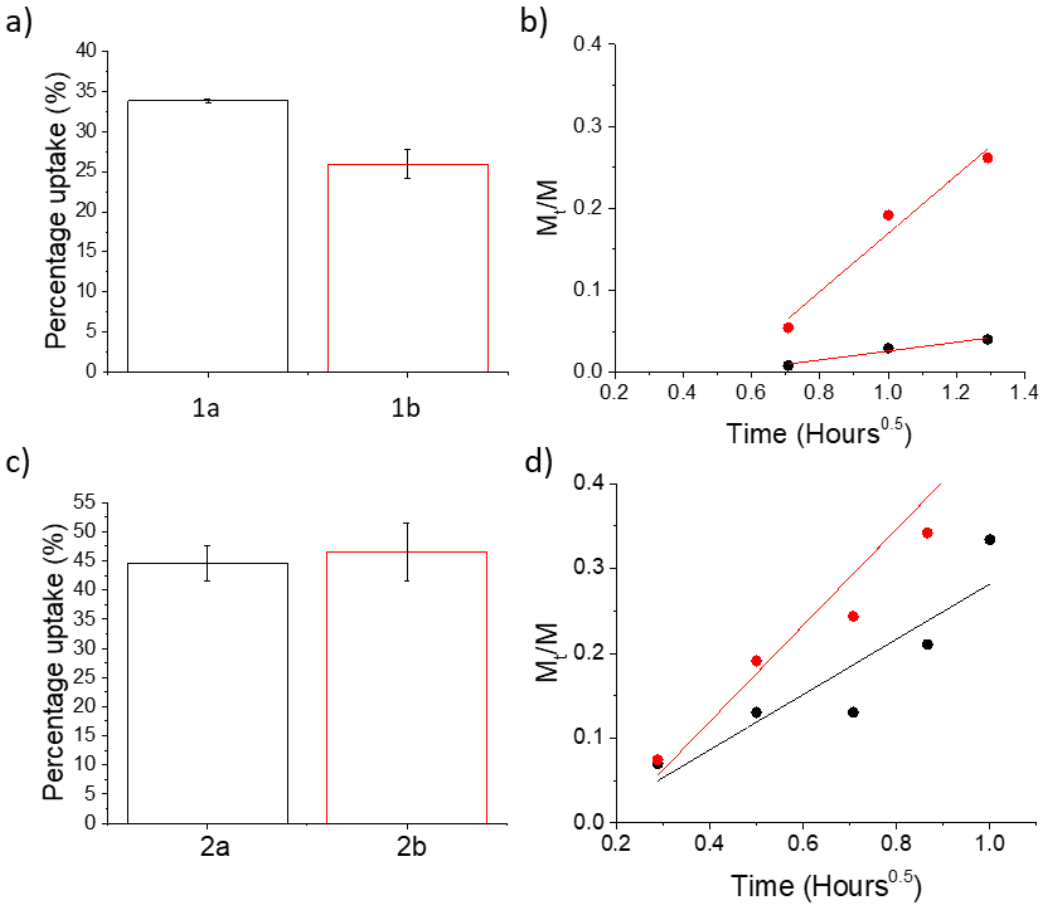

Figure 3.14 Uptake and release of Direct Red 90 in gels **1a**, **1b**, **2a** and **2b**. a) maximum uptake after 16 hours for **1a** and **1b**. b) release kinetics of Direct Red 90 over time for **1a** and **1b.** a) maximum uptake after 16 hours for **1a** and **1b.** b) release kinetics of Direct Red 90 over time for **1a** and **1b**. Linear fits have been added to figures b) and d) for analysis.

3.3.3.4 Thermochromic properties

Upon freezing, the gels changed colour from clear and colourless to dark purple and opaque. We believe this is the result of quinhydrone crystals forming within the pores of the gels. These crystals occur when the ratio of HQ and benzoquinone

is 1:1.[26] To investigate whether the differences in gel growth parameters would lead to a difference of quinhydrone concentration and therefore the thermochromic properties of the gels, gels of **2a** and **2b** were used in UV/Vis studies. Gels formed from **2** were chosen instead of **1**, as they are colourless and more translucent which made them more suitable for UV/Vis analysis. By analysing the absorbance of the crystal peak, we were able to determine a difference in the thermochromic properties of the gels.

Gels of **2a** and **2b** were grown and placed into a 2 mm quartz cuvette. The gel was then frozen for 3 minutes at -15 °C, then allowed to reheat at room temperature for 6 minutes. This was repeated twice. Figure **3.15** shows the colour change observed from a clear gel when at room temperature to a dark purple gel when frozen, the black dot was used as a colour reference point.

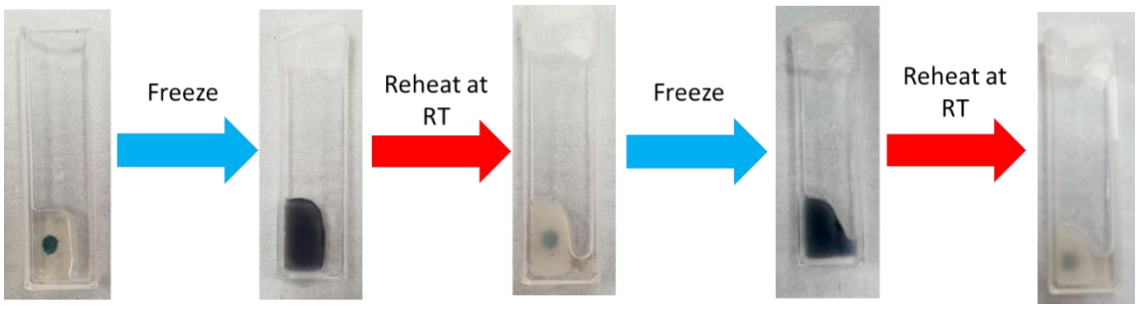

Figure 3.15 Image to show thermochromic change in gel **2a** during freezing and reheating. A black circle is used for colour reference.

Continuous UV/Vis spectra were collected for gels **2a** and **2b** during the first and second heating cycle (Figure **3.16**). In both gels **2a** and **2b**, the colour changed from purple to clear on the first heat cycle. Once re-frozen, the colour changed back to purple with a similar level of absorbance. After the second heat cycle, both gels became more turbid and less clear than the first cycle, which is a lot more apparent in the case of **2b**. The differences in multiple cycles could be potentially linked to underlying network differences developing during the phase changes.

Thermochromic gels have use in a wide range of applications such as temperature sensors, large-area displays and smart-windows. Further development of the gels

as described in this chapter may provide greater opportunities for tuning the thermochromic properties to produce materials of a greater level of complexity.[27]

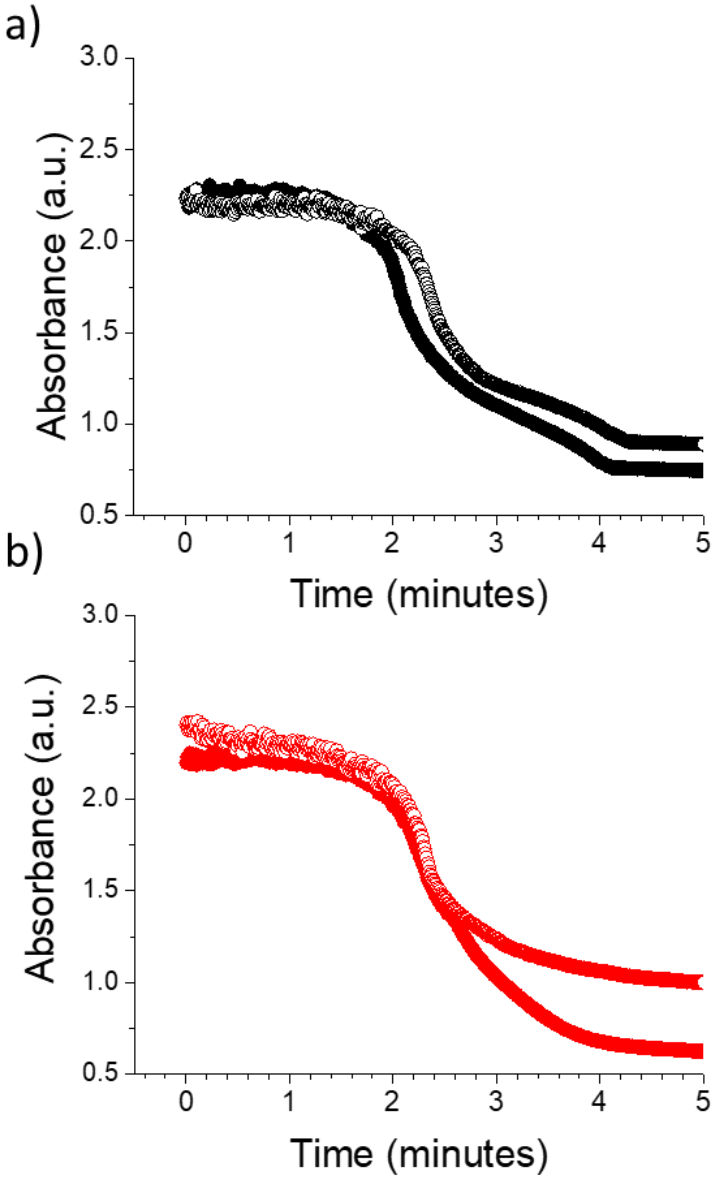

Figure 3.16 UV/Vis absorption data during heating of gels a) **2a** and b) **2b**. The first cycle is shown by full circles and the second cycle is shown as hollow circles.

3.4 Conclusions

This chapter shows how the kinetics of gels formed by electrochemical potentiometry can be controlled by controlling the rate of HQ oxidation and therefore the rate of pH decrease at the electrode surface. The gels that are formed have different physical properties depending upon the current applied. Rheological frequency and strain sweeps show how faster gelation kinetics, from the increase in applied current, result in differences in the rheological properties. Gels formed from worm-like micelles produce stiffer gels when a higher current is applied, and gels formed from smaller aggregates produce weaker gels when a higher current is applied. This is interesting as the different trends in physical properties are unique for each gelator which may allow for new gel properties for existing gelator molecules that usually used to form gels in bulk to be discovered.

In this chapter we also show how the uptake and release studies suggest gels with greater stiffness have larger mesh sizes. Finally, purple crystals forming from quinhydrone are present when the gels are cooled to -15 °C. The thermochromic properties of these gels can be controlled by the applied current. These gels could potentially be used to develop intricate thermochromic devices.

The development of electrochemical LMWG in this chapter provide the fundamental principles to produce electrochemical LMWG with greater level of complexity than is previously published to date.

3.5 References

1. S. Ghosh, V. K. Praveen and A. Ajayaghosh, *Annu. Rev. Mater. Res*, 2016, **46**, 235-262.

2. E. R. Draper and D. J. Adams, *Chem*, 2017, **3**, 390-410.

3. S. H. Huang, L. S. Wei, H. T. Chu and Y. L. Jiang, *Sensors*, 2013, **13**, 10711-10724.

4. J. E. Bressner, B. Marelli, G. Qin, L. E. Klinker, Y. Zhang, D. L. Kaplan and F. G. Omenetto, *J. Mater. Chem. B*, 2014, **2**, 4983-4987.

5. J. Raeburn, B. Alston, J. Kroeger, T. O. McDonald, J. R. Howse, P. J. Cameron and D. J. Adams, *Mater. Horiz*, 2014, **1**, 241-246.

6. E. K. Johnson, D. J. Adams and P. J. Cameron, *J. Am. Chem. Soc*, 2010, **132**, 5130-5136.

7. R. Fernandes, L.-Q. Wu, T. Chen, H. Yi, G. W. Rubloff, R. Ghodssi, W. E. Bentley and G. F. Payne, *Langmuir*, 2003, **19**, 4058-4062.

8. V. Lakshminarayanan, L. Poltorak, D. Bosma, E. J. R. Sudhölter, J. H. van Esch and E. Mendes, *Chem. Comm*, 2019, **55**, 9092-9095.

9. K. Gwon, M. Kim and G. Tae, *Integr. Biol*, 2014, **6**, 596-602.

10. P. S. Kubiak, S. Awhida, C. Hotchen, W. Deng, B. Alston, T. O. McDonald, D. J. Adams and P. J. Cameron, *Chem. Comm*, 2015, **51**, 10427-10430.

11. J. Groll, T. Boland, T. Blunk, J. A. Burdick, D.-W. Cho, P. D. Dalton, B. Derby, G. Forgacs, Q. Li, V. A. Mironov, L. Moroni, M. Nakamura, W. Shu, S. Takeuchi, G. Vozzi, T. B. F. Woodfield, T. Xu, J. J. Yoo and J. Malda, *Biofabrication*, 2016, **8**, 013001.

12. M. Lei, X. Qu, H. Liu, Y. Liu, S. Wang, S. Wu, W. E. Bentley, G. F. Payne and C. Liu, *Adv. Funct. Mater*, 2019, **29**, 1900065.

13. C.M. Xie, X. Lu, K.F. Wang, F.-Z. Meng, O. Jiang, H.P. Zhang, W. Zhi and L.-M. Fang, *ACS Appl. Mater. Inter*, 2014, **6**, 8580-8589.

14. O. Geuli, N. Metoki, N. Eliaz and D. Mandler, *Adv. Funct. Mater*, 2016, **26**, 8003-8010.

15. J. Gong, T. Liu, D. Song, X. Zhang and L. Zhang, Electrochem. Comm, 2009, **11**, 1873-1876.

16. W. Suginta, P. Khunkaewla and A. Schulte, *Chem. Rev*, 2013, **113**, 5458-5479.

17. P. Qi, Y. Wan and D. Zhang, *Biosens. Bioelecron*, 2013, **39**, 282-288.

18. T. Ahuja, I. A. Mir, D. Kumar and Rajesh, *Biomaterials*, 2007, **28**, 791-805.

19. J. F. Betz, Y. Cheng, C.-Y. Tsao, A. Zargar, H.-C. Wu, X. Luo, G. F. Payne, W. E. Bentley and G. W. Rubloff, *Lab Chip*, 2013, **13**, 1854-1858.

20. T. K. Merceron and S. V. Murphy, *Essentials of 3D Biofabrication and Translation*, 2015, 249-270.

21. H. Yi, L.-Q. Wu, W. E. Bentley, R. Ghodssi, G. W. Rubloff, J. N. Culver and G. F. Payne, *Biomacromolecules*, 2005, **6**, 2881-2894.

22. K. Yan, Y. Xiong, S. Wu, W. E. Bentley, H. Deng, Y. Du, G. F. Payne and X.-W. Shi, *ACS Appl. Mater. Inter*, 2016, **8**, 19780-19786.

23. C. A. Schneider, W. S. Rasband, and K. W Eliceiri, *Nat. Methods*, 2012, **9**, 671-675

24. G. P. Stahly, *Cryst. Growth Des*, 2009, **9**, 4212-4229.

25. A. Seeboth, J. Kriwanek and R. Vetter, *J. Mater. Chem*, 1999, **9**, 2277-2278.

CHAPTER 4

Tuning electrochemical hydrogels for biological applications

4.1 Introduction

4.1.1 Hydrogels for biomedical applications

Hydrogels have become very popular in the biomedical field due to their flexibility, softness, high water content and biocompatibility.[1] Their resemblance to living tissue opens up many opportunities for application in tissue engineering. In addition to tissue engineering, hydrogels have many other useful biological applications such as drug delivery systems, wound dressing and hygiene products.[1] Each of these applications require unique specifications such as biocompatibility, antimicrobial properties and certain physical properties like mesh size and stiffness. In this chapter, we develop new oxidation methods of gelation for gels for use in antimicrobial implant coatings and for regenerative medicine.

4.1.2 Antimicrobial gels

The use of medical implants such as intravascular and urinary catheters, heart valve prostheses, artificial hip joints, dental implants and intraocular lenses have increased in recent years due to both an ageing population and an improvement in medical healthcare.[2, 3] Following the increase in medical implant usage, rates of infection due to bacterial adherence followed by biofilm formation on the implant surface has also increased.[3-5] Figure **4.1** describes the process of biofilm formation. Gels with antimicrobial properties can be used to coat medical implants to reduce the formation of microbial biofilms which lead to disease.[6-8]

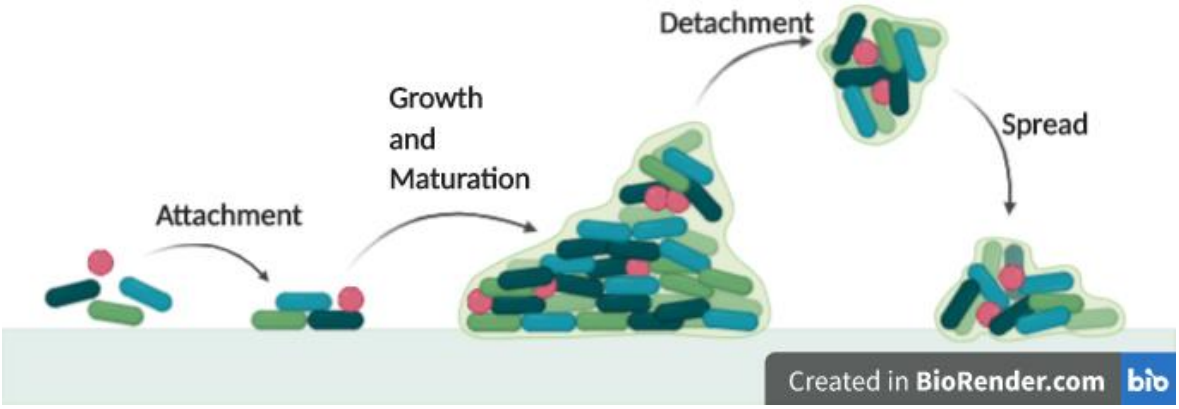

Figure 4.1 Schematic diagram showing the formation of biofilms. Initially, bacteria attach to the tissue. As the bacteria grow and mature, a film is created around the bacteria. Finally, the bacteria detach and spread to another surface.

The biocompatible nature of peptide-based low molecular weight gelators (LMWG) can make them useful building blocks for antimicrobial gels.[9] Antimicrobial gels can either be formed by encapsulation of a known antimicrobial agent into the gel or by developing the hydrogel network to possess antimicrobial activity. Encapsulation of silver and gold nanoparticles can lead to antimicrobial activity.[4, 10-12] However, the mechanism which leads to these antimicrobial properties is unclear.[9] It is possible that bacterial membrane damage is caused by the generation of reactive oxygen species binding to bacterial cell membranes.[9] Furthermore, antibiotics such as amoxicillin,[13] vancomycin,[14] and gentamicin,[15] can be also encapsulated into the gel network. Controlled release of these antibiotics into the area surrounding the biomaterial causes bacteria death.[13, 15, 16]

However, antimicrobial gels formed by the physical encapsulation of antimicrobial agents can be problematic.[17] Accumulation of nanoparticles can be toxic and can cause various health problems and such formulations are prone to a high proportion of burst release.[17-19] In order to prevent antimicrobial resistance development in the use of antibiotic encapsulated gels, it is critical that a sufficient concentration of antibiotic is released, that is above clinically effective concentrations for a sufficient period of time.[20] At least 1 % of bacteria in the stationary phase of biofilm development are tolerant to antibiotics; over time, the number of resistant microorganisms within the stationary phase can increase due to exposure to sub-therapeutic concentrations of antibiotics and therefore greater resistance can develop.[21]

4.1.3 Regenerative medicine

Stiff polystyrene tissue culture plates are usually used to culture cells in vitro. However, in the body, cells attach to the external cellular matrix, which is remarkably less stiff at around 0.01 -10 kPa. Therefore, in vitro the cells are in a highly non-physiologically relevant mechanical environment.[22] Many cell behaviours, including cytoskeletal organization, proliferation and differentiation, are dependent upon the external surface which they are fixed to, whether this is extracellular matrix or polystyrene.[22] Therefore, in vitro study may not reflect the real situation in vivo.

To satisfy the needs of different cells and tissues, a variety of biomaterials that possess adjustable elasticity have been used to study cells in vitro under more physiologically relevant conditions.[22] However, the extent of this adjustability in the elasticity of biomaterials is limited, due to most biomaterials being formed from polymer gels. The rigid nature of the covalent bonding in polymer gels only allows for a small variation in the assembly of the polymers which results in gels with small variations in stiffness. An alternative to forming gels from covalently bonded polymers is to use LMWG.[23] LMWG are held together only by physical interactions, this allows for greater control in adjusting the physical properties of the gels such as stiffness and reversibility.[23]

4.1.4 Dopamine

In order to prepare electrochemical gels for use as a biomaterial especially for use in cell culture, it would be essential to find a biocompatible gelation trigger. HQ which has been used previously to form electrochemical LMWG, like in Chapter 3, is not biocompatible.[24] A typical material safety data sheet of HQ highlight its acute toxicity, corrosive irritation and possible carcinogen properties. Although HQ is not biocompatible, its electrochemical properties are fundamental to the electrochemical gelation of LWMG.[25] Therefore, an alternative to HQ that is biocompatible as well as displaying similar electrochemical properties is required to form electrochemical biomaterials. Under Prof. Dave Adams and my supervision, Euan Herdman, who completed a BSc research project in the group, investigated such alternative to HQ. The chemical found to be biocompatible as well as potentially having similar electrochemical properties to HQ was dopamine (Figure **4.2**).

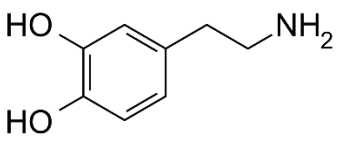

Figure 4.2 Chemical structure of dopamine.

Recently, there has been growing interest in the use of dopamine for surface modification to prevent microbial fouling.[26] The production of polydopamine has been reported to display antimicrobial activity owing to the autoxidation of

catechol in the presence of molecular oxygen to form semiquinone and quinone. During this oxidation process reactive oxygen species such as superoxide anions and hydrogen peroxide (H_2O_2) are generated as by-products.[27] Despite widespread interest in the use of polydopamine as an antimicrobial agent, there is still dispute as to the exact mechanism by which it develops. However, it is known that the self-polymerization process requires alkaline conditions and the presence of oxygen.[28] H_2O_2 is well known for its antimicrobial activity,[4, 29] and the sustained release of H_2O_2 generated as a result of the dopamine self-polymerization process has demonstrated a broad spectrum antimicrobial activity against Gram-positive and Gram-negative organisms.[27]

4.1.5 Summary

The self-assembly of the gelators to form LMWG is controlled by a decrease in the solubility of the gelator in solution. There are many different methods to reduce the solubility of the gelators.[30, 31] Here, we use a gelator where the solubility is controlled by pH. At high pH, the gelator disperses in water. When the pH is lowered, gelation occurs. Conventionally, this would be carried out using a mineral acid or *via* in situ hydrolysis of a lactone (see previous chapters). In this chapter, we show that the autoxidation of dopamine can be used to trigger a reduction in the pH and hence the solubility of gelator **1** in solution (Figure **4.3**). We show how we can control the antimicrobial properties of a gel by controlling the rate of gelation and gel stiffness. Furthermore, we show how the oxidation of dopamine can be controlled electrochemically to produce gels with different rheological properties with cell viability.

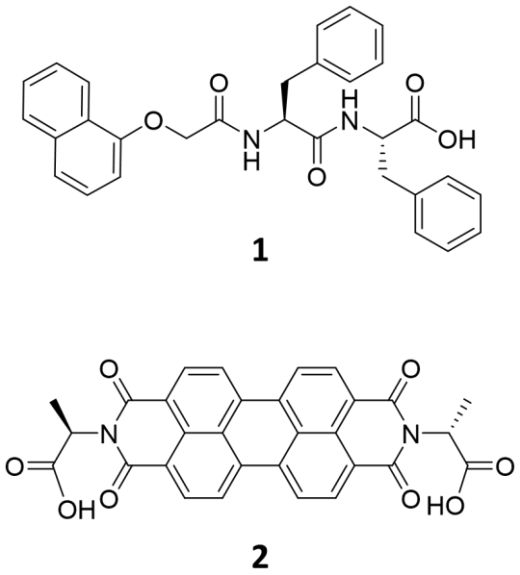

Figure 4.3 Chemical structures for gelators **1** and **2**

4.2 Experimental

4.2.1 Materials

Gelators **1** and **2** (Figure **4.3**) were prepared as previously reported.[32] [33] Gelator **1** was prepared by Prof. Dave Adams and Dr. Bart Dietrich (University of Glasgow) depending on the batch. All other chemicals were purchased from Sigma Aldrich and Fischer scientific and were used as received unless otherwise stated. Lysogeny broth, lysogeny agar and phosphate buffered saline (PBS) were prepared aseptically and autoclaved on site. De-ionised water was used throughout as the solvent.

4.2.2 Dopamine solution

A fresh 0.1 M solution of Dopamine in aqueous KCl (1 M) was prepared for use in electrochemical studies. The pH was adjusted to pH 8 using NaOH (0.01 M).

4.2.3 LMWG solution

LMWG solutions were prepared by weighing out 80 mg of **1** into 14 mL vials then adding deionised H_2O (7.39 mL) and NaOH (aq. 0.1 M, one molar equivalent, 1.61 mL) to a volume of 9 mL. The solution was stirred overnight to ensure all gelator had dissolved. The gelator solutions were then pH adjusted to 8 with HCl (0.5 M) and de-ionised water, ensuring that the final volume was 10 mL which provides solutions at a final concentration of gelator of 8 mg/mL. Solutions were stored at room temperature.

Just before growing gels electrochemically 50 mg of dopamine was added to 10 mL of gelator solution followed by 100 µL of 0.1 M NaCl. The solution was vigorously swirled to ensure the dopamine was dissolved then placed into the electrochemical cell for gel growth.

4.2.4 Electrochemistry set up

As described in Section 3.2.4, an electrochemical cell with dimensions 2.5 cm x 2 cm x 7 cm (HxWxL) containing three electrodes (glassy carbon working electrode, Ag/AgCl (3 M) reference and platinum wire counter electrodes) was set up as shown in Figure **4.4**. The prepared LMWG solution was poured into the

electrochemical cell for cell growth. It is essential that the gelator solution is not left to oxidise over a long period of time, should the solution turn orange a fresh solution should be prepared.

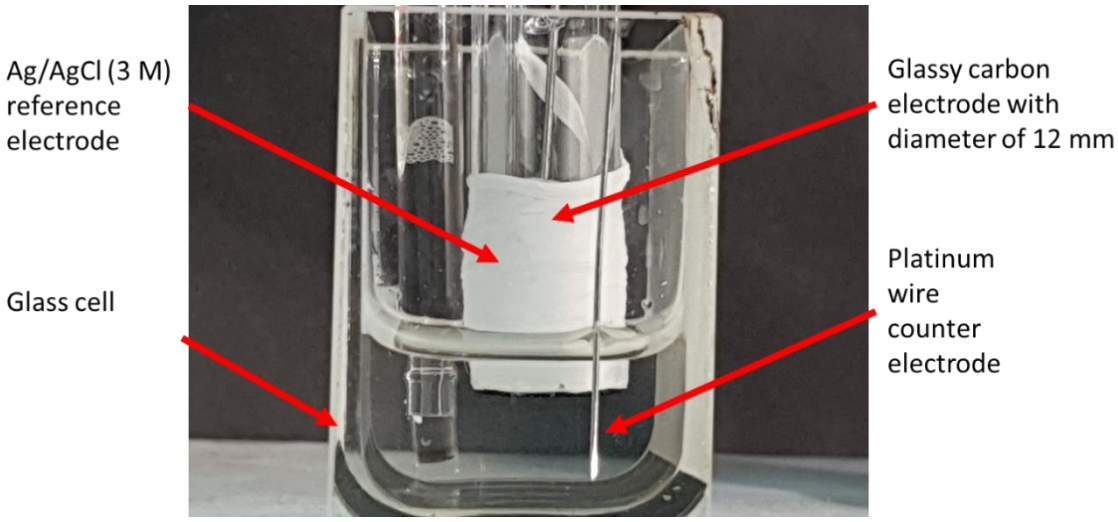

Figure 4.4 Image of electrochemical cell set up. Inside the cubic cell the working electrode is the glassy carbon electrode, the counter electrode is connected to the platinum wire and the reference electrode is the Ag/AgCl (3 M) reference electrode.

Before using the glassy carbon electrode, it is polished using diamond polish with decreasing particle size (10, 3 then 1 μm). Polishing is continued with a fine alumina slurry polish. Polishing was carried out in a figure of 8 motion to ensure a flat electrode surface. The electrode was then placed in distilled water and sonicated for 1 minute to remove and alumina debris.

4.2.5 Cyclic voltammetry

All experiments were run using a Dropsens Potentiostat and a three-electrode system. The working electrode was a glassy carbon electrode, a platinum wire counter was used with a Ag/AgCl (3 M) reference electrode as described in Section 3.2.4. Cyclic voltammetry (CV) measurements were carried out within a potential range of -0.5 to 0.2 V vs. an Ag/AgCl (3 M) reference electrode at a scan rate of 20, 40, 60, 80, 100, 200, 400, 600, 800, 1000 mV/s. Each CV measurement consisted of one scan.

4.2.6 Fast potentiometry

Fast potentiometry was used to grown gels on the working electrode. Gelator solution as describe in Section 3.2.3 was placed into the electrochemical set up (see Section 3.2.4). A current between the range of 1000 and 2000 μA was applied for between 270 to 810 seconds. During this time the potential passed the oxidation potential of dopamine at ~0.5 V which results in a gel being formed on the electrode surface. Once the applied current has stopped the gel was carefully removed from the electrode surface using a scalpel.

4.2.7 Image analysis

Images of gelation were taken every 30 seconds using a mobile phone camera. These images were uploaded to the open source image analysis software 'ImageJ'. The outline of the gel can be traced, and the area of gel calculated.

4.2.8 Rheology

As described in Section 3.2.8, rheological measurements were carried out using an Anton Paar Physical MCR301 rheometer. Parallel plates (12.5 mm diameter, smooth) were used to measure frequency sweeps. For measuring the frequency sweeps, the gels were removed from the electrode surface using a scalpel and placed onto the rheometer. Rheological measurements were recorded at 25 °C. Figure **3.4**a) shows the gel carefully placed onto the bottom parallel plate while b) shows the top plate once it has been lowered to a gap of 2 mm.

a)

b)

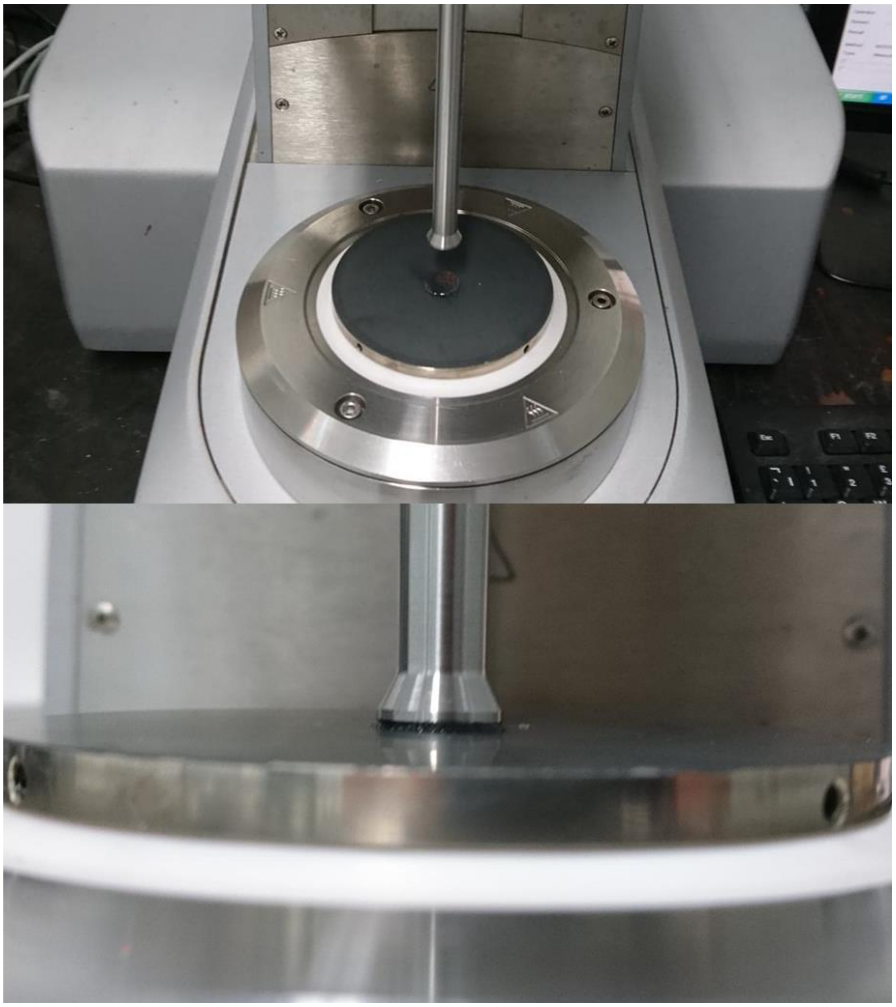

Figure 4.5 Images of an electrochemically grown gel a) carefully placed on the bottom parallel plate. b) The top parallel plate is lowered and sandwiches the gel between the bottom and top plate.

Frequency sweep: Frequency scans were performed from 1 rad/s to 100 rad/s under a constant strain of 0.5%. Measurements were performed in duplicate and errors were calculated from the standard deviation.

4.2.9 Small angle neutron scattering (SANS)

Small Angle Neutron Scattering was carried out by Ana María Fuentes Caparrós and Kate McAulay (both University of Glasgow) at the Institut Laue Langevin with help from Ralf Schweins (Institut Laue Langevin). The data were fitted and interpreted by Dave Adams.

The solutions were prepared as described above in D_2O using NaOD (0.1 M) and DCl (0.1 M) to adjust the pH. SANS measurements were performed using the D11 instrument at the Institut Laue Langevin, Grenoble, France. A neutron beam with a fixed wavelength of 6 Å and divergence of $\Delta\lambda/\lambda$ = 9% was used to carry out measurements over a Q range ($Q = 4\pi\sin(\theta/2)/\lambda$) of 0.001 to 0.3 $Å^{-1}$ using three sample-detector distances of 1.5 m, 8 m, and 39 m.

Gels were prepared in UV spectrophotometer grade, quartz cuvettes (Hellma) with a 2 mm path length. These were placed in a temperature-controlled sample rack during the measurements. Prior to measurement but post irradiation, the samples were wrapped in tinfoil to prevent any further accidental light irradiation.

The data were then reduced to 1D scattering curves of intensity vs. Q using the facility provided software. The electronic background was subtracted, the full detector images for all data were normalized and scattering from the empty cell was subtracted. The scattering from D_2O was also measured and subtracted from the data. The instrument-independent data were then fitted to the models discussed in the text using the SasView 4.2.0 software package version.[34]

4.2.9.1 Cell viability studies

Cell viability studies were carried out by Sam Donnelly (University of Glasgow). Electrochemical gels were grown and placed into 30 mL of pH 7.14 water solution to allow for any residual dopamine to diffuse out of the gel pores. Bulk dopamine gels were prepared by adding the dopamine solution as described in into a 12 well plate and allow to gel overnight, The gels were removed from the 12 well plate by adding pH 7.14 water on top of the gel which caused the gel to float and could easily be lifted out of the plate. The gels were then placed into 30 mL of pH 7.14 water solution to allow for any residual dopamine to diffuse out of the gel pores.

4.2.9.2 Seeding cells

The cells were seeded in a 12-well tissue culture plate (Croning) at a density of around 10,000 cells per well. The media was removed *via* a pipette from the flask of cells and washed twice with PBS buffer to maintain physiological. 3 mL of Trypsin-EDTA solution was then used to remove the cells from the culture vessel into suspension. The plate was placed in the incubator for 5 minutes, checking for

cell detachment. 3 mL of media was added to the cells to stop trypinisation. The cells were then transferred to a plastic universal centrifuge at 1400 rpm for 4 minutes. Finally, the media was poured off and resuspending in 1 mL of media for counting.

4.2.9.3 Cell counting

These steps follow on after resuspension in 1 mL. 10 µL of cell suspension was removed and placed in a 0.5 mL Eppendorf tube followed by 10 µL of trypan blue. This mixture was pipetted onto the cell counting chamber of the haemocytometer. Using a microscope, we were able to count the number of cells within the counting grids. The total approximate number of cells per 1 mL could calculated using Equation **4.1**. The cells were then resuspended in the appropriate volume and seeded for later use.

$$Number\ of\ cells = \frac{number\ counted}{number\ of\ grids\ counted} \times 2 \times 10^4\ cells/mL$$

Equation 4.1 Used for counting the total number of cells within a cell counting grid.

4.2.9.4 Adding gels

The cells were seeded at an appropriate density (10,000 cells/mL in 96 well plate), where they are left to adhere in the plate for 48 hours. Afterwards, the gels are placed in the wells on top of the cells. These were left, feeding where possible, until we used them for staining. Three wells were left with no gel to act as 2D controls.

4.2.9.5 Live/dead staining

We used a 1000 µL assay solution per sample in the 12 well plate. The assay solution was made up from 4 µM ethidium homodimer-1 and 2 µM Calcein-AM reagents. We added the calculated amount of each dye to PBS to create the volume of solution relevant to the number of samples. Ethidium homodimer-1 was used as it stains dead cells nuclei red indicating loss of plasma membrane integrity as it is a cell-impemeable dye. Calcein-AM was used as it is a cell-permeable dye

which indicates intracellular esterase activity seen in live cells by staining with green fluorescence.

The media was removed from the samples and washed twice with PBS. The assay solution was added to the samples and left in an incubator for 10 minutes. After this period, the assay solution was removed and the samples were again, washed twice with PBS. The PBS was not removed from the samples to prevent cell drying during imaging

4.2.10 Bacterial susceptibility assay

These data were collected by Sophie Coulter and Garry Laverty (Queens University, Belfast). *Staphylococcus aureus* NCTC 10788, *Staphylococcus epidermidis* ATCC 12228, *Pseudomonas aeruginosa* ATCC 15692 *and Escherichia coli* ATCC 15597 were subcultured for 18 hours at 37 ^{o}C in Lysogeny broth and adjusted to an optical density reading of 0.3 at 550 nm in PBS, corresponding to $1x10^{8}$ CFU/mL, and further diluted (1 in 50) in broth.

100 µL of bacterial suspension was then plated into each well of a microtiter plate containing 100 µL of gelator. Control wells included bacteria in broth as a growth control (100% survival), PBS alone as a negative, sterility control and 2% w/v (hydroxypropyl)methyl cellulose (HPMC) as an inert hydrogel to examine the effect of gelation on bacterial viability.

Inoculated microtiter plates were incubated for 24 hours at 37 ^{o}C and 20 µL samples were taken from each well, serially diluted in PBS (10^{-1} to 10^{-8}) and transferred to Lysogeny agar plates for colony counting *via* the Miles and Misra technique.[35] Each experiment was performed in triplicate and results were displayed as the mean (Log_{10} CFU/mL) of nine replicates.

4.2.11 pH measurements

pH measurements were recorded using a Hannah PC turtle FC500 pH probe with a given error of ± 0.1.

4.2.12 UV/vis spectroscopy

Measurements were carried out on an Agilent Cary 60 UV−Vis spectrophotometer. Gel samples for UV-vis absorptions were placed into a placed in a demountable 2 mm quartz cuvette. Samples were irradiated with a 365 nm light emitting diode (LED) for 15 minutes and the spectra collected.

4.3 Results and discussion

4.3.1 Dopamine autoxidation

Dopamine oxidises in air to produce dopamineoquinone and protons (Figure **4.6**).[36, 37] The quinone undergoes intramolecular Michael addition forming aminochrome.[37] This aminochrome can further polymerise into neuromelanin which is dark brown in colour. Several studies on the kinetic behaviour of dopamine autoxidation have been carried out.[38-40] The summary of these kinetic studies suggest that the autoxidation of dopamine is strongly pH-dependent with the rate of autoxidation faster at higher pH.[40] The increase in rate is due to the abundance of hydroxide ions which are required in the intramolecular Michael addition step. Babbit, Lloyd and more recently Salomäki et al. report the rate constant for the formation of aminochrome is first order.[38, 39, 41] At low pH, the Michael addition is the rate limiting step.[38] If we are able to control the rate of dopamine oxidation, we should be able to control the gelation kinetics of self-assembly.

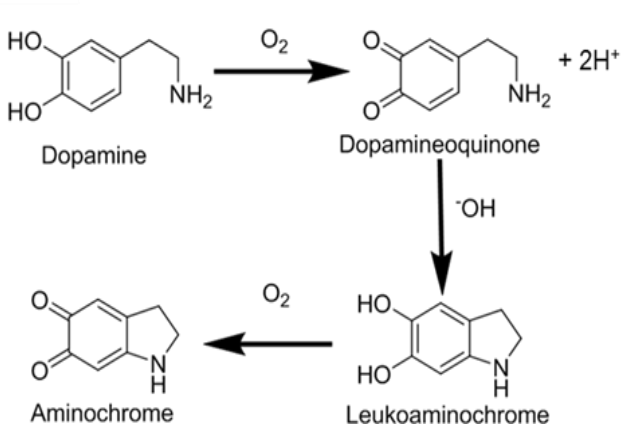

Figure 4.6 Oxidation pathway of dopamine, initial oxidation step produces protons which lowers the pH of the bulk gelator solution, this triggers self-assembly of the gelator molecules. A Michael addition and further oxidation forms the brown pigment leukoaminochrome and aminochrome.

Solutions of **1** were prepared at different initial pH values of 7, 8, 9 and 10 at a concentration of 8 mg/mL. The apparent pK_a of **1** is 6.8 and hence **1** is expected to be de-protonated in all these solutions.[42] All solutions were viscous, as expected as **1** assembles into worm-like micelles at these pH values.[43] In all cases, no

gelation occurs with time for these solutions. However, a gel was formed when dopamine (3 mg) was added to a solution of gelator **1** (16 mg in 2 mL) at pH 8**.** To determine whether the effect of gelation was due to the oxidation products of dopamine or the electrostatic interactions between dopamine and the gelator in solution, two gelator solutions were prepared, one under a nitrogen atmosphere and the other under air. After 16 hours, the solution of **1** and dopamine which was under nitrogen did not form a gel whereas a gel was formed from the mixture in air. Furthermore, a brown colour gradient could be observed with a dark brown colour at the gel and air interface which faded into the bulk solution as shown in Figure **4.7**. This led us to conclude that the oxidation of dopamine in air triggers gelation.

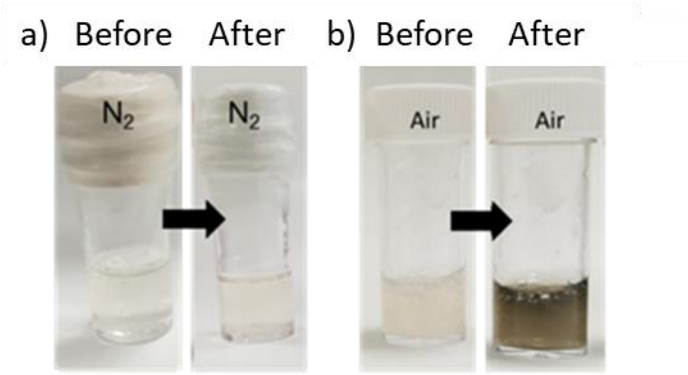

Figure 4.7 a) and b) show solutions of **1** (8 mg/mL, 2 mL sample) with dopamine (6 mg) under an atmosphere of a) N_2 and b) air. The left-hand sample in both a) and b) show the solution before gelation and the right-hand sample shows the solution after 16 hours. Oxidation products of dopamine cause brown colour when the solution is left in air, which is absent under N_2.

4.3.1.1 Effect of pH on dopamine autoxidation

To investigate the effect of pH on the rate of dopamine oxidation and gelation, dopamine (3 mg/mL) was added to stock solutions of **1** (8 mg/mL) at a pH of 7, 8, 9 or 10. After 16 hours, in all cases, the sample could be inverted without flow. Again, the dark brown colour gradient starting from the gel/air interface was observed (Figure **4.8**). For the samples at the higher initial pH, the brown colour extended further into the bulk solution; for the sample starting at pH 7 the brown colour was only observed near the gel-air interface. We assume that this brown

colour corresponds to the presence of dopamine oxidation products and polydopamine which are highly coloured.[44] In all cases, after 16 hours, the pH of the solution was between 7.0 and 7.3.

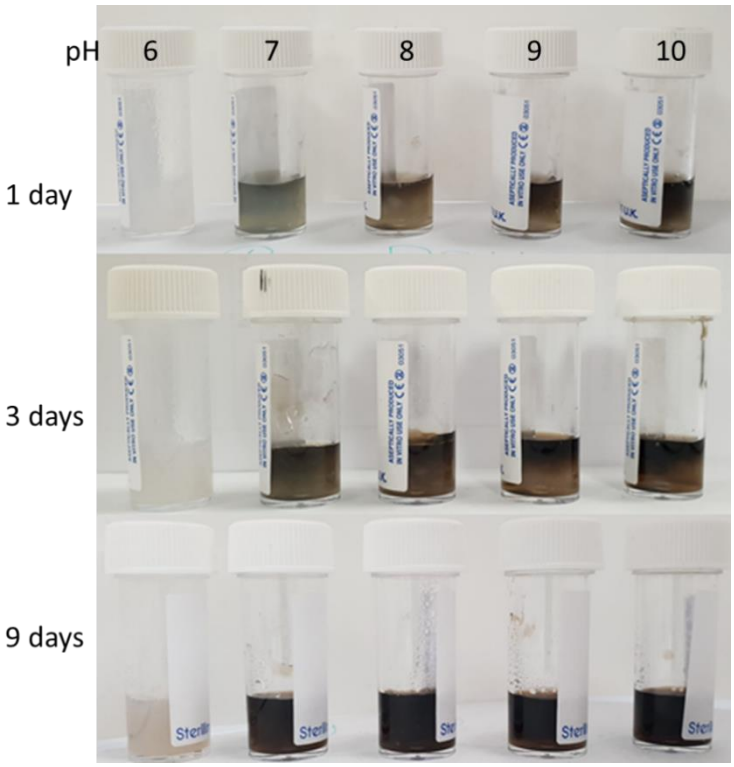

Figure 4.8 Images of gels containing **1** and dopamine over 1, 3 and 9 days. The initial pH of the gelator solutions vary from pH 6, 7, 8, 9 and 10.

Rheological analysis was carried out to further investigate the effect of the initial pH of the gelator solution pH on the final gel properties. Frequency and strain sweeps were used to determine the stiffness and breaking points of the gels (Figure **4.9**a). All gels show frequency independence at the measured 0.1-100 rad/s angular frequency. Remarkably, a linear relationship between the gel stiffness and the pH of the starting solution was observed (Figure **4.9**). We describe this linear relationship as an effect of the first order rate kinetics of dopamine oxidation.[38] As the pH decreases, the rate of dopamine oxidation is slower, and this results in stiffer gels. This phenomenon of gel stiffness being controlled with the rate of gelation has been previously seen in other low molecular weight hydrogels.[45]

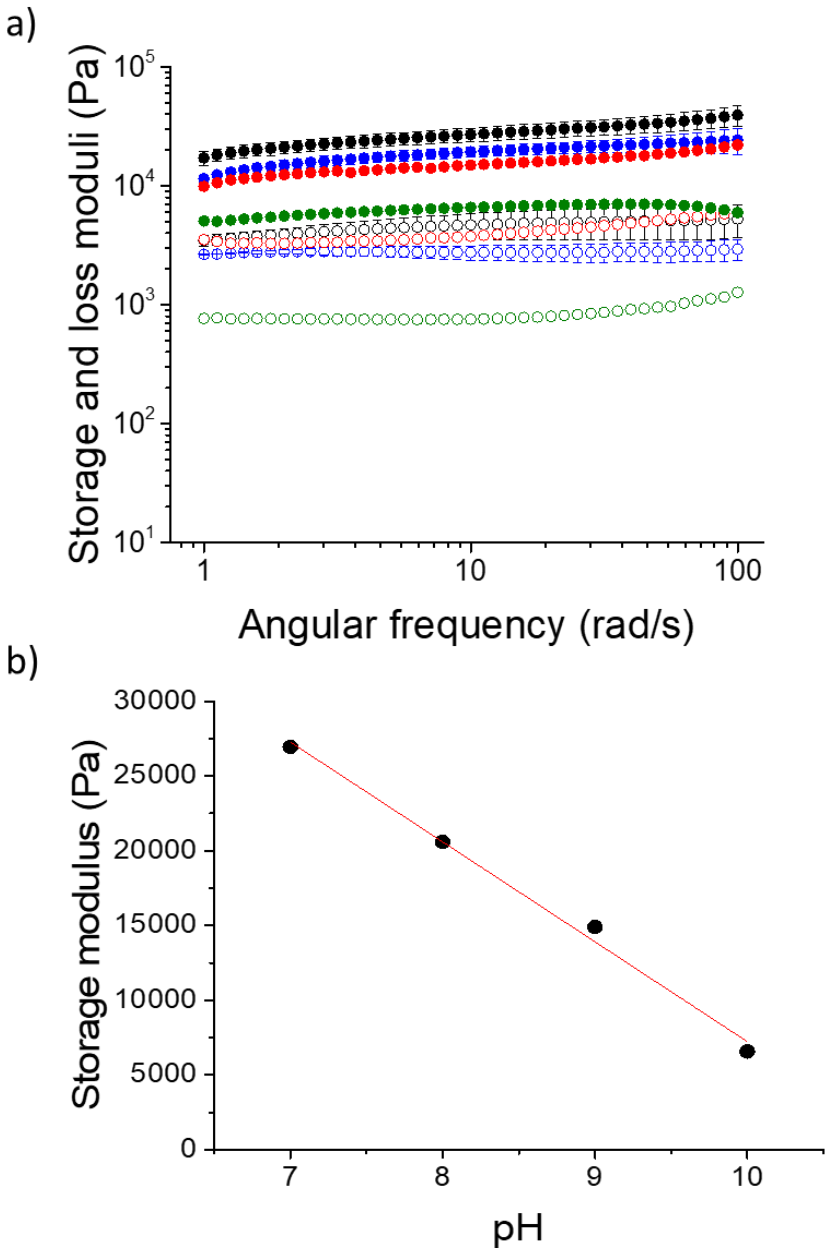

Figure 4.9 a) Frequency sweep showing the storage and loss moduli of gels formed from **1** on adding dopamine to at an initial pH of 7 (black), 8 (blue), 9 (red) and 10 (green), storage moduli have closed circles, loss moduli have open circles. b) Storage moduli at a frequency of 10 rad/s versus pH. The linear regression (r^2) is 0.98988.

4.3.1.2 Small angle neutron scattering (SANS)

We further probed the fibre properties of the gels using small angle neutron scattering (SANS). The collection of small angle neutron scattering data was carried out by Ana María Fuentes Caparrós and Kate McAulay, the data was interpreted by Dave Adams (all University of Glasgow).

For the gels formed from initial pH values of 7, 8, and 9, the data can be fitted to a core-shell model combined with a power law to take into account the scattering at low Q. The full scattering data and fits are shown in **Figure 4.10** and Table **4.1**. The fits imply that the core is larger for the gels formed from the initial pH 7 solutions, whilst those formed from the solutions at pH 8 and 9 are very similar. There is a hydrated shell around the fibres, which increase in size as the initial pH is lower. The scattering length density (SLD) is higher than would be expected from the structure of polydopamine and we suspect that this implies that the coating is highly hydrated. This suggests that the slow oxidation at the initially lower pH results in a polydopamine 'shell' forming around the fibres. The data for the sample that was initially pH 10 fits best to a cylinder combined with a power law. This implies that at the initially high pH, the fast rate means no coating forms. Hence, it is likely that the gel stiffness is affected by the presence of a polydopamine coating in some cases, which may result in cross-links between fibres.

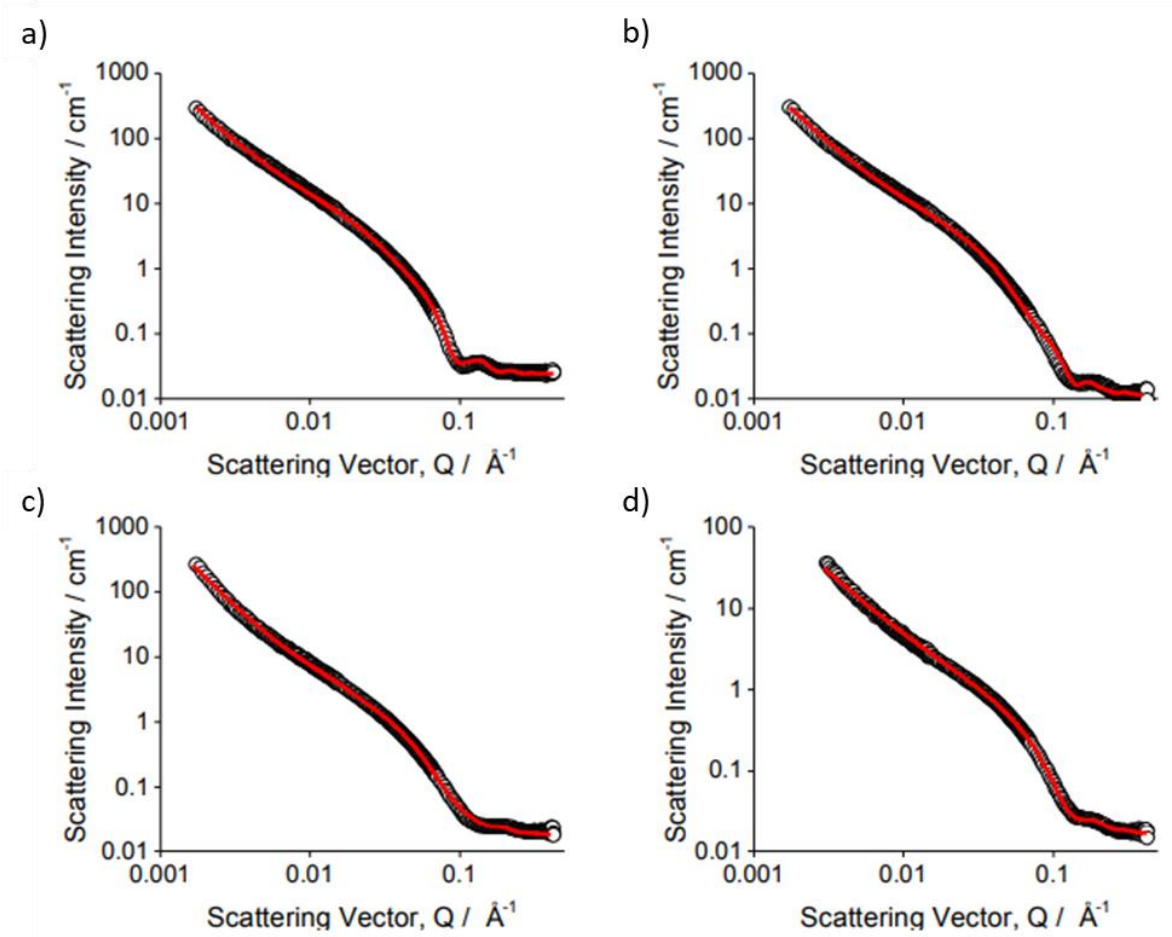

Figure 4.10 SANS data (black circles) and fits described in Table **4.1** (red lines) for gels formed over time from solutions of gelator 1 and dopamine starting at a pH of a) 7, b) 8, c) 9, d) 10.

Table 4.1 Fitting parameters obtained for gels formed from solutions of gelator **1** and dopamine starting at an inital pH of 7, 8, 9, or 10. The data for the gels formed from solutions at an initial pH of 7, 8 and 9 were fitted to a core-shell model combined with a power law. The data for the gels formed from solutions at an initial pH of 10 were fitted to a cylinder model combined with a power law. * Due to the fit not fully capturing the data at low Q, the data were fitted over the range of 0.003<Q $Å^{-1}$.

	Initially pH 7	Initially pH 8	Initially pH 9	Initially pH 10*
Background (cm^{-1})	0.024 ± $4.77x10^{-5}$	0.011 ± $4.06x10^{-5}$	0.020 ± $5.00x10^{-5}$	0.015 ± $6.89x10^{-5}$
Scale	0.051 ± 0.002	0.033 ± 0.0001	0.0019 ± $1.19x10^{-6}$	0.0034 ± $1.00x10^{-5}$
Length (Å)	971 ± 15	>1000	294 ± 4	>3000
Radius (Å)	38.0 ± 0.03	27.1 ± 0.03	29.9 ± 0.04	26.7 ± 0.03
Thickness (Å)	79.7 ± 0.3	44.8 ± 0.1	30.0 ± 0.2	
Scattering Length Density (Shell, $x10^{-6}$ $Å^{-2}$)	6.21 ± 2	6.00 ± 0.1	5.85 ± 0.1	
Scale	$3.44x10^{-5}$ ± $8.47 x10^{-6}$	$4.30x10^{-5}$ ± $8.69x10^{-6}$	$4.25x10^{-5}$ ± 1.17x10-6	$2.23x10^{-4}$ ± $4.64x10^{-5}$
Power Law	2.50 ± 0.01	2.45 ± 0.01	2.44 ± 0.01	1.97 ± 0.01
χ^2	14.7	39.7	18.4	6.98

4.3.1.3 Bacteria susceptibility

Bacterial susceptibility assays were performed to assess antimicrobial activity of the gels and to examine whether there was any correlation between final gel stiffness, initial pH, polydopamine/H_2O_2 production and antimicrobial activity. In order to do this, bacterial susceptibility assays were performed against clinically relevant Gram-positive and Gram-negative organisms with the ability to reduce bacterial viability measured using a colony counting method. A (hydroxypropyl)methyl cellulose (HPMC) control was employed as an inert gelator to ensure that the process of gel removal had no effect on the bacterial viability.[46, 47] These data was collected by Sophie Coulter and Garry Laverty (Queens University, Belfast).

Antimicrobial activity was observed against the Gram-positive bacteria *Staphylococcus aureus* when pH 10 was used to initiate gelation and

Staphylococcus epidermidis when both pH 9 and 10 were used to initiate gelation (Figure **4.11**). We highlight again that all gels once formed were at a pH of between 7.0 and 7.3. In each case, at least a three log reduction in bacterial counts was observed and this was used to denote clinical significance.[48] Remarkably, the antimicrobial properties increased as the gel stiffness decreased This contrasts with other studies relating to the antimicrobial activity of peptide gelators. For example, work by Jiang et al. demonstrated a correlation between an increase in storage modulus and more effective bacterial inhibition and suggested that increased storage modulus provides the required mechanical support for individual nanofibres and fibrous networks to direct their desirable chemical and biological functionalities against bacteria.[46] This leads us to believe that the differences observed in antimicrobial activity seen here are likely due to the production of polydopamine and reactive oxygen species rather than the gelator itself. If the gelator alone were responsible for the antimicrobial activity, then it would be expected that an increase in stiffness should result in an increase in antimicrobial activity in line with other studies.

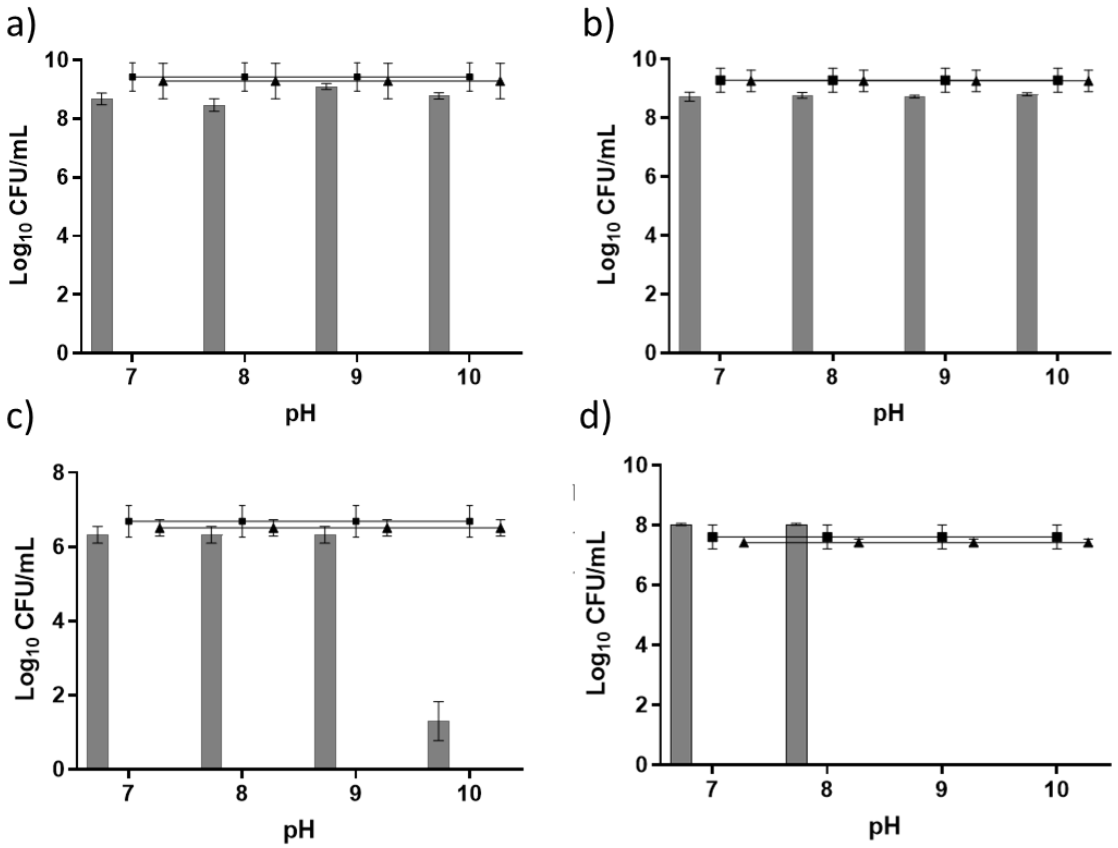

Figure 4.11 Bacterial susceptibility assays for a) *Pseudomonas aeruginosa* ATCC 15692 b) *Escherichia coli* ATCC 15597 c) *Staphylococcus aureus* NCTC 10788 and d) *Staphylococcus epidermidis* ATCC 12228. In both parts, gels of **1** formed at different initial pH values with dopamine are shown as grey bars, positive control as black triangles, HPMC controls as black square.

We suggest that with increasing pH used for initiating gelation, there is an increase in the rate of polydopamine production and therefore a subsequent increase in H_2O_2 release. Ball et al. investigated the kinetics of the formation of polydopamine films under various pH conditions and found that the thickness of the film formed increased from pH 5.5 to pH 8 indicating that more polydopamine was produced under increasing alkaline conditions.[49] The decrease in gel stiffness and fibre entanglement observed for gels produced under a higher pH may promote diffusion of H_2O_2 through the network pores to enable increased interaction with bacterial cell membranes and intracellular targets (e.g. DNA) thereby enabling a bactericidal effect.[50] The lack of activity observed for Gram-negative organisms may be due to differences in the membrane architecture or detoxification of reactive oxygen species. The additional outer lipopolysaccharide membrane in

Gram-negative organisms well documented for its ability to limit the influx and uptake of antibiotic molecules, including reactive oxgen species.[51] Bacteria also demonstrate an ability to reduce the damaging effects of reactive oxygen species through the production of neutralising molecules such as the exopolysaccharide Psl in biofilm forming isolates of *P. aeruginosa*.[52] Interestingly, work by Forooshani et al. found the sustained release of low doses of H_2O_2, generated during polydopamine production, was sufficient to achieve broad spectrum activity against both Gram-positive and Gram-negative bacteria.[27] Antibacterial efficacy may therefore be a concentration dependent effect reliant on the rate at which H_2O_2 or other reactive oxygen species are produced within the system. Gram-negative microorganisms demonstrate increased resistance to reactive oxygen species, requiring increased exposure time or concentration to achieve significant apoptosis events.[27]

4.3.2 Electrochemical oxidation of dopamine

To investigate whether the electrochemical oxidation of dopamine could be used to grow gels, a comparison between the electrochemical properties of HQ, used in Chapter 3, was carried out. Figure **4.12** a) shows the electrochemical reversibility of HQ. When HQ is oxidised around 0.5 V it produces benzoquinone and protons. We can compare this to dopamine (Figure **4.12** b), when we apply a potential of around 0.6 V the oxidation products aminochrome and protons are formed. This suggests there is potential for using dopamine as an alternative trigger to HQ for pH triggered gelation.

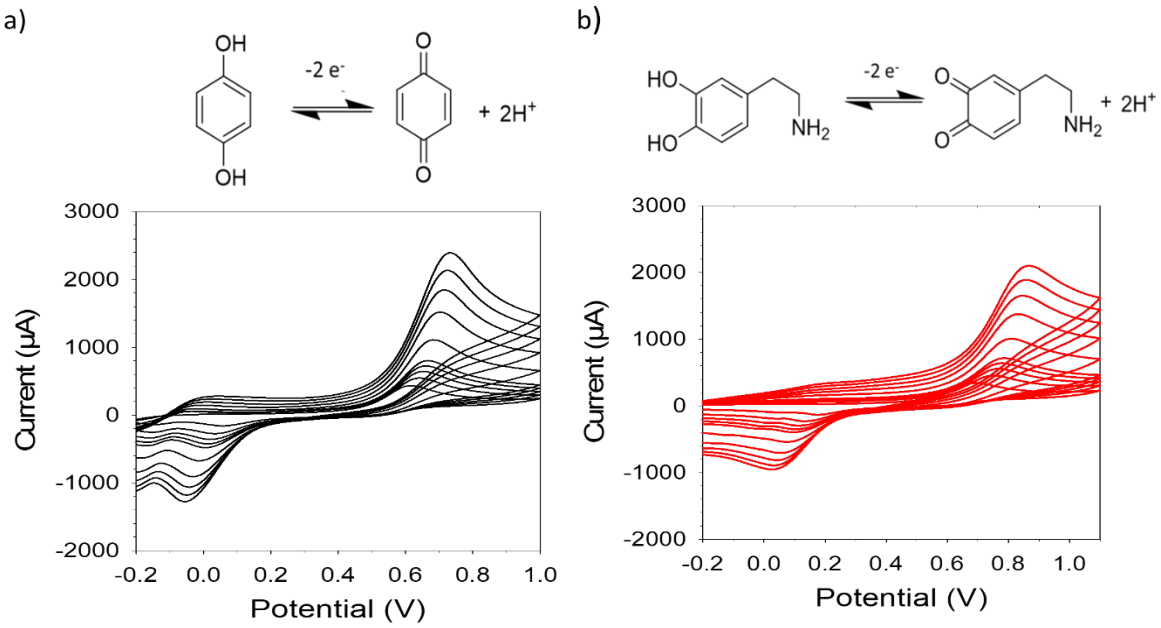

Figure 4.12 The cyclic voltammetry with increasing scan rate for a) HQ (5 mM) and b) dopamine (5 mM), both in a KCl (1 M) solution. Scan rates measured at 0.02, 0.04, 0.06, 0.08, 0.10, 0.20, 0.40, 0.60, 0.80 and 1.00 V/s vs Ag/AgCl (3M) ref. electrode.

To electrochemically control the oxidation of dopamine, dopamine (5 mg/mL) was added to a 10 mL solution of **1**. Cyclic voltammetry was swept passed the oxidation of dopamine which resulted in a thin film of gel on the electrode surface (Figure **4.13**). This showed that the oxidation of dopamine could trigger gelation. With the potential for using these materials in regenerative medicine it would be ideal for us to control gel stiffness in order to replicate in vivo conditions. As demonstrated in Chapter 3, two current values within the oxidation range of the trigger can be used to grow gels at different rates. The lower current oxidises dopamine slowly therefore gelation is slower and *vice versa*.

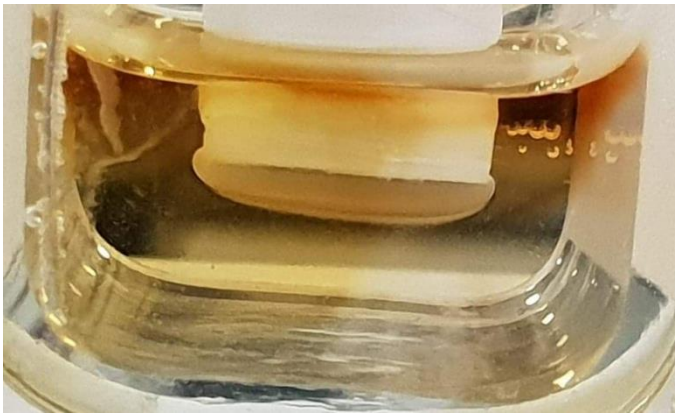

Figure 4.13 Thin film gel formed from gelator **1** on a glassy carbon electrode.

Two current values, 500 μA and 1250 μA were chosen to grow gels. Gels grown at 500 μA we will call **1a** and gels formed at 1250μA we will call **1b**. These gels were grown by fast potentiomenty for 540 s and 270 s respectively, this ensured the gel thicknesses were even (Figure **4.14**). Like in Chapter 3 it is important for the gel thickness for all samples to be equal to ensure rheological data is comparable.

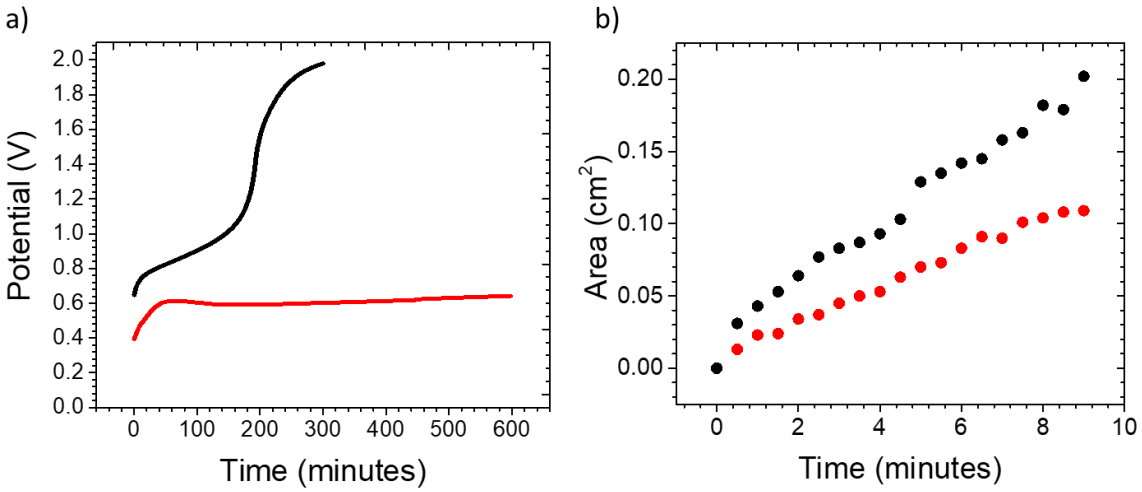

Figure 4.14 a) Fast potentiometry for gel **1a** grown at 500 μA (red) and gel **1b** at grown at 1250 μA (black). b) corresponding gel growth areas for **1a** (red) and **1b** (black).

4.3.2.1 Rheology

The rheological properties of gels **1a** and **1b** were measured. Both gels measured showed linear viscoelastic properties in the measured frequency range of 1-100 rad/s with reproducible data shown in Figure **4.15**. The frequency sweeps showed

significant differences between the stiffness of **1b** compared to **1a**, with **1b** being stiffer. These data suggest there are structural differences within the networks of the gels.

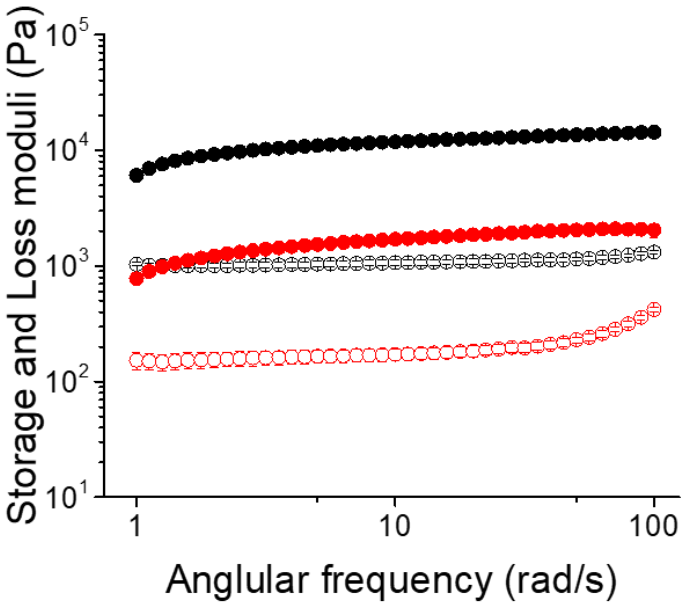

Figure 4.15 Rheological frequency sweep of **1a** (red) and **1b** (black). In both cases the full circles represent the storage modulus and the hollow circles show the loss modulus. Frequency sweeps were measured under a constant strain of 0.5 %

4.3.2.2 Cell viability

The autoxidation of dopamine required a minimum concentration of 3 mg/mL of gelator solution to form a gel after 16 hours. This resulted in the dopamine to gelator ratio of 0.375:1. This high level of dopamine aided its antimicrobial properties. In comparison, the electrochemical oxidation of dopamine only required a ratio of dopamine to gelator of 0.00424:1. This low level of dopamine may allow for cells to be cultured within the gels.

Cell viability studies were conducted to determine whether the gels were cytotoxic. The cell viability studies were carried out by Sam Donnelly (University of Glasgow). Gels were grown and placed into pH 7.14 water solution to allow for any residual dopamine to diffuse out of the gel pores, this would also lower the dopamine to gelator ratio. After 16 hours, the gels were placed into 12 well plates and a combination of cells and cell media were placed on top of the gels and into

an incubator at 37 °C. After 24 hours a live dead study was carried out to determine the cell viability of the gels. We observed gels grown by HQ oxidation were not cell viable however, gels grown by dopamine oxidation were cell viable. In addition, we tested the cell viability of gel **1** formed by the autoxidation of dopamine. As predicted the high concentration of dopamine present in the bulk gel samples lead to cell death. Figure **4.16** show the live stained cells in the presence of the electrochemically oxidised dopamine gel after 24 hours as well as the viability of the gels.

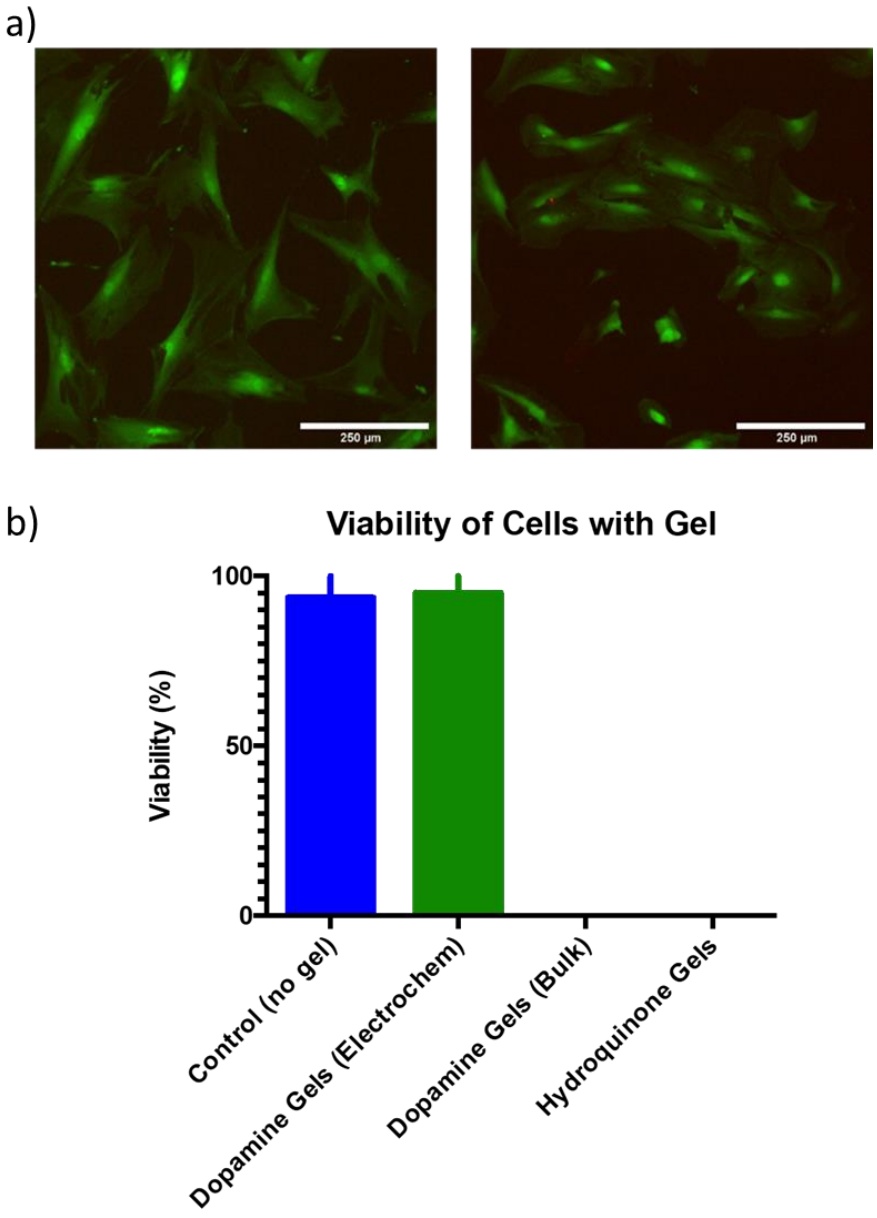

Figure 4.16 a) Image of stained cells in gel **1a** after 24 hours b) Cell viability of **1** formed from the electrochemical oxidation of dopamine, the electrochemical oxidation of HQ as well as from the autoxidation of dopamine and 2D control.

As the gelator molecule used to form gels **1a** and **1b** does not have cell binding sites, there is potential for development of electrochemical gels using gelators with cell binding sites, this would allow the cells to bind directly to the gel fibres. The gels themselves will provide a hypoxic environment that can better simulate in vivo conditions as a lot of the tissue in the body is hypoxic particularly in tumours. The gels could also be used to house drugs, cytokines or growth factors which influence the cells overtime. There is also a therapeutic interest in the future for drug release within the body.[53]

4.3.2.3 Photoconductive gels

Preparing thin film gels electrochemically has great potential for use in optoelectronics such as organic photovoltaic devices (OPV). However, using a trigger such as HQ could lead to recombination of the radical anion produced when irradiating the gelator, as HQ is a known radical scavenger.[54, 55] A possible recombination mechanism for HQ and gelator **2** is shown in Figure **4.17**.

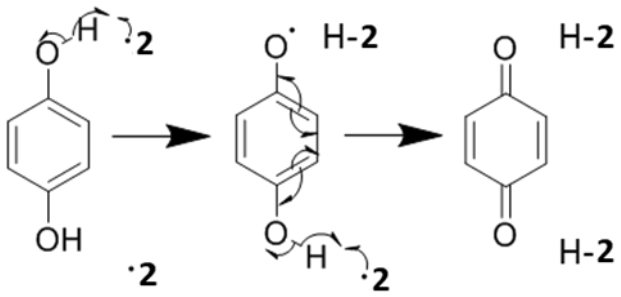

Figure 4.17 A possible recombination mechanism for HQ and **2.**

To identify whether radical scavenging behaviour is observed for electrochemical gels formed by HQ and dopamine triggers, a known photoconductive gel was prepared using gelator **2** on a glassy carbon electrode (Figure **4.3**).

Gel **2** was prepared with either HQ and dopamine and placed into a 2 mm quartz cuvette for UV-Vis studies. When the radical anions from **2** are present, peaks are typically observed around 735, 820 and 1000 nm, this can vary depending upon the aggregation of the gelator molecules.[56] Figure **4.18** shows the UV-Vis spectroscopy for gel **2** prepared using the electrochemically triggers HQ and dopamine before and after irradiation with light at 365 nm wavelength for 10

minutes. The spectra produced from the HQ-triggered gel show a broad peak between 700 and 900 nm before irradiation. This could potentially be from an aggregate formed of **2** and HQ. Although, there is no literature which identifies the aggregates formed between HQ and **2**, Chua et al. show how conjugated small molecules, similar to **2** can absorbed infra-red light when in the presence of HQ.[57] After irradiation of the HQ-triggered gel, no peaks within the radical anion region between 735-1000 were observed. This suggests HQ is quenching the radical anion produced by the gelator. The broad peak that was observed between 700 and 900 nm before irradiation has disappeared, which may be a result in a change of the aggregated structure between **2** and the scavenged product benzoquinone. This further aids to the theory that HQ is being used to scavenge the radical from **2**.

In contrast, gel **2** prepared using dopamine does not have any peaks within the 700 and 900 nm range before irradiation. After irradiation peaks at 735, 820 and 920 nm are observed, which fall within the range where we would expect to see the radicals of **2** to be formed.[56]

From these data we show how different triggers used to prepare electrochemically grown hydrogels by oxidation, can influence the optoelectronic properties of the gel. This development in electrochemically grown hydrogels may now allow for the preparation of intricate OPV devices with enhanced photoconductive properties compared to gels prepared in bulk.

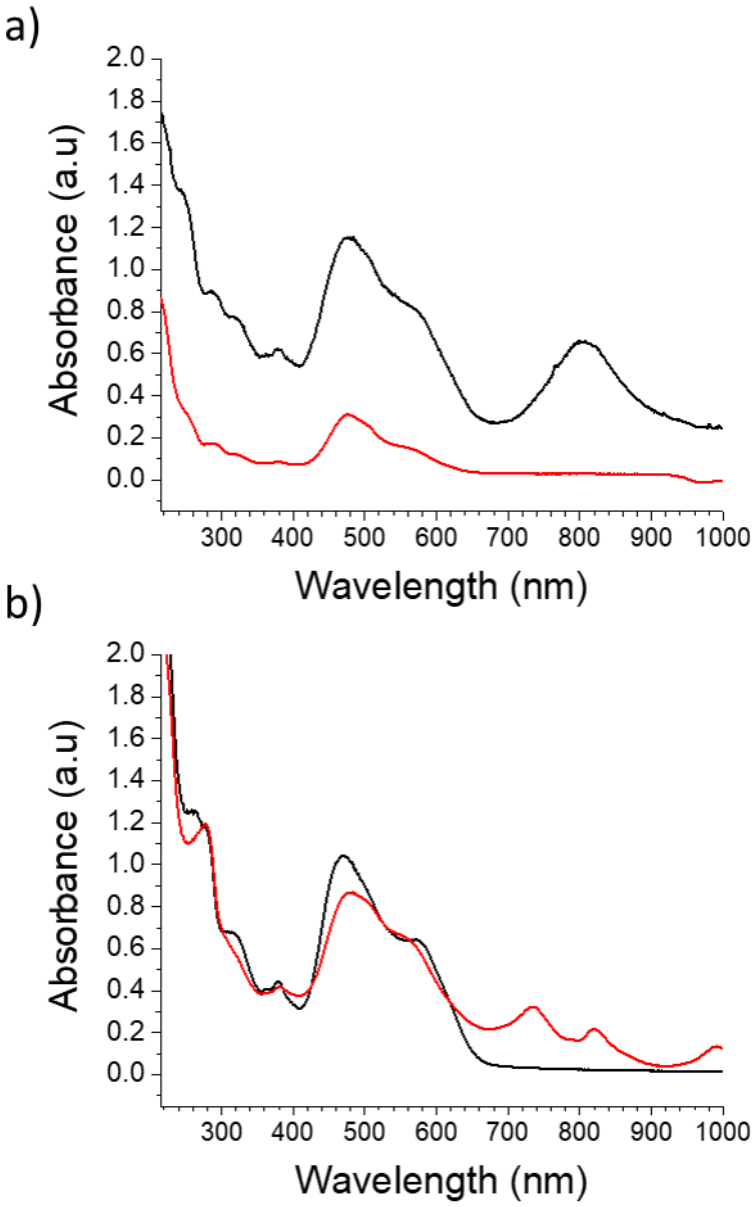

Figure 4.18 UV-Vis spectra of gel **2** prepared using a) HQ before (black) and after irradiation at 365 nm for 10 minutes (red) and using b) dopamine before (black) and after irradiation at 365 nm for 10 minutes (red).

4.4 Conclusion

In the first section of this chapter, we presented a new gelation trigger method for low molecular weight hydrogels. Using this method, the gel stiffness can be controlled by the initial starting pH of the gelator solution. SANS data show how the composition of the gel fibres are similar at low Q therefore, the differences in gel stiffness are due to the entanglement of the fibres. We demonstrate that weaker gels show greater antimicrobial properties towards Gram-positive bacteria and attribute this to the production of reactive oxygen species as a result of the autoxidation of dopamine to produce polydopamine. This suggests potential to control the antimicrobial properties of a gel by controlling the mechanical properties of gelation.

In the second part of this chapter, we used the dopamine oxidation as an electrochemical trigger. Using this method, the gel stiffness can be controlled by the applied current. We demonstrate that electrochemical gels grown by dopamine are cell viable. This suggests a new method to develop an extracellular matrix that it suitable for a range of biomedical applications. In addition, we have identified that dopamine triggered electrochemical gelation is suitable for preparing photoconductive gels, which opens up a new route for OPV device fabrication.

4.5 References

1. E. Caló and V. V. Khutoryanskiy, *Eur. Polym. J*, 2015, **65**, 252-267.

2. A. P. G. McCloskey, B.F., Laverty, G, *Pathogens*, 2014, **3**, 791-821.

3. C. Potera, *Science*, 1999, **283**, 1837-1839.

4. E. M. Hetrick and M. H. Schoenfisch, *Chem. Soc. Rev*, 2006, **35**, 780-789.

5. E. M. Kojic and R. O. Darouiche, *Clin. Microbiol. Rev*, 2004, **17**, 255-267.

6. A. Rai, S. Pinto, M. B. Evangelista, H. Gil, S. Kallip, M. G. S. Ferreira and L. Ferreira, *Acta Biomater*, 2016, **33**, 64-77.

7. I. C. Saldarriaga Fernández, H. C. van der Mei, M. J. Lochhead, D. W. Grainger and H. J. Busscher, *Biomaterials*, 2007, **28**, 4105-4112.

8. G. P. Giammona Gaetano, Palumbo Fabio Salvatore, Maraldi Susanna, Scarponi Sara and Romanò Carlo Luca, intechopen, *Hydrogels*, 2018, **9**, 180-200.

9. A. Salomé Veiga and J. P. Schneider, *J. Pept. Sci*, 2013, **100**, 637-644.

10. S. Li, S. Dong, W. Xu, S. Tu, L. Yan, C. Zhao, J. Ding and X. Chen, *Adv. Sci*, 2018, **5**, 1700527.

11. A. Panáček, L. Kvítek, R. Prucek, M. Kolář, R. Večeřová, N. Pizúrová, V. K. Sharma, T. j. Nevěčná and R. Zbořil, *J. Phys. Chem. B*, 2006, **110**, 16248-16253.

12. J. F. Hernández-Sierra, F. Ruiz, D. C. Cruz Pena, F. Martínez-Gutiérrez, A. E. Martínez, A. de Jesús Pozos Guillén, H. Tapia-Pérez and G. Martínez Castañón, *Nanomed. Nanotechnol*, 2008, **4**, 237-240.

13. C. H. Chang, Y. H. Lin, C. L. Yeh, Y. C. Chen, S. F. Chiou, Y. M. Hsu, Y. S. Chen and C. C. Wang, *Biomacromolecules*, 2010, **11**, 133-142.

14. C. H. Liao, C. S. Chen, Y. C. Chen, N.-E. Jiang, C. J. Farn, Y.S. Shen, M.L. Hsu and C. H. Chang, *J. Microbiol. Immunol. Infect*, 2019, DOI: accepted: 25/09/19.

15. H. Li, J. Yang, X. Hu, J. Liang, Y. Fan and X. Zhang, *J. Biomed. Mater. Res. A*, 2011, **98A**, 31-39.

16. S. Marchesan, Y. Qu, L. J. Waddington, C. D. Easton, V. Glattauer, T. J. Lithgow, K. M. McLean, J. S. Forsythe and P. G. Hartley, *Biomaterials*, 2013, **34**, 3678-3687.

17. J. L. Fox, *Nat. Biotechnol*, 2013, **31**, 379-382.

18. S. Prabhu and E. K. Poulose, *Int. Nano Lett*, 2012, **2**, 32.

19. D. M. Wen H, Yang Y, Lyu J, Shao A, Cheng X, Chen L, *Xu L PLos ONE*, 2017, **19**, 9.

20. C. Pan, Z. Zhou and X. Yu, *J. Orthop. Surg. Res*, 2018, **13**, 220.

21. E. Maisonneuve and K. Gerdes, *Cell*, 2014, **157**, 539-548.

22. F. Han, C. Zhu, Q. Guo, H. Yang and B. Li, *J. Mater. Chem. B*, 2016, **4**, 9-26.

23. E. R. Draper and D. J. Adams, *Chem*, 2017, **3**, 390-410.

24. F. W. Kari, J. Bucher, S. L. Eustis, J. K. Haseman and J. E. Huff, *Food Chem. Toxicol*, 1992, **30**, 737-747.

25. J. Raeburn, B. Alston, J. Kroeger, T. O. McDonald, J. R. Howse, P. J. Cameron and D. J. Adams, *Mat. Horiz*, 2014, **1**, 241-246.

26. L. Su, Y. Yu, Y. Zhao, F. Liang and X. Zhang, *Sci. Rep*, 2016, **6**, 24420.

27. P. Kord Forooshani, E. Polega, K. Thomson, M. S. A. Bhuiyan, R. Pinnaratip, M. Trought, C. Kendrick, Y. Gao, K. A. Perrine, L. Pan and B. P. Lee, *Front. Chem*, 2019, **7**, 631.

28. W. Zheng, H. Fan, L. Wang and Z. Jin, *Langmuir*, 2015, **31**, 11671-11677.

29. B. J. Juven and M. D. Pierson, *J. Food Prot*, 1996, **59**, 1233-1241.

30. A. R. Hirst, B. Escuder, J. F. Miravet and D. K. Smith, *Angew. Chem. Int. Edit*, 2008, **47**, 8002-8018.

31. P. Terech and R. G. Weiss, *Chem. Rev*, 1997, **97**, 3133-3160.

32. L. Chen, S. Revel, K. Morris, L. C. Serpell and D. J. Adams, *Langmuir*, 2010, **26**, 13466-13471.

33. E. R. Draper, E. G. B. Eden, T. O. McDonald and D. J. Adams, *Nat. Chem*, 2015, **7**, 848.

34. www.sasview.org.

35. A. A. Miles, S. S. Misra and J. O. Irwin, *J .Hyg. (Lond),* 1938, **38**, 732-749.

36. S. Senoh, C. R. Creveling, S. Udenfriend and B. Witkop, *J. Am. Chem. Soc*, 1959, **81**, 6236-6240.

37. E. Herlinger, R. F. Jameson and W. Linert, *J. Chem. Soc. Perkin. Trans. 2*, 1995, **2**, 259-263.

38. M. Salomäki, L. Marttila, H. Kivelä, T. Ouvinen and J. Lukkari, *J. Phys. Chem. B*, 2018, **122**, 6314-6327.

39. R. V. Lloyd, *Chem. Res. Toxicol*, 1995, **8**, 111-116.

40. D. C. Tse, R. L. McCreery and R. N. Adams, *J. Med. Chem*, 1976, **19**, 37-40.

41. T. E. Young and B. W. Babbitt, *J. Org. Chem*, 1983, **48**, 562-566.

42. E. R. Cross and D. J. Adams, *Soft Matter*, 2019, **15**, 1522-1528.

43. E. R. Draper, O. O. Mykhaylyk and D. J. Adams, *Chem. Comm*, 2016, **52**, 6934-6937.

44. T. F. Wu and J. D. Hong, *Biomacromolecules*, 2015, **16**, 660-666.

45. E. R. Cross, S. Sproules, R. Schweins, E. R. Draper and D. J. Adams, *J. Am. Chem. Soc,* 2018, **140**, 8667-8670.

46. L. Jiang, D. Xu, T. J. Sellati and H. Dong, *Nanoscale*, 2015, **7**, 19160-19169.

47. A. P. McCloskey, S. M. Gilmore, J. Zhou, E. R. Draper, S. Porter, B. F. Gilmore, B. Xu and G. Laverty, *RSC. Adv*, 2016, **6**, 114738-114749.

48. G. A. Pankey and L. D. Sabath, *Clin. Infect. Dis*, 2004, **38**, 864-870.

49. V. Ball, D. D. Frari, V. Toniazzo and D. Ruch, *J. Colloid. Interf. Sci*, 2012, **386**, 366-372.

50. H. I. Zgurskaya, C. A. López and S. Gnanakaran, *ACS Infect. Dis,* 2015, **1**, 512-522.

51. J. van der Heijden, L. A. Reynolds, W. Deng, A. Mills, R. Scholz, K. Imami, L. J. Foster, F. Duong and B. B. Finlay, *mBio*, 2016, **7**, e01238-01216.

52. S. L. Chua, Y. Ding, Y. Liu, Z. Cai, J. Zhou, S. Swarup, D. I. Drautz-Moses, S. C. Schuster, S. Kjelleberg, M. Givskov and L. Yang, *Open Biol*, 2016, **6**, 160162.

53. K. D. Patel, R. K. Singh, E.-J. Lee, C.-M. Han, J.-E. Won, J. C. Knowles and H.-W. Kim, *Surf. Coat. Technol*, 2014, **242**, 232-236.

54. E. Bendary, R. R. Francis, H. M. G. Ali, M. I. Sarwat and S. El Hady, Ann. Agric. Sci, 2013, **58**, 173-181.

55. B. D. Beake, R. B. Moodie and J. P. B. Sandall, *J. Am. Chem. Soc. Perkin Trans. 2*, 1994, **5**, 957-960.

56. R. O. Marcon and S. Brochsztain, *J. Phys. Chem. A*, 2009, **113**, 1747-1752.

57. M. H. Chua, Q. Zhu, K. W. Shah and J. Xu, *Polymers-Basel*, 2019, **11**, 98.

CHAPTER 5

Tuning hydrogel properties for photoconductive hydrogels

5.1 Introduction

Organic photovoltaic devices (OPV) can consist of a heterojunction of two different materials one which is positively doped (p) that accepts electrons and another that is negatively doped (n) which donates electrons.[1] [2] When combined, these heterojunctions can convert light energy to electrical energy.[2, 3] These cascade of events begin when light energy excites an electron from the highest occupied molecular orbital (HOMO) of the n-type material into its lowest unoccupied molecular orbital (LUMO).[2, 3] This electron hole pair (exciton) diffuses across the phase boundary between the p-type material and n-type material. As a result, there is a charge separation, then the electron hops into the lower energy conductance band of the n-type material, leaving the hole in the p-type.[2] In order to generate electricity, a space charge region is created due to the build-up of charge between junction which results in an internal electrical field, and the electron and holes travel to separate electrodes.

The lifetime that the exciton can diffuse between the p and n-type materials is limited, so the distance it can travel before it collapses is small approximately 10-20 nm,[4] therefore the optimal size of the heterojunction is smaller than the maximum distance. Bulk heterojunctions consist of micro-phase separated materials which are small enough to allow the exciton to travel.[4] Multicomponent LMWG have been used as bulk heterojunctions due to the nature of the small fibres, where one fibre consists of a p-type gelator network whereas the other consists of a n-type gelator network.[5, 6] To optimise the morphology of the bulk heterojunction, further understanding of the self-assembly in these systems is required.[1] If we can understand and control how the p and n-type gelators self-assemble and interact with each other in both single and multicomponent networks then we could potentially control the photoconductive properties of the gels.

5.1.1 Low molecular weight hydrogels

The gelators used in this chapter are 4,4-stilbene diphenylalanine referred to as **1**, and N,N'-di(L-alanine)-perylene-3,4:9,10-tetracarboxylic acid bisimide referred to as **2**.[7] (Figure **5.1**). Both consist of a hydrophobic aromatic core, with symmetrical amino acid groups on the periphery. **1** is a p-type material so can

accept electrons,[8] whereas **2** is a n-type material that can donate electrons.[8] There is potential for functionalisation on the aromatic core to alter the electronic properties of the material making them better suited for use in p-n heterojunctions.

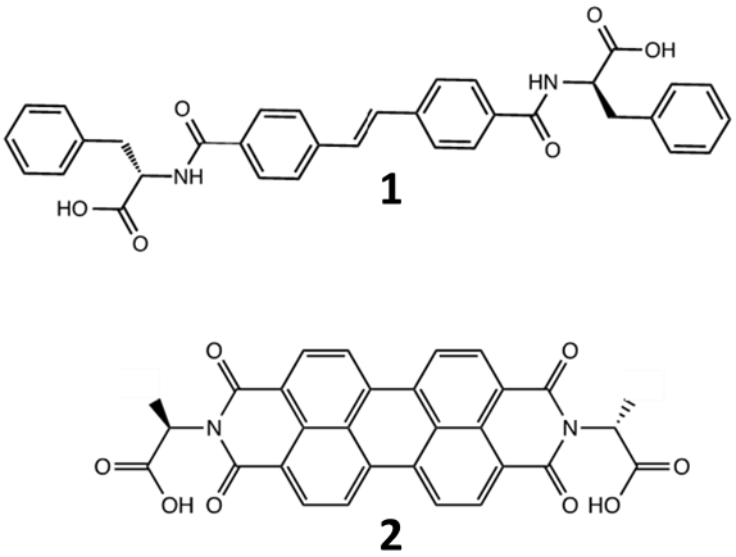

Figure 5.1 Chemical structures for gelators **1** and **2**.

5.1.2 Multicomponent hydrogels

Typically, research into low molecular weight hydrogels describes systems using a single molecule but this does not need to be the case.[9] Using two molecules, which can each independently form single component hydrogels, can result in them self-assembling in the same container to form a multicomponent system.[10] There is potential to fine tune the gelators and conditions to provide hydrogels with varying properties.[10]

There are three ways in which fibres can self-assemble in multicomponent systems (Figure **5.2**).[10, 11] The first way is self-sorting (Figure **5.2**a) where the fibres are composed of only a single gelator. The second way is an ordered system where there is a specific mixed pattern in composition of gelator (Figure **5.2**b). Finally, a system where both gelators assemble randomly could be formed (Figure **5.3**)

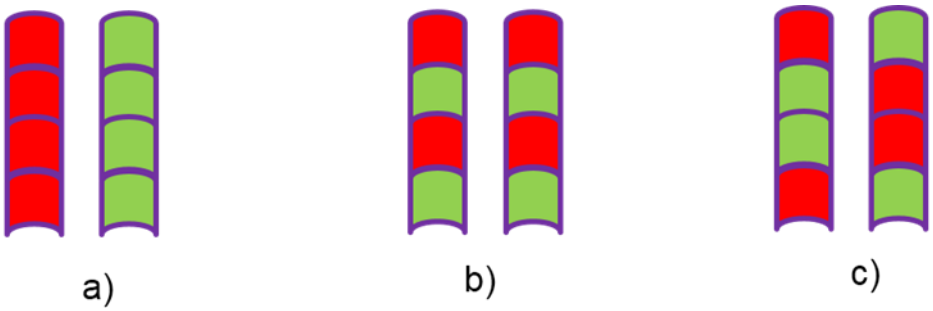

Figure 5.2 Schematic diagram showing three possible molecular assembly methods in a multicomponent system of two gelators including a) self-sorting, b) ordered sorting and c) random sorting.

While this primary assembly level is used to define the system, useful properties often arise from the next level of hierarchy, such as how these fibres interact (Figure **5.3**).[12] Conceptually, the degree of fibre entanglement can vary from low, where there is little overlap and no interaction (similar to an interpenetrating polymer network), to high, where strong interactions lead to fibres coiling around each other. Controlling entanglement provides further potential variation in final properties from self-assembly alone.

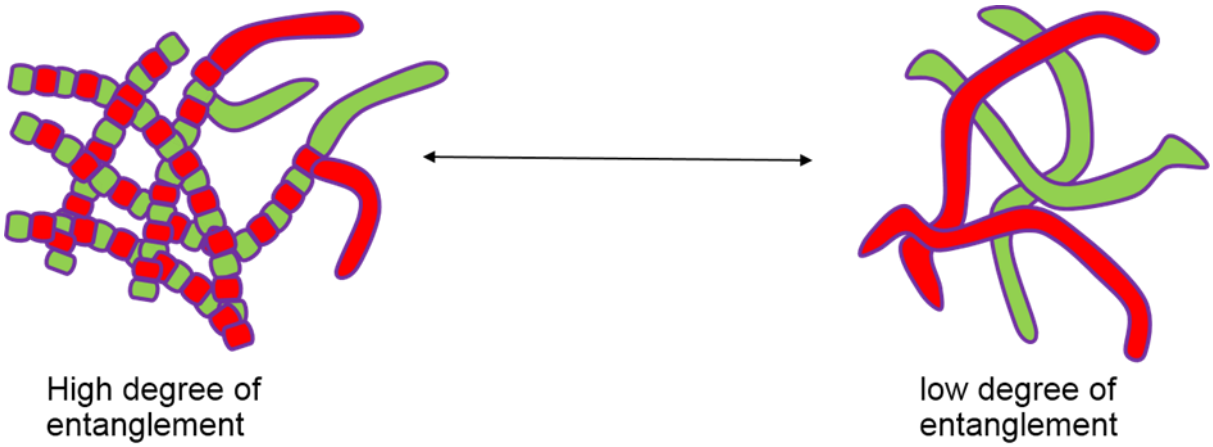

Figure 5.3 Cartoon showing the hypothetical situations (left) self-sorted fibres have significant interaction, (right) were self-sorted fibres do not interact. Conceptually, a heterojunction occurs where the green and red fibres interact.

Bulk heterojunctions have been formed using self-sorted low molecular weight gels.[5, 6, 13] Being able to control the molecular assembly and level of entanglement, especially with networks formed from p-type and n-type fibres,[8] could propel the use of these cheap and easily synthesised materials in the field of organic photovoltaics.[9] An increased entanglement gives a larger p-n interface, but too much entanglement would promote recombination of the charged species. However, too little entanglement would limit the amount of charge transfer and so careful tuning would be required to make this system usable.[8, 14]

By controlling both self-assembly and entanglement, multicomponent hydrogels have the potential to be used as exciting new functional materials.[15, 16] Development of these materials is hindered by the inability to fully understand and control the self-assembly process. The Adams group have previously shown methods where we can control the formation of one network over another by adjusting the concentration of glucono-δ-lactone (GdL) added to a multicomponent gelator solution.[17] As the pH decreases past the pK_a of the first gelator, its self-assembly is triggered, then as soon as the pK_a of the second gelator is reached, self-assembly of the second gelator occurs. It is also possible to remove one network from another post-gelation to spatially control the network.[15]

To achieve a further degree of control over the self-assembly of these multicomponent systems, we can attempt to vary the kinetics of the process. Here, we show how the rate of gelation can be controlled by selecting the temperature during gelation. Increasing the temperature will increase the rate of GdL hydrolysis,[18] therefore resulting in a quicker decrease in the pH.[19] Depending on how fast the pH is dropped will equate to a different amount of time spent above, between and below the pK_a values of the gelators. This may result in different fibre assemblies, different degrees of entanglement and finally, different hydrogel properties. If we can gain control over both the molecular assembly and degree of entanglement with p- and n-type gelators, we should then be able to develop materials with optimum photoconductivies. Electron paramagnetic resonance (EPR) is used to determine how much electron transfer occurs in each gel.

5.1.3 Measuring self-assembly

The challenge with exploiting multicomponent LMWG systems is that there is no way of controlling or predicting in advance the interactions between the fibres which control the properties of the final gel. In addition, many of these LMWG are kinetically trapped, and multiple states are possible from the same mixtures. It is also extremely difficult to identify what has been formed. This is a major hurdle for developing and using mixed LMWGs for useful materials.

Difficulties arise when choosing a method to characterise self-assembly over time due to the multiple levels at which the self-assembly occurs.[20] Characterisation of the gel needs to occur on both a molecular and on a supramolecular level where initial formation of fibres and their entanglement can be observed in real time.[21]

Molecular self-assembly can be observed by ^{1}H NMR spectroscopic characterisation, which can be used to measure percentage assembly over time.[22] When the gelator is in solution, the protons are detectable by ^{1}H NMR spectroscopy, but as soon as the gelator molecules start to self-assemble and form fibrous structures they become relatively stationary so are no longer detectable by ^{1}H NMR spectroscopy.[19]

Possible methods to observe the fibres and their interactions include scanning and transmission electron microscopy. Images of a dried or cryo-frozen gels can be used to observe the overlapping of fibres,[23] possible identifying fibres of different thicknesses.[24] However, this method does not represent the three dimensional hydrogel network due to drying of the gel distorting the network therefore producing inaccurate comparison of the wet hydrogel.[25] Rheological methods can be used to characterise the mechanical properties of the hydrogel which are highly dependent upon the supramolecular network.[26] The storage and loss moduli can be recorded under a fixed strain and frequency during gelation which portrays the transition of a liquid to hydrogel.

Given that self-assembly is triggered when the pH lowers past the pK_a, the pH evolution of the self-assembly process can be recorded. Only with the combination of the characterisation evolution methods (pH, ^{1}H NMR spectroscopy and rheology) can we begin to understand the molecular and supramolecular assemblies.

5.2 Experimental

5.2.1 Materials

The gelators **1** and **2** were prepared as previously reported.[11, 15] Gelator **1** was prepared by Prof. Dave Adams (University of Glasgow). Gelator **2** was prepared by myself or Dr. Emily Draper (University of Glasgow) depending on the batch. depending upon the batch. All other chemicals were purchased from Sigma Aldrich and were used as received unless otherwise stated. Deuterium oxide (D_2O) was used throughout as the solvent. A stock solution of sodium deuteroxide (NaOD) at a concentration of 0.1 M was prepared in D_2O from the commercially available 40 wt% solution.

5.2.2 Preparation of solutions of 1, 2 and 1+2

For each single component solution, the gelator was added to D_2O and NaOD (0.1 M, one molar equivalent for **1** and two molar equivalents for **2**). The solution was stirred overnight to ensure all gelator had dissolved to provide solutions at a final concentration of each gelator of 5 mg/mL. For the multicomponent solution, single component solutions were prepared as above at a concentration of 10 mg/mL. The two single component solutions were then mixed in a ratio of 1:1 to provide a solution in which the concentration of **1** and **2** were 5 mg/mL (so total gelator concentration of 10 mg/mL). All solutions were stored at room temperature.

5.2.3 Preparation of gels of 1, 2 and 1+2

For each single component gel, 2 mL of gelator solution was added to 10 mg of GdL in a 7 mL Sterlin vial. The vial was gently swirled to ensure all the GdL had dissolved then placed into a water bath at a controlled temperature of 15, 20, 25, 30 or 40 °C for 16 hours. For the multicomponent gel, 1 mL of each gelator solution were added together. This was added to 20 mg of GdL (10 mg/mL) in a 7 mL Sterilin vial. The vial was gently swirled to ensure all the GdL had dissolved and placed into the water bath for 10-30 hours depending on the experiment.

5.2.4 Nuclear Magnetic Resonance (NMR)

^{1}H NMR spectra were recorded using a Bruker Avance III 500 MHz spectrometer with the temperature internally controlled. Samples were run in D_2O/NaOD with ethanol (2 µL/mL) added as an internal standard. For the kinetic measurements, ethanol was added to 2 mL of the solution. 1 mL of this solution was used to record a standard measurement prior to the addition of GdL (i.e. a time zero measurement). After the standard measurement was obtained, GdL (5 mg/mL) was added to the remaining 1 mL of the solution which was added to the NMR tube and inserted into the spectrometer. Due to the experimental limitations, there was a time delay of around 5 minutes from addition of GdL to the first sample acquisition. Spectra were recorded every 5 minutes until the gelator's proton peaks were no longer detectable. This took between 10-30 hours depending on the sample. Example spectra recorded over time are shown in Figure **5.4**, Figure **5.5**, and Figure **5.6**. The referenced proton environment was used to determine the percentage assembly over time.

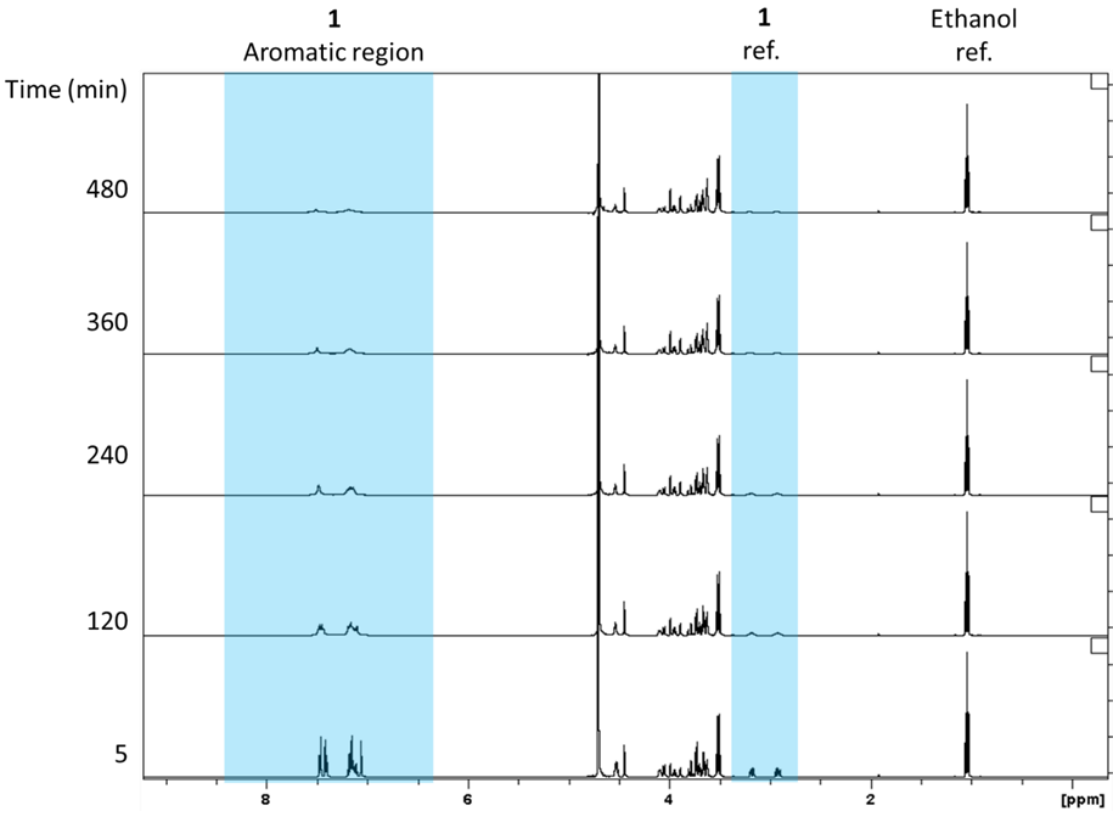

Figure 5.4 ^{1}H NMR spectra recorded over time after addition of GdL to a solution of 1 in D_2O/NaOD. The time at which the data were collected is shown on the left, with the peaks arising from 1 being shown in blue. The peaks between around 3.5 and 4.3 ppm are from GdL and its hydrolysis products. The peak at 4.5 ppm is from the solvent. The methyl groups from the ethanol standard against which the peaks of **1** are integrated are at just over 1 ppm. The proton environment labelled **1** ref. was used to determine the percentage assembly over time.

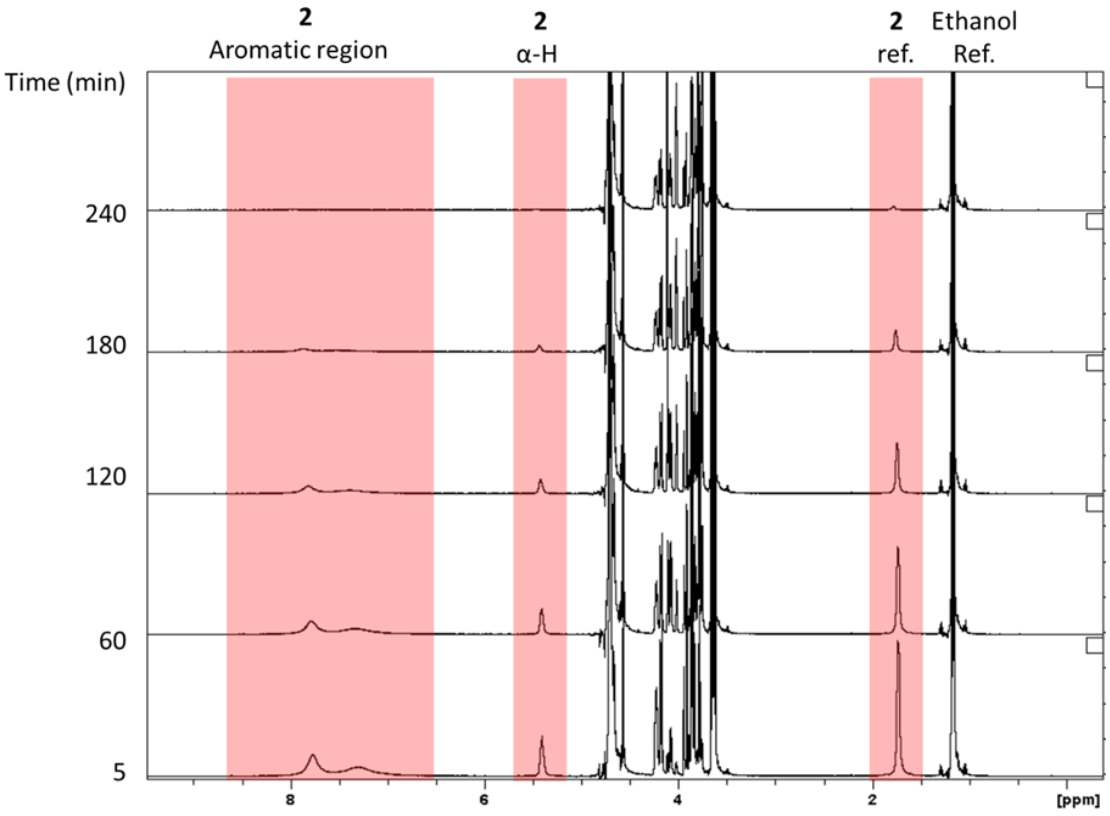

Figure 5.5 ^{1}H NMR spectra recorded over time after addition of GdL to a solution of **2** in D_2O/NaOD. The time at which the data were collected is shown on the left, with the peaks arising from **2** being shown in pink. The peaks between around 3.5 and 4.3 ppm are from the solvent. The methyl groups from the ethanol standard against which the peaks of **2** are integrated are at just over 1 ppm. The proton environment labelled **2** ref. was used to determine the percentage assembly over time.

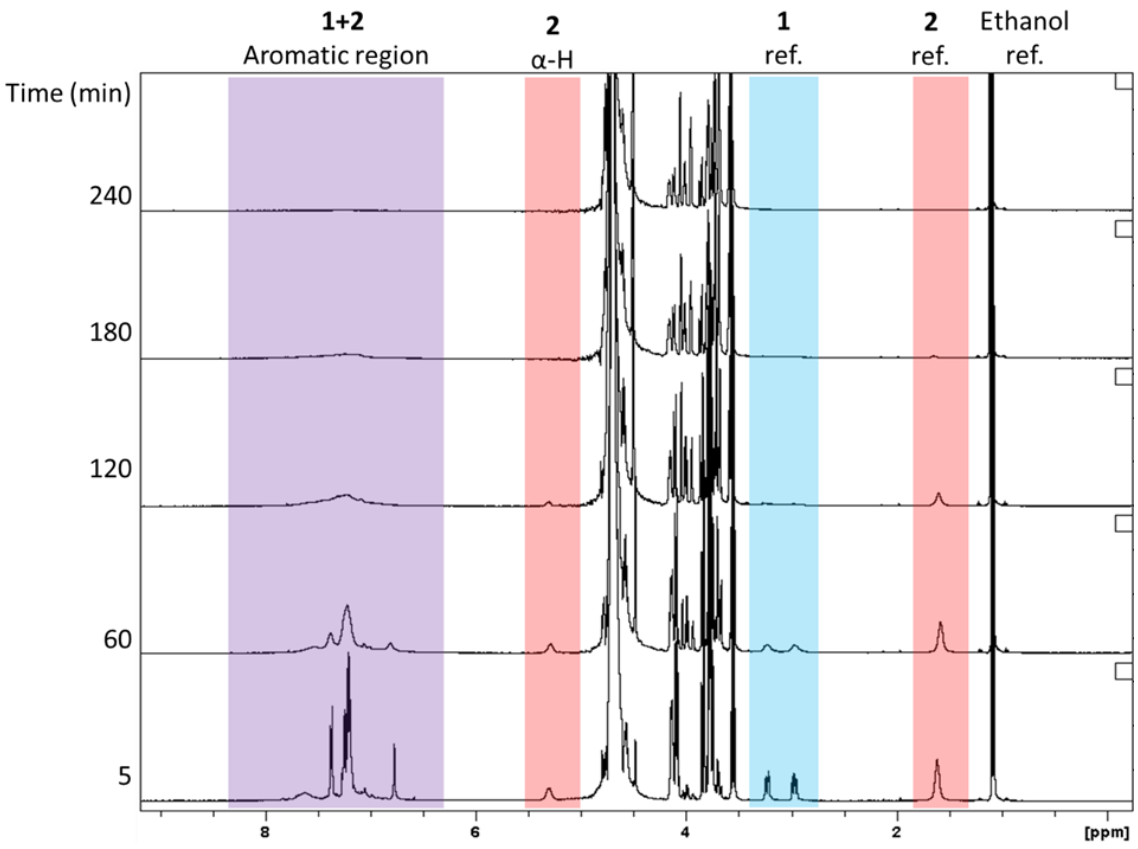

Figure 5.6 ^{1}H NMR spectra recorded over time after addition of GdL to a solution of both 1 and 2 in D_2O/NaOD. The time at which the data were collected is shown on the left, with the peaks arising from 1 being shown in blue, the peaks from 2 in pink and where peaks from both **1** and **2** in purple. The peaks between around 3.5 and 4.3 ppm are from GdL and its hydrolysis products. The peak at 4.5 ppm is from the solvent. The methyl groups from the ethanol standard against which the peaks of **1** and **2** are integrated are at just over 1 ppm. The proton environments labelled **1** ref and **2** ref. were used to determine the percentage assembly over time.

5.2.5 Rheological measurements

Rheological measurements were carried out using an Anton Paar Physical MCR301 or MCR101 rheometer. A vane and cup geometry was used to measure the frequency and strain sweeps. Parallel plates were used to measure time sweeps. For measuring the frequency and strain sweeps, 2 mL of gelator solution was added to GdL in a Sterilin vial as described in Section 5.2.3. This was immersed in a water bath at a controlled temperature for 16 hours. The rheological measurements were then recorded at room temperature. For measuring the time sweep, 2 mL of

the gelator solution was added to GdL as described above. The solution was then placed on the temperature-controlled plate. A time delay of 15 seconds was maintained from addition of GdL to sample acquisition.

Strain sweep: Strain scans were measured from 0.01 % to 100 % with a constant frequency of 10 rad/s.

Frequency sweep: Frequency scans were performed from 1 rad/s to 100 rad/s under a constant strain of 0.5 %.

Time sweep: Time sweeps were measured with an angular frequency of 10 rad/s with a strain of 0.5 %.

5.2.6 pH measurements

pH measurements were recorded using a Hanna PC turtle FC500 pH probe with a given error of ±0.1. For measuring the pH of gelation over time, 2 mL of gelator solution was added to GdL in a Sterilin vial and this was immersed in a water bath at a controlled temperature. The probe tip was then inserted into the gel with parafilm used to seal the top of the vial/tip. A time delay of 15 seconds was maintained from addition of GdL to sample recording. The pH measurements were recorded every 30 seconds for between 16-36 hours depending on the experiment.

5.2.7 Electron paramagnetic resonance (EPR)

The EPR data were collected by Dr. Stephen Sproules (University of Glasgow). To prepare samples for EPR, 1 mL of a gelator solution was added to GdL as described in Section 5.2.3. Using a needle and syringe, the solution was added to a soda glass capillary tube until it reached a 1 cm mark. The top was sealed with adhesive tack to prevent sample evaporation. The sample was irradiated with an LED light source powered by a 70 mA TTi QL564P power supply. All EPR data were recorded at X-band frequency (9.67 GHz) on a Bruker ELEXSYS E500 spectrometer equipped with an ER 4102ST-O optical transmission resonator. Spectra represent 5 scan averages collected over a 5 mT sweep width centred at 344.4 mT, with modulation frequency = 100 kHz, modulation amplitude = 0.2 mT, receiver gain = 60 dB, time constant = 40.96 s, conversion time = 10.24 s, and microwave power = 0.63 mW. Spin counts of solution samples were quantified by double integration of the first

derivative spectrum and calibrated to a 0.5 mg/mL aqueous solution of TEMPO recorded under identical conditions.

5.2.8 Small angle neutron scattering (SANS)

For the SANS experiments, Prof. Dave J. Adams and Dr Emily Draper conducted the measurements and interpreted the data. Two sets of solutions were prepared for **1**, **2**, and **1+2**. The first was prepared in D_2O using NaOD as described in Section 5.2.2, and the second the solvents were switched to H_2O and NaOH. The solutions were then mixed to prepare solutions with different ratios of H_2O to D_2O, ensuring the final concentration of gelator remained the same. These samples were then gelled using GdL in a thermostat oven to ensure that the temperature was constant. Solutions of H_2O and D_2O were mixed to provide the appropriate backgrounds.

5.3 Results and discussion

5.3.1 Controlling the rate of gelation in single component hydrogels

To investigate the self-assembly and final properties of the multicomponent system, first we analysed the single component systems. Single component solutions of **1** (5 mg/mL) and **2** (5 mg/mL) were prepared with a pD of 10.5. At this pD, the carboxylic acid groups on the gelator were de-protonated.[20] 2 mL of gelator solution was added to GdL (5 mg/mL) in a Sterilin vial and the pD was recorded over time whilst the temperature was controlled. As the hydrolysis of GdL is slow,[22] this allows for the self-assembly process to monitored over time. The slow hydrolysis of GdL lowered the pH and reduced the solubility of the gelator molecules, triggering self-assembly. The hydrolysis of GdL is temperature dependent.[14] Buffering between the protonated/de-protonated carboxylic acid of the gelator can be observed at each temperature during GdL hydrolysis where the decrease in pD vs time deviates from a negative linear gradient (Figure **5.7**). In both **1** and **2** systems, at the different temperatures, the buffering occurs at different times and pD values for each temperature where the samples at higher temperature show faster buffering and pD decrease. This suggests that the pK_a values of both gelators are temperature dependent which is expected as the degree of dissociation of an acid, to which pK_a is related, increases with increasing temperature.[27]

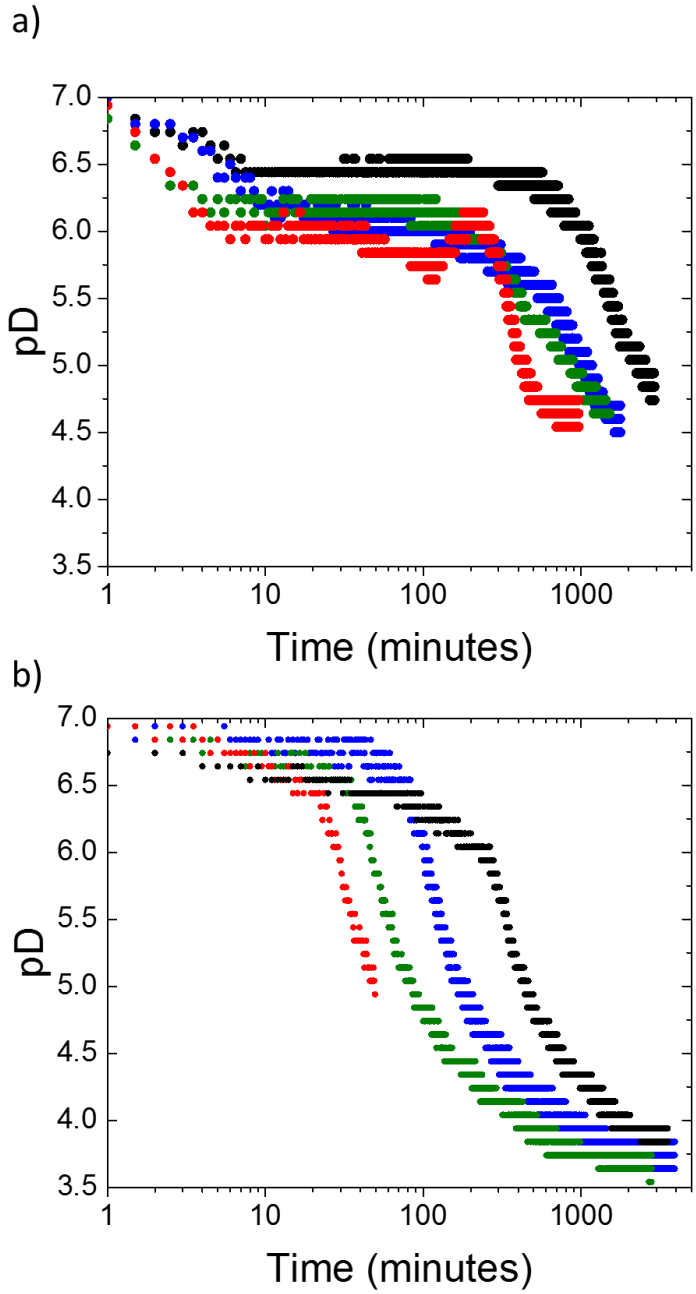

Figure 5.7 Temperature controlled pD evolution for a) **1** and b) **2**. The temperatures of pD evolution are 15 ˚C (black), 20 ˚C (blue), 30 ˚C (green) and 40 ˚C (red).

Alongside pD measurements, rheological time sweeps were carried out at 15, 20, 30 and 40 ˚C to further analyse the structural properties of the samples over time and to confirm that a gel had been formed. 2 mL of gelator solution was added to GDL (5 mg/mL) for analysis. For both systems, self-assembly of gelator molecules into a gel was faster at higher temperatures as the sharp increase in G′ occurred earlier for the higher temperatures (Figure **5.8**). Gel **2** had a relatively sharp

increase in G′ before a slower increase was observed. The sharp increase in G′ corresponds to the short pK_a buffering time observed in the pD versus time measurements as seen in Figure **5.7**, implying that self-assembly occurs quicker in **2** than **1**. The rheological time sweeps observed for gel **1** suggest that the formation of the gel network occurs earlier, which is expected as the pK_a is higher.[28] The variation between the rates of G′ increase over time for **1** suggests a multistage self-assembly process.

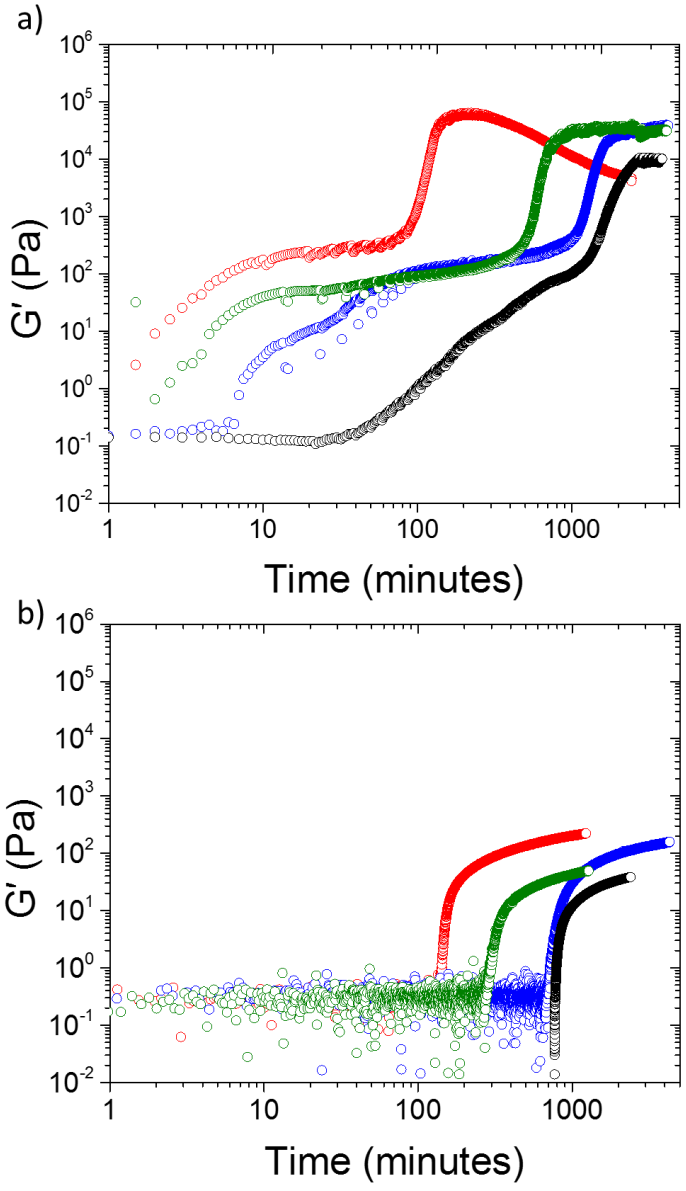

Figure 5.8 Temperature controlled rheological time sweep for a) **1** and b) **2**. For clarity, the data for G″ is not shown. The data shown are 15 ˚C (black), 20 ˚C (blue), 30 ˚C (green) and 40 ˚C (red). Time sweeps were measured with an angular frequency of 10 rad/s with a strain of 0.5 %.

^{1}H NMR spectroscopy was used in parallel to the pD and rheological time sweeps to analyse the self-assembly over time. When the gelator is in solution the protons are detectable by ^{1}H NMR, but as soon as the gelator molecules start to self-assemble and form larger aggregated structures, they become relatively stationary so are no longer detectable by ^{1}H NMR spectroscopy.[29] From these data, we observe a decrease in intensity of the gelator proton peaks over time as gelation is occurring.[29] A spectrum of gelator solution with an ethanol internal standard was recorded before each set of gelation measurements to act as a reference for 0 % assembly. After the addition of GdL (5 mg/mL), a spectrum was recorded every 5 minutes. The spectra were then normalized against the ethanol standard and compared to the gelator solution reference. The intensity of the gelator protons in relation to the standard (no assembly) and to a gelled sample with an integral of 0 (fully assembled) was described as the 'percentage assembled'.

The rate of percentage assembly for both **1** and **2** increased as temperature increased (Figure **5.9**), with complete assembly occurring earlier for the higher temperatures. It is possible to identify a variation in the rate of percentage increase between gel **1** and **2**. The rate of percentage assembly increase with time for **1** is more linear than **2** at all temperatures which suggests a different but sequential self-assembly mechanism. It is possible to observe a decrease in percentage assembly for **1**, which may be a result of the gelator buffering around its pK_a before becoming fully assembled.

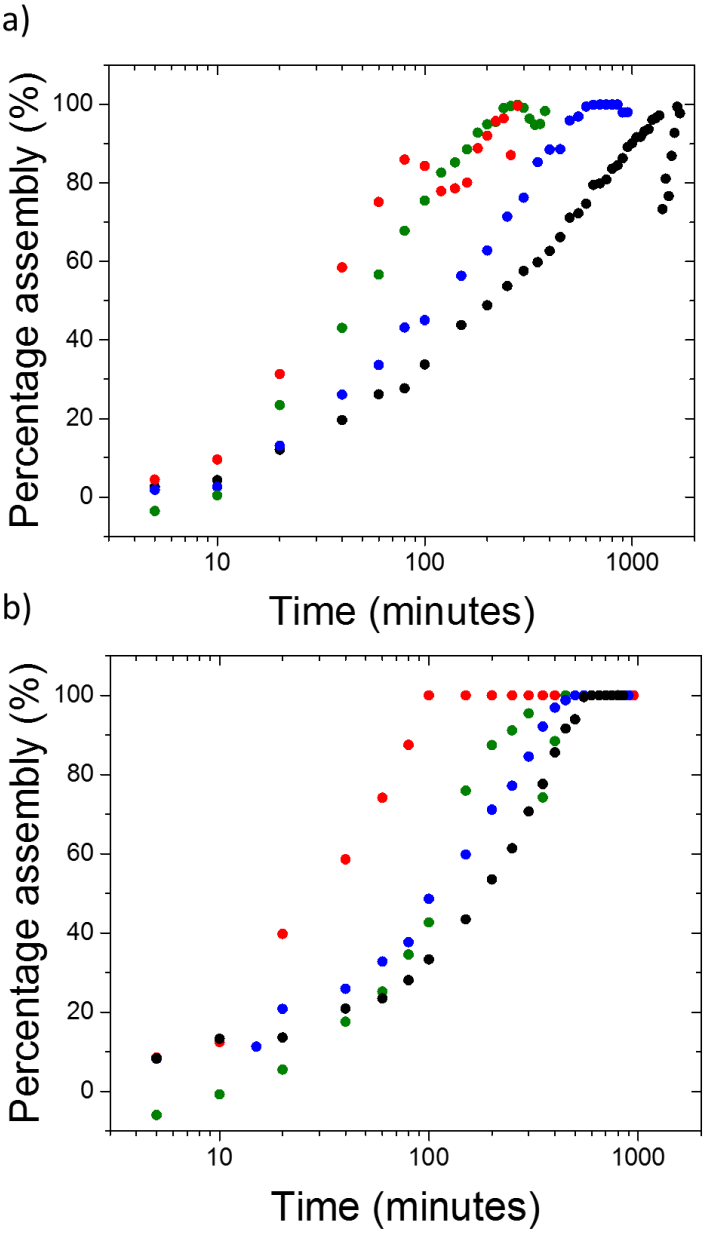

Figure 5.9 Graph showing temperature-controlled percentage assembly of a) **1** and b) **2** using ^{1}H NMR. The data shown are 15 ˚C (black), 20 ˚C (blue), 30 ˚C (green) and 40 ˚C (red).

Overlaying the data from the pD, time sweep and ^{1}H NMR experiments makes for an easier comparison over the same time scale (Figure **5.10** and Figure **5.11**). For **1,** we observe that the increase in percentage assembly occurs in parallel to the increase in G' as the pD decreases to the pK_a of the gelator. This suggests that the majority of gelator **1** forms fewer long fibres before entangling and immobilizing

water. This would also correspond to the linearity of percentage assembly in terms of ^{1}H NMR.

For **2,** we observe a different trend than for **1**. Using ^{1}H NMR spectroscopy at 15, 20, 30 and 40 °C, we can determine that the gelator becomes fully assembled before the increase in G' is observed by rheology, which occurs once the pH at which pK_a occurs is reached. This suggests that the majority of gelator **2** forms short fibres before these become long enough to entangle and immobilise water. This would also correspond to the deviation from linearity in the percentage assembly data. It is difficult with these three characterization methods to confirm the self-assembly mechanism. This may be improved when measuring the kinetics of gelation by SANS as we have shown for other gelator systems.[8, 20, 30, 31]

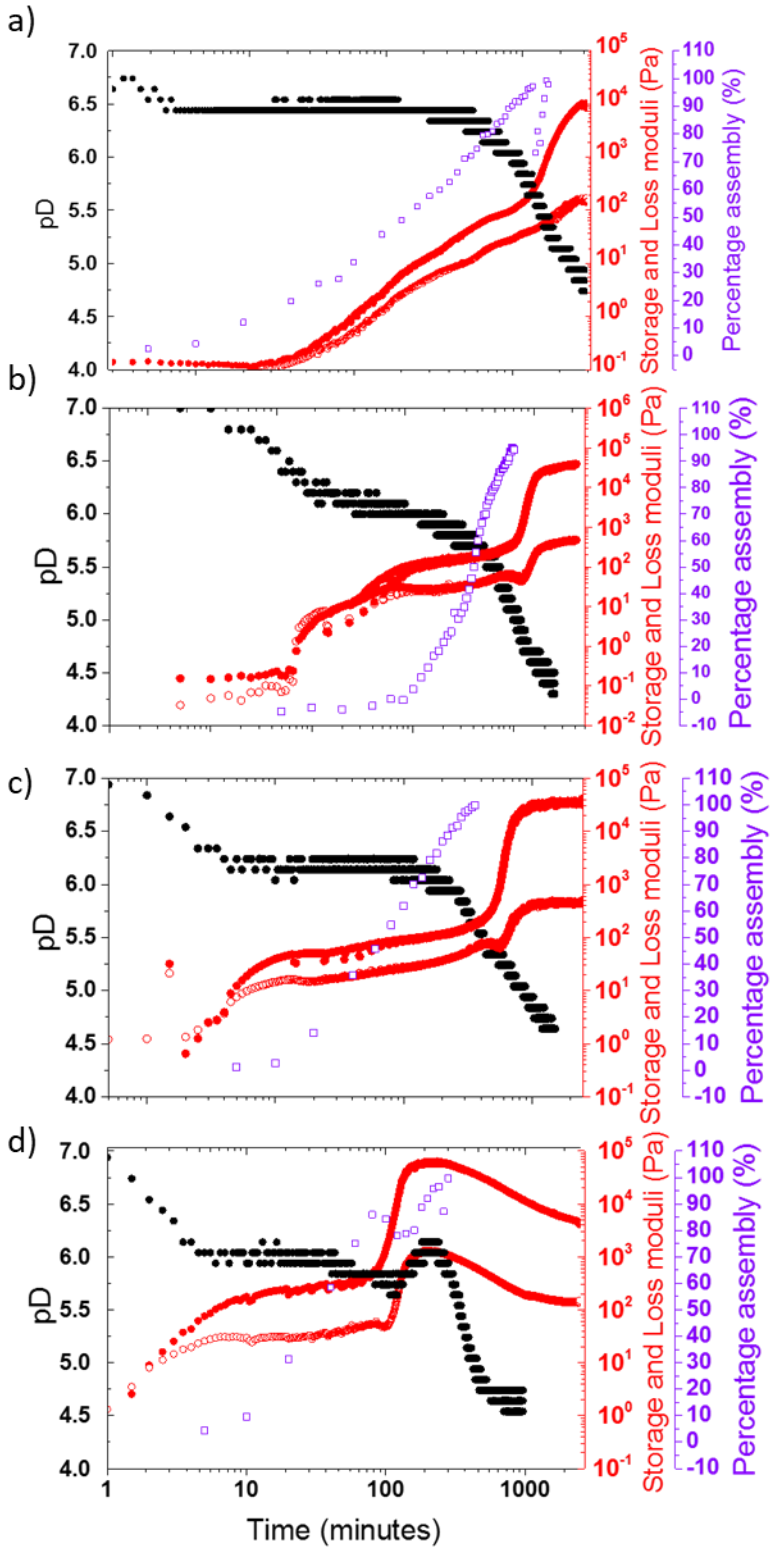

Figure 5.10 Monitoring the gelation of **1** over time at a) 15 ˚C, b) 20 ˚C, c) 30 ˚C and d) 40 ˚C. The change in intensity of peaks from ^{1}H NMR spectroscopy during gelation of the referenced peak of CH_3 at 1.7 ppm from **1** (purple hollow squares) are compared to the change in pD during gelation of **1** (black). The change in G′ (red full circle) and G″ (red hollow circle) over time for gel **2** (red data) is also shown.

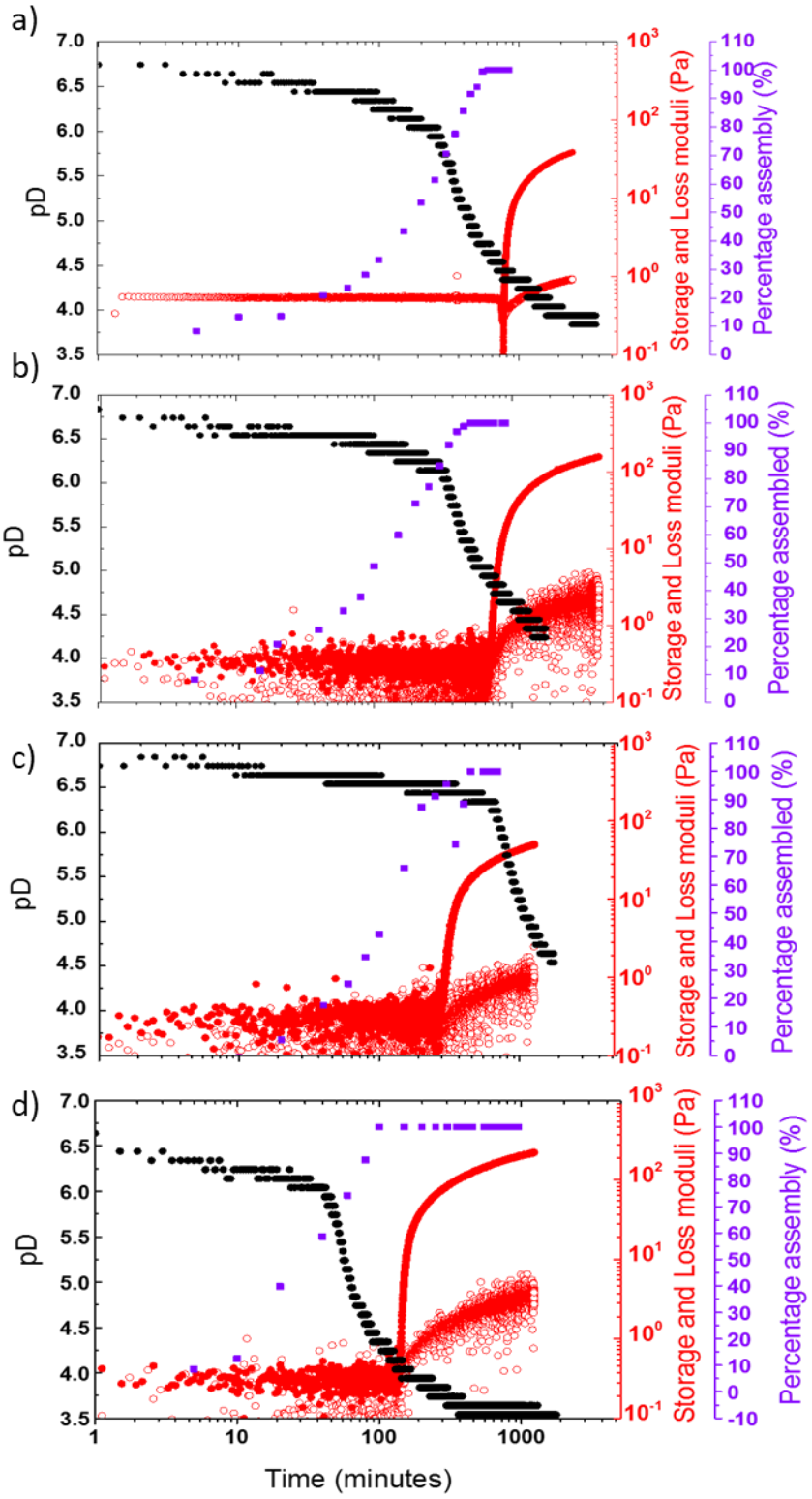

Figure 5.11 Monitoring the gelation of **2** over time at a) 15 ˚C, b) 20 ˚C, c) 30 ˚C and d) 40 ˚C. The change in intensity of peaks from ^{1}H NMR spectroscopy during gelation of the referenced peak of CH_3 at 3.0 ppm from **2** (purple full squares) are compared to the change in pD during gelation of **2** (black). The change in G′ (red full circle) and G″ (red hollow circle) over time for gel **2** (red data) is also shown.

5.3.2 Controlling the rate of gelation to tune optoelectronic properties in multicomponent hydrogels

To analyse the self-assembly of a multicomponent gel system of **1+2** at 25 and 30 °C, data from the pD, time sweep and ^{1}H NMR experiments were overlaid. While gelation at 25 °C results in sequential assembly of the gelators as shown by the rates at which the peaks disappear from the NMR spectra for **1** and **2,** at 30 °C the results are less clear (Figure **5.12**). The signals for **1** and **2** disappear simultaneously throughout the gelation process, although **1** still assembles at a faster rate than **2**. These data are consistent with either random/ordered sorting, self-sorting (assuming the structures would rather self-sort even when they assemble at the same rate), or a mixture of random/ordered sorting and self-sorting occurring.[1, 32]

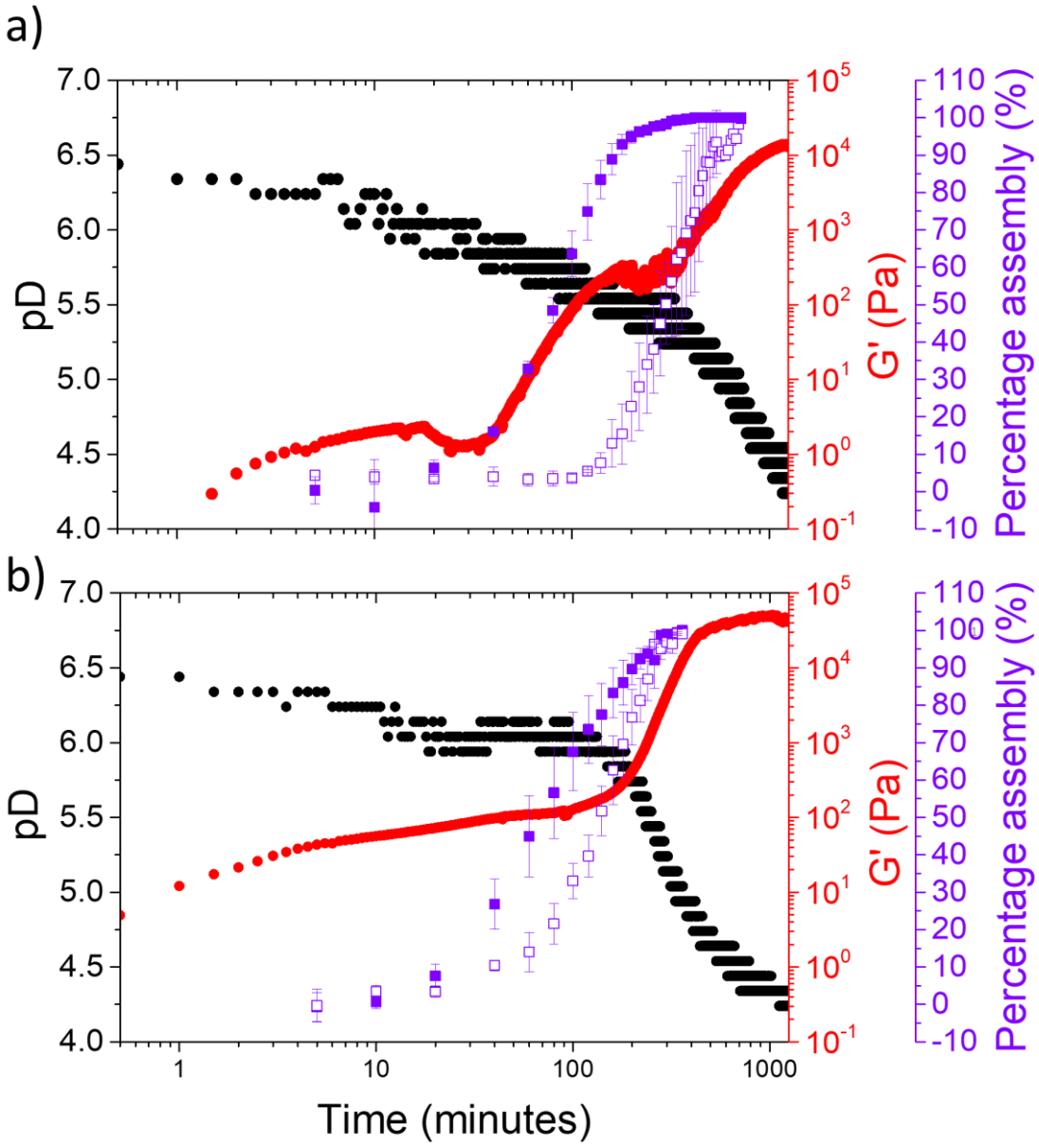

Figure 5.12 Monitoring the gelation of **1+2** at a) 25 °C and b) 30 °C. The gelation of the individual components 1 and 2 are followed by the change in intensity of reference peaks from ^{1}H NMR spectroscopy during gelation. The reference peaks for gelator **1** are taken at 1.7 ppm (CH_3) and shown as whole purple squares. The reference peaks for gelator **2** are taken at 3.0 ppm (CH_3) and shown as hollow purple squares. These data are compared to the change in pH during gelation of **1+2** (black) and the change in G′ over time for gel **1+2** (red data) is also shown.

Rheological measurements in Figure **5.13** and Figure **5.14** show that G' was an order of magnitude greater than G" and independent of the frequency applied, which suggests a hydrogel was formed in all cases. The gels formed

from **1** or **2** alone are stiffer when prepared at 30 °C as compared to 25 °C, as is the mixed gel. The final strength and stiffness of gel **1**+**2** was weaker than the addition of the single component gel values of **1** and **2**. This implies that the addition of two gelator networks does not simply equate to the addition of the networks strengths and stiffnesses, but results in new values that are representative of the combination and interactions between the networks formed. It is not clear from these data whether the networks are composed of two self-sorted systems or mixed systems.[11] The data does suggest however that, the variation in G' and G" at 25 °C and 30 °C corresponds to a difference in network interaction between both the single and multicomponent gels at the two temperatures.

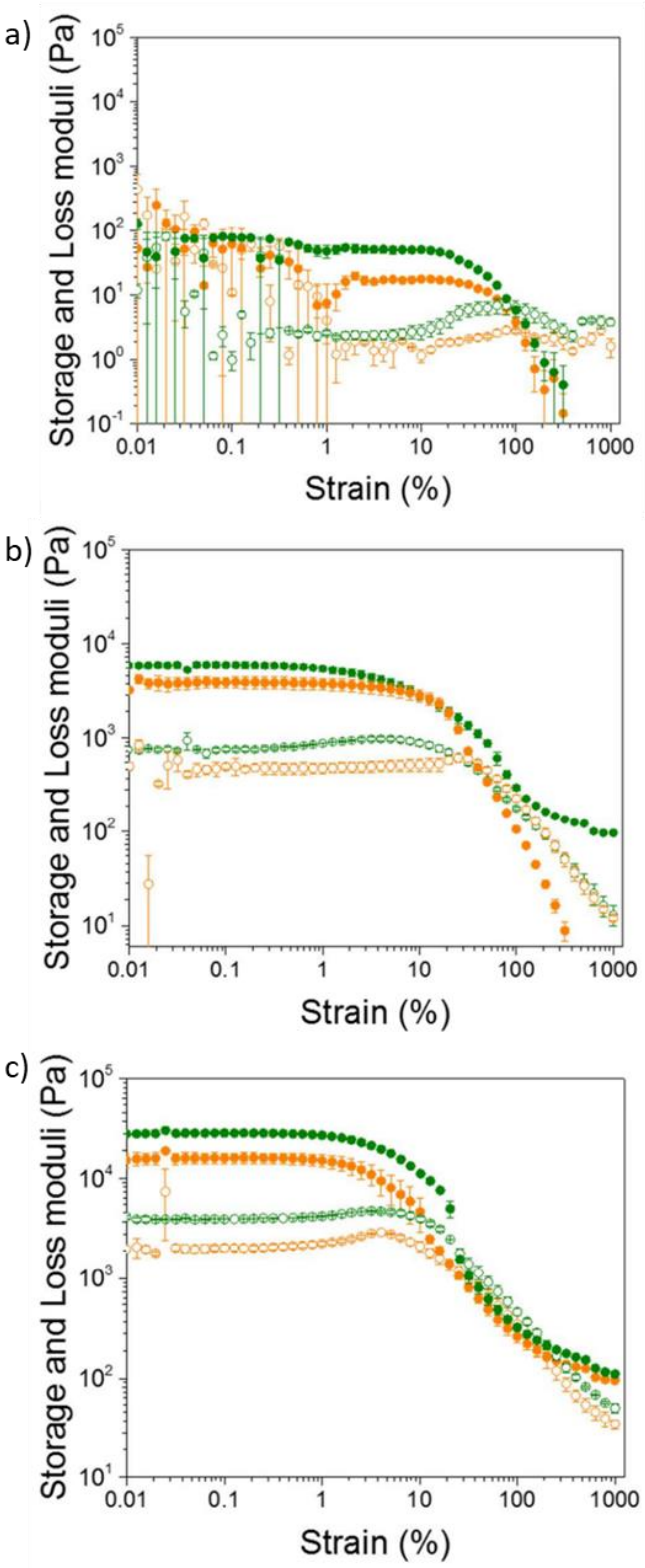

Figure 5.13 Strain sweep data for a) **1**, b) **2**, and c) **1**+**2**. In all cases, the data in orange were collected from samples prepared at 25 °C and the green data were from samples prepared at 30 °C. In all cases, the storage modulus (G′) is represented by the closed symbols and the loss modulus (G″) is represented by open symbols. Strain sweeps were measured from 0.01 % to 100 % with a constant frequency of 10 rad/s.

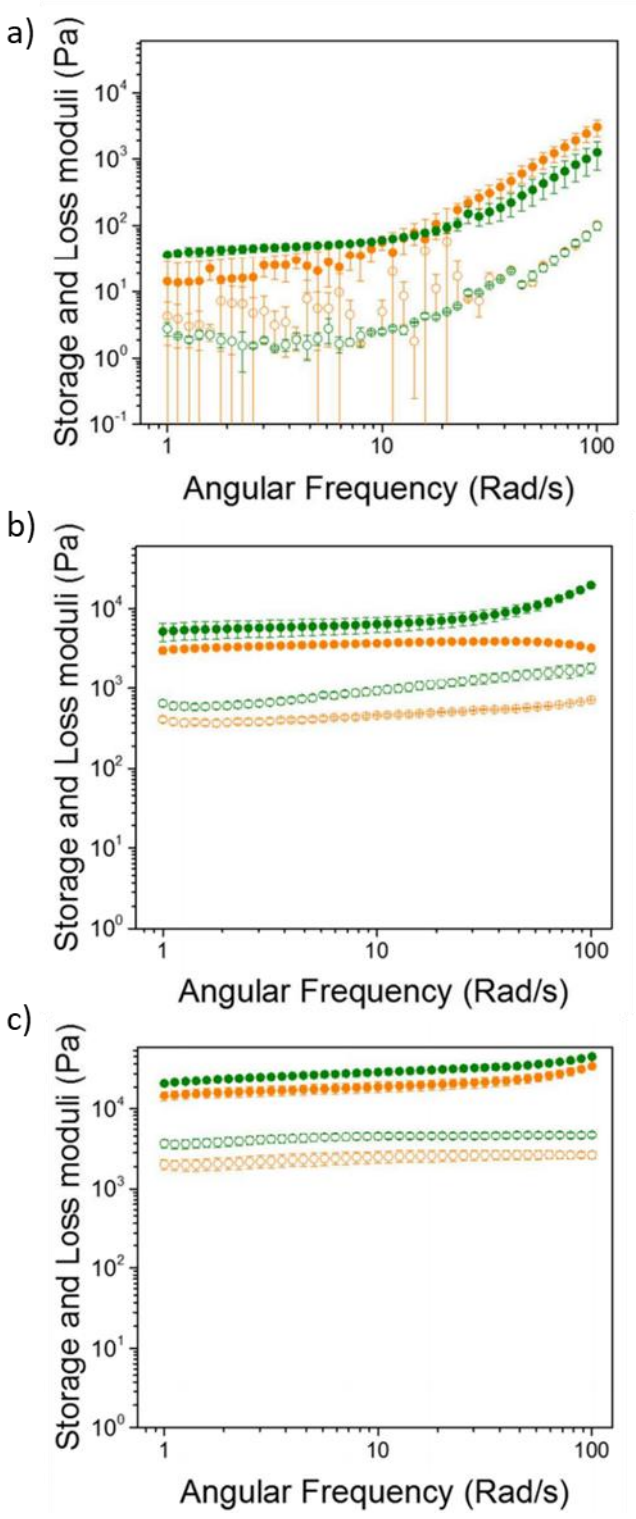

Figure 5.14 Frequency sweep data for a) **1**, b) **2**, and c) **1**+**2**. In all cases, the data in orange were collected from samples prepared at 25 °C and the green data were from samples prepared at 30 °C. In all cases, the storage modulus (G′) is represented by the closed symbols and the loss modulus (G″) is represented by open symbols. Measurements were performed in duplicate and errors were calculated from the standard deviation. Frequency sweeps were performed from 1 rad/s to 100 rad/s under a constant strain of 0.5 %.

5.3.3 Small angle neutron scattering

Small angle neutron scattering combined with contrast matching has been previously used to probe the self-assembled networks formed by a number of LMWG.[19, 33-35] The scattering intensity in SANS is determined by the contrast difference between the LMWG and the solvent, which can be changed by altering the ratio of D_2O and H_2O. Depending on the chemical composition of the LMWG it will have a unique scattering length density therefore, the contrast matching ratio of H_2O and D_2O between two different LMWG will be different. It is therefore possible to selectively choose a solvent ratio that will effectively scatter **1** or **2** and vice versa. These data can then be compared to the sample in pure D_2O where both **1** and **2** scatter. Consequently, it should be possible to probe the individual networks of the multicomponent system.

Prof. Dave J. Adams and Dr Emily R. Draper conducted the following SANS measurements and interpreted the data. Contrast matching for **1** occurred at 45 % D_2O in H_2O (v/v), while contrast matching for **2** occurred at 60 % D_2O in H_2O (v/v). Figure **5.15** shows the SANS data for **1**, **2** and **1**+**2** in a multicomponent gel at 45 % D_2O and 60 % D_2O. In 45 % D_2O, only **2** scatters well which fits to a cylindrical model coupled with a power law to take into the account at low Q. The fits imply that the structures have a radius of 7.2 ± 0.1 nm, and a length that is outside the meaningful range of the fit (>1000 nm). In 60 % D_2O, only **1** scatters well and the data can be fitted to a flexible cylinder model. The fit implies that the structures have a radius of 3.2 ± 0.2 nm, a Kuhn length of 6.0 ± 0.3 nm, and a length that is again outside the meaningful range of the fit. Table **5.1** and Table **5.2** show parameters from fits to the scattering data for samples in 45 % and 60 % D_2O. Figure **5.16** and Figure **5.17** show the individual SANS data and fits.

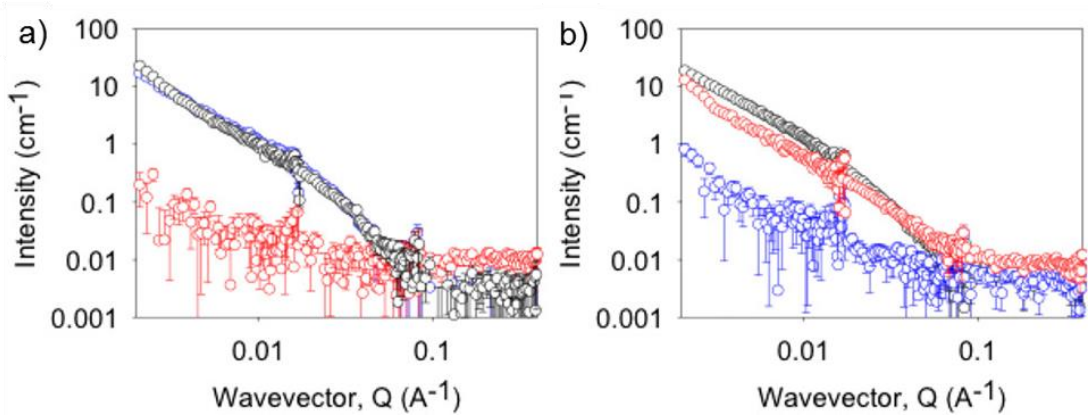

Figure 5.15 Scattering of **1** alone (red), **2** alone (blue), and (**1**+**2**) (black) in a) 45% D_2O and b) 60% D_2O.

Table 5.1 Parameters from fits to the scattering data in 60% D_2O.

	1 alone (60 % D_2O, 25 °C)	**1**in (**1+2**) (60 % D_2O, 25 °C)	**1** alone (60 % D_2O, 30 °C)	**1** in (**1+2**) (60 % D_2O, 30 °C)
Background (cm^{-1})	0.009	0.007	0.003	0.002
Kuhn Length (nm)	6.0 ± 0.3	11.8 ± 0.4	6.3 ± 0.5	22.5 ± 0.7
Length (nm)	> 1000	> 1000	> 1000	> 1000
Radius (nm)	3.2 ± 0.2	6.1 ± 0.4	3.2 ± 0.4	6.1 ± 0.5
Scale	$2.07 \times 10^{-3} \pm 4.48 \times 10^{-4}$	$1.96 \times 10^{-3} \pm 4.86 \times 10^{-5}$	$1.98 \times 10^{-3} \pm 5.7 \times 10^{-4}$	$1.47 \times 10^{-3} \pm 6.63 \times 10^{-5}$
x^2	1.21	2.53	2.01	4.21

Table 5.2 Parameters from fits to the scattering data in 45% D_2O. A * indicates that the parameter was fixed during the fitting process.

	2 alone (45 % D_2O, 25 °C)	**2** in (**1**+**2**) (45 % D_2O, 25 °C)	**2** alone (45 % D_2O, 30 °C)	**2** in (**1**+**2**) (45 % D_2O, 30 °C)
Background (cm^{-1})	0.002*	0.002*	0.003*	0.004*
Power Law	2.20 ± 0.02	2.34 ± 0.02	2.29 ± 0.03	2.12 ± 0.01
Power Law Scale	1.74 X 10^{-5} ± 2.4 x 10^{-6}	1.00 X 10^{-5} ± 9.23 X 10^{-8}	1.10 X 10^{-5} ± 1.91 X 10^{-6}	3.60 X 10^{-5} ± 2.86 X 10^{-6}
Length (nm)	> 1000	> 1000	> 1000	> 1000
Radius (nm)	7.2 ± 0.1	6.1 ± 0.1	6.6± 0.1	7.0 ± 0.1
Scale	2.20 x 10^{-3} ± 7.37 x 10^{-5}	2.09 x 10^{-3} ± 4.1 x 10^{-5}	2.29 x 10^{-3} ± 9.26 x 10^{-6}	1.66 x 10^{-3} ± 6.99 x10^{-5}
x^2	2.11	1.88	2.22	1.38

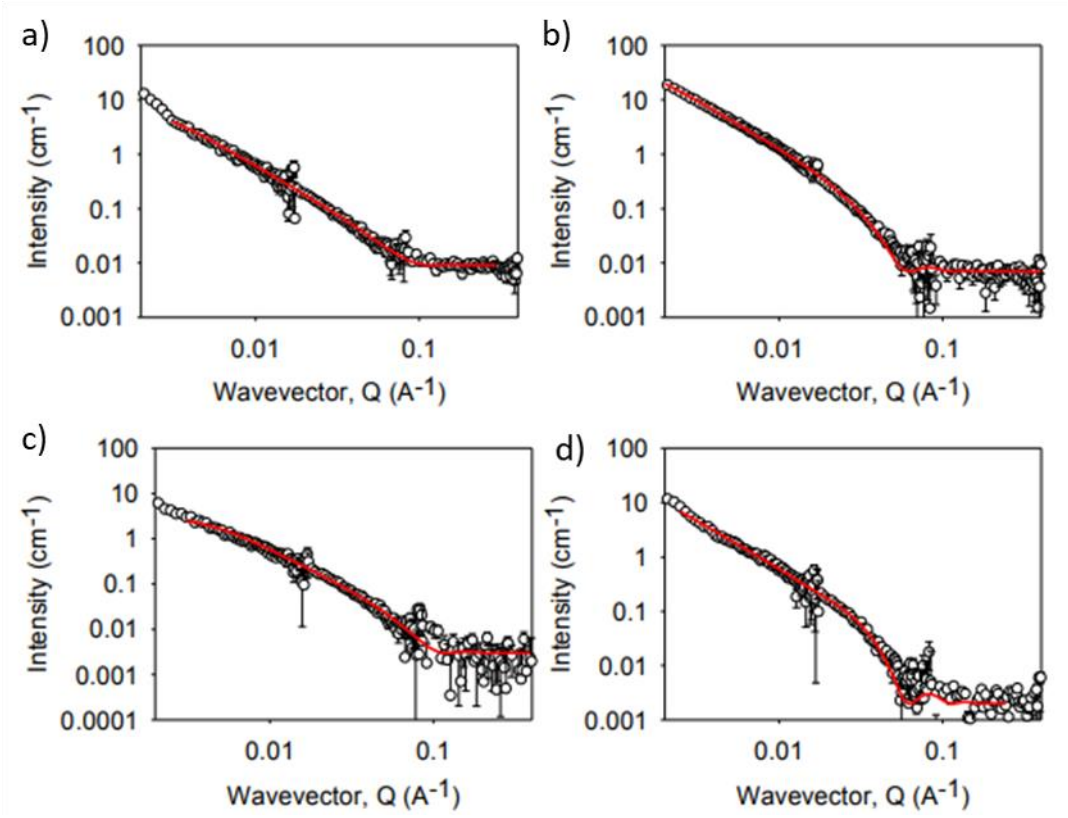

Figure 5.16 Scattering data and fits for a) **1** alone (60 % D_2O, 25 °C); b) **1** in (**1**+**2**) (60 % D_2O, 25 °C); c) **1** alone (60 % D_2O, 30 °C); d) **1** in (**1**+**2**) (60 % D_2O, 30 °C).

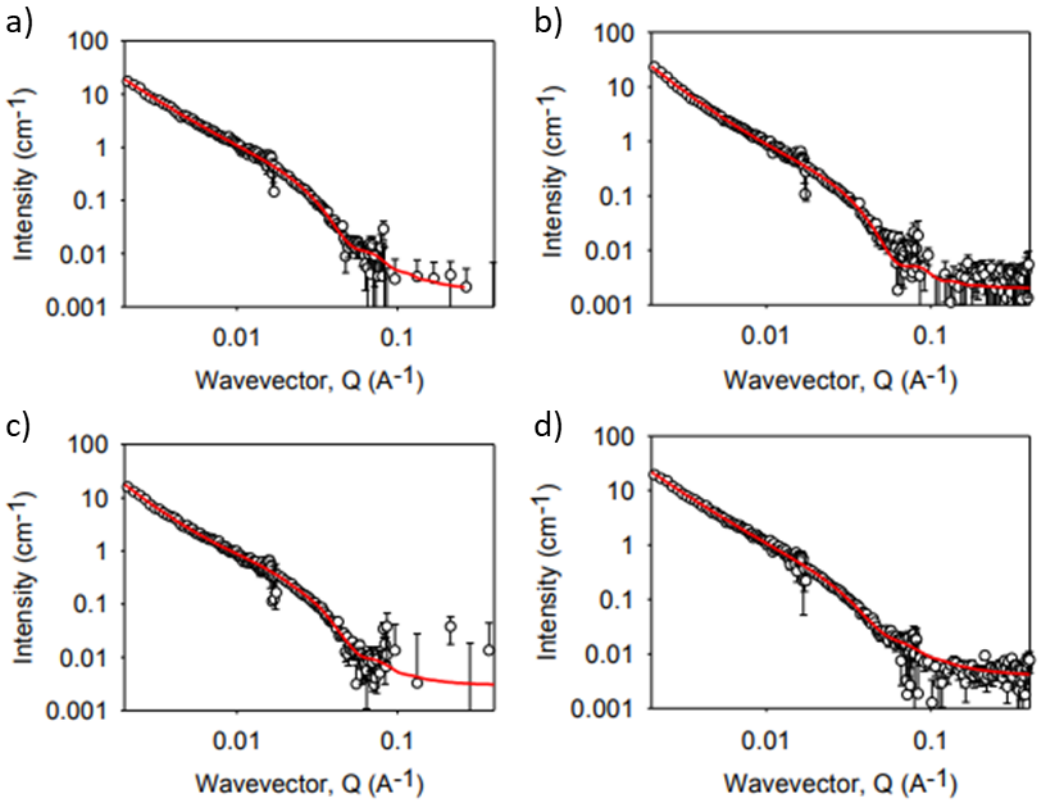

Figure 5.17 Scattering data and fits for a) **2** alone (45 % D_2O, 25 °C); b) **2** in (**1**+**2**) (45 % D_2O, 25 °C); c) **2** alone (45 % D_2O, 30 °C); d) **2** in (**1**+**2**) (45 % D_2O, 30 °C).

Previous data has shown how **1** and **2** can sequentially self-assemble into self-sorted systems.[8] It is therefore possible that the formation of one network may template the self-assembly of another network. If this templating can be controlled then we may be able to tune the physical properties of multicomponent LMWG. When comparing the scattering of **2** in the single component solution as well as the multicomponent system we observe very similar scattering. The data can again be fitted to a cylinder model coupled with a power law, with the fit implying that the structures have a radius of 6.1 ± 0.1 nm, and a long length. We can therefore conclude that **2** forms the same structures when self-assembled in the multicomponent system as in the single component system. When comparing the scattering of **1** in the single component solution as well as the multicomponent system we observe very different scattering. The data can be fitted to a flexible cylinder model shows that the structures have a radius of 6.1 ± 0.4 nm, a Kuhn length of 11.8 ± 0.4 nm, and a long length. Therefore, we can conclude that the structures formed by **1** are heavily dependent on the presence of **2**. We believe

this is the first example that has determined differences in the fibrous structures formed in a self-sorted system at this length scale.

5.3.4 Electron paramagnetic resonance

All EPR measurement were carried out by Dr Steven Sproules, and the data interpreted by myself. To investigate whether the difference in self-assembly and rheology equates to a difference in photoconductivity properties, EPR was used to measure the radical anion content. When this system is used as a bulk heterojunction (where the fibres of **1** and **2** are sufficiently close in space to allow electron transfer), it is the network level assembly that is important. In a self-sorted system, electron transfer will occur between fibres, so the points at which the fibres touch is important. On irradiating **2** with UV light, the radical anion is formed, which is EPR active.[36] Adding **1** means that the radical anion can be formed by irradiating at higher wavelengths.[8]

As expected, no radical anion is formed when gels of **2** formed at either temperature are irradiated at 420 nm (Figure **5.18**).[8] As shown previously, UV light is needed for gels of **2** alone to form the radical anion. In comparison, the radical anion was formed in the mixed gel of **1** and **2**. Despite the primary structures being very similar, there are differences in the amount of radical anion that is formed from the gels. Significantly more radical anion is formed from the gel prepared at 30 °C. This strongly implies that the networks are different, with more opportunity for electron transfer from **1** to **2** at 30 °C.

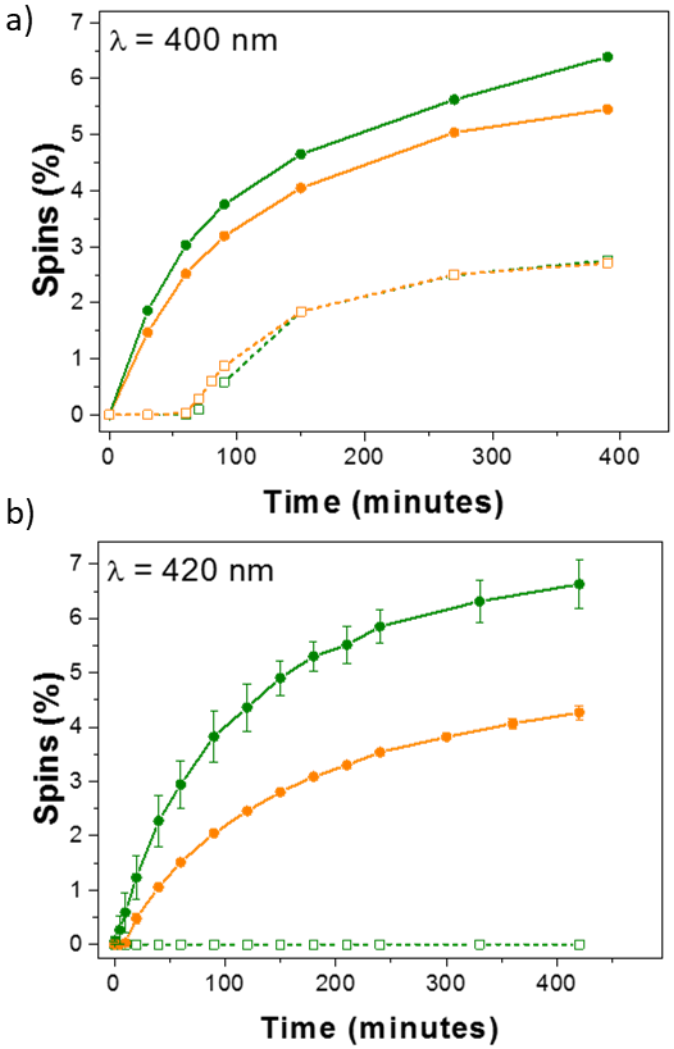

Figure 5.18 EPR data recorded over time showing the growth in EPR signal during irradiation with an LED light source at (a) 400 nm and (b) 420 nm, for (**1**+**2**) in full circles, and **2** only in hollow squares. In all cases, the data in orange were from samples prepared at 25 °C and the green data were from samples prepared at 30 °C. There was no growth observed for **2** alone at 420 nm.

5.4 Conclusions

We show a method of using a combination of ^{1}H NMR spectroscopy, pD, and rheological measurements over time to analyse gelation self-assembly over multiple hierarchies. Using these analytical methods, we were able to show how self-assembly in both single component and multicomponent hydrogel networks can be controlled by temperature. An increase in temperature resulted in an increase in the rate of GdL hydrolysis and subsequently the rate of gelation. Furthermore, we demonstrated how different components within a multicomponent gel can be differentiated by small-angle neutron scattering using contrast-matching experiments. With results showing that although the underlying self-assembled structures are very similar; instead, it is the organization of these structures that is affected that results in the differences in physical properties.

The rate of self-assembly can be used to vary the networks that are formed within multicomponent gels, leading directly to changes in the efficiency of electron transfer. The assembly kinetics can therefore be used to prepare different networks from the same primary building blocks and primary self-assembled structures. We expect that these advances will allow multicomponent systems to become effective electronic materials.

5.5 References

1. M. d. Loos, B. L. Feringa and J. H. v. Esch, *Euro. J. Org. Chem*, 2005, **17**, 3615-3631.

2. P. Terech and R. G. Weiss, *Chem. Rev*, 1997, **97**, 3133-3160.

3. A. Ali and S. Ahmed, *J. Agric. Food Chem*, 2018, **66**, 6940-6967.

4. S. S. Panda, H. E. Katz and J. D. Tovar, *Chem. Soc. Rev*, 2018, **47**, 3640-3658.

5. E. Caló and V. V. Khutoryanskiy, *Euro. Poly. J*, 2015, **65**, 252-267.

6. M. E. Parente, A. Ochoa Andrade, G. Ares, F. Russo and Á. Jiménez-Kairuz, *Int. J. Cosmet. Sci*, 2015, **37**, 511-518.

7. D. A. Gyles, L. D. Castro, J. O. C. Silva and R. M. Ribeiro-Costa, *Euro. Poly. J*, 2017, 88, 373-392.

8. D. B. Brown, D. Rehmann, *Mater. Matt*, 2016, **11**, 86-89

9. J. Zhuang, S. Lin, L. Dong, K. Cheng and W. Weng, *ACS Biomater. Sci. Eng*, 2018, **4**, 1528-1535.

10. T. Ling, J. Lin, J. Tu, S. Liu, W. Weng, K. Cheng, H. Wang, P. Du and G. Han, J. Mater. Sci-mater. M, 2013, **24**, 2709-2718.

11. E. R. Draper and D. J. Adams, *Chem*, **3**, 390-410.

12. S. Ghosh, V. K. Praveen and A. Ajayaghosh, *Annu. Rev. Mater. Res*, 2016, **46**, 235-262.

13. L. E. Buerkle and S. J. Rowan, *Chem. Soc. Rev*, 2012, **41**, 6089-6102.

14. B. Ding, Y. Li, M. Qin, Y. Ding, Y. Cao and W. Wang, *Soft Matter*, 2013, **9**, 4672-4680.

15. L. Chen, J. Raeburn, S. Sutton, D. G. Spiller, J. Williams, J. S. Sharp, P. C. Griffiths, R. K. Heenan, S. M. King, A. Paul, S. Furzeland, D. Atkins and D. J. Adams, *Soft Matter*, 2011, **7**, 9721-9727.

16. E. R. Draper, H. Su, C. Brasnett, R. J. Poole, S. Rogers, H. Cui, A. Seddon and D. J. Adams, *Angew. Chem*, 2017, **129**, 10603-10606.

17. R. Huang, Y. Wang, W. Qi, R. Su and Z. He, *Mater. Lett*, 2014, **128**, 216-219.

18. F. Trausel, F. Versluis, C. Maity, J. M. Poolman, M. Lovrak, J. H. van Esch and R. Eelkema, *Acc. Chem. Res*, 2016, **49**, 1440-1447.

19. B. Ozbas, J. Kretsinger, K. Rajagopal, J. P. Schneider and D. J. Pochan, *Macromolecules*, 2004, **37**, 7331-7337.

20. H. McEwen, E. Y. Du, J. P. Mata, P. Thordarson and A. D. Martin, *J. Mater. Chem. B*, 2017, **5**, 9412-9417.

21. Lin Chen, Tom O. McDonald and D. J. Adams, *RSC Adv,* 2013, **3**, 8714-8720.

22. C. Colquhoun, E. R. Draper, E. G. B. Eden, B. N. Cattoz, K. L. Morris, L. Chen, T. O. McDonald, A. E. Terry, P. C. Griffiths, L. C. Serpell and D. J. Adams, *Nanoscale*, 2014, **6**, 13719-13725.

23. D. J. Adams, M. F. Butler, W. J. Frith, M. Kirkland, L. Mullen and P. Sanderson, *Soft Matter*, 2009, **5**, 1856-1862.

24. D. J. Adams, *Macromol. Biosci*, 2011, **11**, 160-173.

25. A. Z. Cardoso, A. E. Alvarez Alvarez, B. N. Cattoz, P. C. Griffiths, S. M. King, W. J. Frith and D. J. Adams, *Faraday Discuss*, 2013, **166**, 101-116.

26. R. Fernandes, L.-Q. Wu, T. Chen, H. Yi, G. W. Rubloff, R. Ghodssi, W. E. Bentley and G. F. Payne, *Langmuir*, 2003, **19**, 4058-4062.

27. E. K. Johnson, D. J. Adams and P. J. Cameron, *J. Am. Chem. Soc*, 2010, **132**, 5130-5136.

28. X. Pang and I. Zhitomirsky, *Mater. Chem. Phys*, 2005, **94**, 245-251.

29. Q. Lu, Y. Huang, M. Li, B. Zuo, S. Lu, J. Wang, H. Zhu and D. L. Kaplan, *Acta Biomater*, 2011, **7**, 2394-2400.

30. D. Maniglio, W. Bonani, G. Bortoluzzi, E. Servoli, A. Motta and C. Migliaresi, *J. Bioact. Compat. Pol*, 2010, **25**, 441-454.

31. A. P. Tabatabai, D. L. Kaplan and D. L. Blair, *Soft Matter*, 2015, **11**, 756-761.

32. J. E. Bressner, B. Marelli, G. Qin, L. E. Klinker, Y. Zhang, D. L. Kaplan and F. G. Omenetto, *J. Mater. Chem. B*, 2014, **2**, 4983-4987.

33. N. Kojic, M. J. Panzer, G. G. Leisk, W. K. Raja, M. Kojic and D. L. Kaplan, *Soft Matter*, 2012, **8**, 6897-6905.

34. M. Cheong and I. Zhitomirsky, *Colloids Surf. A. Physicochem. Eng. Asp*, 2008, **328**, 73-78.

35. R. Ma, R. F. Epand and I. Zhitomirsky, Colloids. Surf. B, 2010, **77**, 279-285.

36. J. Raeburn, B. Alston, J. Kroeger, T. O. McDonald, J. R. Howse, P. J. Cameron and D. J. Adams, *Mater. Horiz*, 2014, **1**, 241-246.

37. E. K. Johnson, L. Chen, P. S. Kubiak, S. F. McDonald, D. J. Adams and P. J. Cameron, *Chem. Comm*, 2013, **49**, 8698-8700.

38. Z. Jin, G. Güven, V. Bocharova, J. Halámek, I. Tokarev, S. Minko, A. Melman, D. Mandler and E. Katz, *ACS Appl. Mater. Inter*, 2012, **4**, 466-475.

39. S. He, B. Ren, X. Liu and Z. Tong, *Macromol. Chem. Phys*, 2010, **211**, 2497-2502.

40. L.-Q. Wu, R. Ghodssi, Y. A. Elabd and G. F. Payne, *Adv. Funct. Mater,* 2005, **15**, 189-195.

41. C. Maerten, T. Garnier, P. Lupattelli, N. T. T. Chau, P. Schaaf, L. Jierry and F. Boulmedais, *Langmuir*, 2015, **31**, 13385-13393.

42. G. F. Payne and S. R. Raghavan, *Soft Matter*, 2007, **3**, 521-527.

43. Y. Wang, Z. Zhang, M. Wang, C. Guo, H. Liu, H. Zeng, X. Duan, Y. Zhou and Z. Tang, *Cellulose*, 2018, **25**, 105-115.

44. K. M. Gray, B. D. Liba, Y. Wang, Y. Cheng, G. W. Rubloff, W. E. Bentley, A. Montembault, I. Royaud, L. David and G. F. Payne, *Biomacromolecules*, 2012, **13**, 1181-1189.

45. Y. Liu, J. L. Terrell, C.-Y. Tsao, H.-C. Wu, V. Javvaji, E. Kim, Y. Cheng, Y. Wang, R. V. Ulijn, S. R. Raghavan, G. W. Rubloff, W. E. Bentley and G. F. Payne, *Adv. Funct. Mater*, 2012, **22**, 3004-3012.

46. J. Wang, X. Miao, Q. Fengzhao, C. Ren, Z. Yang and L. Wang, RSC Adv, 2013, **3**, 16739-16746.

47. T. Jiang, Z. Zhang, Y. Zhou, Y. Liu, Z. Wang, H. Tong, X. Shen and Y. Wang, *Biomacromolecules*, 2010, **11**, 1254-1260.

48. H. He, X. Cao, H. Dong, T. Ma and G. F. Payne, *Adv. Funct. Mater*, 2017, **27**, 1605665.

49. F. Wang, P. Huang, D. Huang, Y. Hu, K. Ma, X. Cai and T. Jiang, *J. Mater. Chem. B*, 2018, **6**, 2304-2314.

50. Y. Li, Y. Liu, T. Gao, B. Zhang, Y. Song, J. L. Terrell, N. Barber, W. E. Bentley, I. Takeuchi, G. F. Payne and Q. Wang, *ACS Appl. Mater. Inter*, 2015, **7**, 10587-10598.

51. X. Pang and I. Zhitomirsky, *Surf. Coat. Technol,* 2008, **202**, 3815-3821.

52. Y. Zhang and C. Ji, *Anal. Chem*, 2010, **82**, 5275-5281.

53. S. Wu, K. Yan, Y. Zhao, C.-C. Tsai, J. Shen, W. E. Bentley, Y. Chen, H. Deng, Y. Du, G. F. Payne and X. Shi, *Adv. Funct. Mater*, 2018, **28**, 1803139.

54. A. A. Rowe, A. J. Bonham, R. J. White, M. P. Zimmer, R. J. Yadgar, T. M. Hobza, J. W. Honea, I. Ben-Yaacov and K. W. Plaxco, *PLOS ONE*, 2011, **6**, e23783.

55. M. D. M. Dryden and A. R. Wheeler, *PLOS ONE*, 2015, **10**, e0140349.

56. A. Butterworth, D. K. Corrigan and A. C. Ward, *Anal. Methods*, 2019, **11**, 1958-1965.

57. A. Ainla, M. P. S. Mousavi, M.-N. Tsaloglou, J. Redston, J. G. Bell, M. T. Fernández-Abedul and G. M. Whitesides, *Anal. Chem*, 2018, **90**, 6240-6246.

58. T. K. Merceron and S. V. Murphy, *Essentials of 3D Biofabrication and Translation*, 2015, **14**, 249-270.

59. H. Yi, L.-Q. Wu, W. E. Bentley, R. Ghodssi, G. W. Rubloff, J. N. Culver and G. F. Payne, *Biomacromolecules*, 2005, **6**, 2881-2894.

60. C. Maerten, L. Jierry, P. Schaaf and F. Boulmedais, *ACS Appl. Mater. Inter*, 2017, **9**, 28117-28138.

61. P. S. Kubiak, S. Awhida, C. Hotchen, W. Deng, B. Alston, T. O. McDonald, D. J. Adams and P. J. Cameron, *Chem. Comm*, 2015, **51**, 10427-10430.

62. J. Groll, T. Boland, T. Blunk, J. A. Burdick, D.-W. Cho, P. D. Dalton, B. Derby, G. Forgacs, Q. Li, V. A. Mironov, L. Moroni, M. Nakamura, W. Shu, S. Takeuchi, G. Vozzi, T. B. F. Woodfield, T. Xu, J. J. Yoo and J. Malda, *Biofabrication*, 2016, **8**, 013001.

63. M. Lei, X. Qu, H. Liu, Y. Liu, S. Wang, S. Wu, W. E. Bentley, G. F. Payne and C. Liu, *Adv. Funct. Mater,* 2019, **29**, 1900065.

64. J. Gong, T. Liu, D. Song, X. Zhang and L. Zhang, Electrochem. Comm, 2009, **11**, 1873-1876.

65. W. Suginta, P. Khunkaewla and A. Schulte, *Chem. Rev*, 2013, **113**, 5458-5479.

66. P. Qi, Y. Wan and D. Zhang, *Biosens. Bioelectro*, 2013, **39**, 282-288.

67. T. Ahuja, I. A. Mir, D. Kumar and Rajesh, *Biomaterials,* 2007, **28**, 791-805.

68. J. F. Betz, Y. Cheng, C.-Y. Tsao, A. Zargar, H.-C. Wu, X. Luo, G. F. Payne, W. E. Bentley and G. W. Rubloff, *Lab Chip*, 2013, **13**, 1854-1858.

69. C.-M. Xie, X. Lu, K.-F. Wang, F.-Z. Meng, O. Jiang, H.-P. Zhang, W. Zhi and L.-M. Fang, *ACS Appl. Mater. Inter*, 2014, **6**, 8580-8589.

70. M. B. Thomas, N. Metoki, D. Mandler and N. Eliaz, *Electrochim. Acta*, 2016, **222**, 355-360.

71. O. Geuli, N. Metoki, N. Eliaz and D. Mandler, *Adv. Funct. Mater*, 2016, **26**, 8003-8010.

72. Q. Chen, U. P. de Larraya, N. Garmendia, M. Lasheras-Zubiate, L. Cordero-Arias, S. Virtanen and A. R. Boccaccini, *Colloids Surface B*, 2014, **118**, 41-48.

73. K. D. Patel, R. K. Singh, E.-J. Lee, C.-M. Han, J.-E. Won, J. C. Knowles and H.-W. Kim, *Surf Coat. Tech*, 2014, **242**, 232-236.

74. L. Q. Wu, A. P. Gadre, H. Yi, M. J. Kastantin, G. W. Rubloff, W. E. Bentley, G. F. Payne and R. Ghodssi, *Langmuir*, 2002, **18**, 8620-8625.

75. J. Thiele, Y. Ma, S. M. C. Bruekers, S. Ma and W. T. S. Huck, *Adv. Mater*, 2014, **26**, 125-148.

76. K. Yan, Y. Xiong, S. Wu, W. E. Bentley, H. Deng, Y. Du, G. F. Payne and X.-W. Shi, *ACS Appl. Mater. Inter*, 2016, **8**, 19780-19786.

77. V. Lakshminarayanan, L. Poltorak, D. Bosma, E. J. R. Sudhölter, J. H. van Esch and E. Mendes, *Chem. Comm*, 2019, **55**, 9092-9095.

78. K. Gwon, M. Kim and G. Tae, *Integr. Biol*, 2014, **6**, 596-602.

79. S.-H. Huang, L.-S. Wei, H.-T. Chu and Y.-L. Jiang, *Sensors*, 2013, **13**, 10711-10724.

80. K. Yan, Y. Liu, J. Zhang, S. O. Correa, W. Shang, C.-C. Tsai, W. E. Bentley, J. Shen, G. Scarcelli, C. B. Raub, X.-W. Shi and G. F. Payne, *Biomacromolecules*, 2018, **19**, 364-373.

81. Y. Wang, Y. Liu, Y. Cheng, E. Kim, G. W. Rubloff, W. E. Bentley and G. F. Payne, *Adv. Mater*, 2011, **23**, 5817-5821.

82. G. G. Leisk, T. J. Lo, T. Yucel, Q. Lu and D. L. Kaplan, *Adv. Mater*, 2010, **22**, 711-715.

83. Y. Liu, E. Kim, R. V. Ulijn, W. E. Bentley and G. F. Payne, *Adv. Funct. Mater*, 2011, **21**, 1575-1580.

84. J. Li, D. Maniar, X. Qu, H. Liu, C.-Y. Tsao, E. Kim, W. E. Bentley, C. Liu and G. F. Payne, *Biomacromolecules*, 2019, **20**, 969-978.

85. G. R. Weiss, *Gels*, 2018, **4**, 1-27.

86. L. L. E. Mears, E. R. Draper, A. M. Castilla, H. Su, Zhuola, B. Dietrich, M. C. Nolan, G. N. Smith, J. Doutch, S. Rogers, R. Akhtar, H. Cui and D. J. Adams, *Biomacromolecules*, 2017, **18**, 3531-3540.

87. E. R. Cross and D. J. Adams, *Soft Matter*, 2019, **15**, 1522-1528.

88. E. R. Cross, S. Sproules, R. Schweins, E. R. Draper and D. J. Adams, *J. Am. Chem. Soc*, 2018, **140**, 8667-8670.

89. C. A. Schneider, W. S. Rasband, and K. W Eliceiri, *Nat. Methods*, 2012, **9**, 671-675

90. M. Wallace, J. A. Iggo and D. J. Adams, *Soft Matter*, 2015, **11**, 7739-7747.

91. M. Wallace, J. A. Iggo and D. J. Adams, *Soft Matter*, 2017, **13**, 1716-1727.

92. M. Wallace, D. J. Adams and J. A. Iggo, *Anal. Chem*, 2018, **90**, 4160–4166.

93. M. P. Foster, C. A. McElroy and C. D. Amero, *Biochemistry*, 2007, **46**, 331-340.

94. E. R. Draper, J. R. Lee, M. Wallace, F. Jackel, A. J. Cowan and D. J. Adams, *Chem. Sci*, 2016, **7**, 6499-6505.

CHAPTER 6

Conclusions

Within this thesis, new methods to probe the self-assembly of gelation as well as the ability to control the self-assembly of gelation have been developed. These methods are applied to either bulk or electrochemical gelation.

In Chapter 2, a new electrochemical method to probe the surface chemistry of self-assembled hydrogel fibres to determine their pK_a was developed. Not only were we able to determine the pK_a of a gelator, we were also able to determine whether a gel would form and what its rheological stiffness would be. This is the first example of electrochemistry being used to determine the rheological properties of gels. Furthermore, a method was developed to probe in the real time the self-assembly kinetics of a gelator into a gel using multiple pulse amperometry. Finally, we expanded this method to complex multicomponent systems and were able to observe the surface chemistry for individual components within the gel. In the future this work could be applied to high-throughput screening methods to determine the rheological properties of new gelator molecules and complex systems.

Chapter 3 introduced a new development in controlling the rate of gelation in electrochemically fabricated hydrogels. Rheological frequency and strain sweeps show how faster gelation kinetics, from the increase in applied current, result in differences in the rheological properties. Gels formed from worm-like micelles produce stiffer gels when a higher current is applied, and gels formed from smaller aggregates produce weaker gels when a higher current is applied. This development is interesting as the different trends in physical properties are unique for each gelator which may allow for new gel properties for existing gelator molecules that usually used to form gels in bulk to be discovered. Chapter 3 also shows how the uptake and release studies suggest gels with greater stiffness have larger mesh sizes. Finally, purple crystals forming from hydroquinone are present when the gels are cooled to -15 °C. The thermochromic properties of these gels can be controlled by the applied current. These gels could potentially be used to develop intricate thermochromic devices. In conclusion, the development of electrochemical LMWG Chapter 3 provide the fundamental principles to produce electrochemical LMWG with greater level of complexity than is previously published to date.

Chapter 4 introduces a new gelation trigger method for low molecular weight hydrogels. Using this method, the gel stiffness can be controlled by the initial starting pH of the gelator solution. SANS data show how the composition of the gel fibres are similar at low Q therefore, the differences in gel stiffness are due to the entanglement of the fibres. We demonstrate that weaker gels show greater antimicrobial properties towards Gram-positive bacteria and attribute this to the production of reactive oxygen species as a result of the autoxidation of dopamine to produce polydopamine. This suggests potential to control the antimicrobial properties of a gel by controlling the mechanical properties of gelation.

The second part of Chapter 4 developed on from the electrochemically fabricated gel work in Chapter 3. Dopamine oxidation was controlled electrochemically and used to trigger gelation on an electrode surface. Gels grown by electrochemical oxidation of dopamine were found to be cell viable which gives a new potential method to develop an extracellular matrix that is suitable for a range of biomedical applications. In addition, we have identified that dopamine triggered electrochemical gelation is suitable for preparing photoconductive gels, which opens up a new route for OPV device fabrication.

Finally, in Chapter 5 a new method to control the self-assembly of both single component and multicomponent gel networks by temperature was shown. This method was analysed by the combination of ^{1}H NMR spectroscopy, pD, and rheological measurements over time. Furthermore, we demonstrated how different components within a multicomponent gel can be differentiated by small-angle neutron scattering using contrast-matching experiments. Results showed that although the underlying self-assembled structures are very similar; instead, it is the organization of these structures that is affected that results in the differences in physical properties. Lastly, we showed how the rate of self-assembly can be used to vary the networks that are formed within multicomponent gels leads directly to changes in the efficiency of electron transfer. We expect that these advances will allow multicomponent systems to become effective electronic materials.

In conclusion, this thesis shows new methods to analyse and control the self-assembly of gelation leading to exciting new materials. These materials have been shown to be of use to a wide range of applications including antimicrobial coatings, OPV devices, thermochromic materials and biomedical materials. Many of the described methods are novel or go beyond the state of the art. The ability to prepare low molecular weight gels electrochemically with the potential for biomedical applications has been achieved where others have previously only suggested it to be possible.

This work has ignited the potential for further electrochemical analysis methods to probe soft materials which will advance the field. Future work could see new high throughput laboratory equipment developed that could determine rheological properties of gels which are cheaper than mechanical rheometers and could be used by interdisciplinary groups without specialised knowledge of existing characterising methods. Developing dopamine as a bulk gelation trigger will allow for existing gelator molecules to form new physical and antimicrobial properties which will allow for new or improved use in applications. Furthermore, future work to control gelation electrochemically could provide new materials with higher spatiotemporal control than existing bulk gelation methods. There is potential in both biomedical and optoelectronic fields to create gels with defined networks that will allow for cell differentiation, greater electron transfer efficiency or a combination of both.